POTENTIAL ROLE OF IRON CHELATION IN EXPERIMENTAL SEPSIS

by

Danielle Fokam

Submitted in partial fulfillment of the requirements

for the degree of Master of Science

at

Dalhousie University

Halifax, Nova Scotia

November 2019

© Copyright by Danielle Fokam, 2019

DEDICATION PAGE

I dedicate this thesis to my beloved grandma, Lydie Kuitchou.

Bien qu'ayant les yeux remplis de larmes, je tiens à te rédiger ces quelques mots. Le célèbre écrivain Victor Hugo avait dit : « Tu n'es plus là où tu étais, mais tu es partout là où je suis ». J'ai toujours été honorée de porter ton nom et à travers lui, je sais que tu vis en moi. J'espère que de là-haut tu es fière de celle que je suis et du travail que j'ai accompli. Tu me manques Bomboh!

Je t'aime ♥

TABLE OF CONTENTS

LIST OF TABLES

LIST OF FIGURES

ABSTRACT

Sepsis is a life-threatening medical condition characterized by a dysregulated immune response to an infection. The increasing incidence, remaining high mortality and enormous costs burden, make sepsis a real public health problem. Early appropriate treatment boosts chances of surviving sepsis, but there is no specific approved treatment for the dysregulated immune response available to date. However, some lifesaving measures are available. The main goal of sepsis treatment is to control the source of the infection, surgically and/or by using antibiotics. The fact that iron is a nutrient required for bacterial growth and involved in the immune response, makes it a potential therapeutic target for sepsis. The present research has been designed to study the effect of the novel, highly specific iron chelator, DIBI, in relevant experimental murine models of bacterial sepsis. It has been found that DIBI alone or in combination with antibiotic treatment was able to decrease sepsis-induced leukocyte (hyper-) activation, preserve capillary perfusion, and reduce bacterial growth. These results strongly suggest DIBI as a promising adjunct treatment for bacterial sepsis.

LIST OF ABBREVIATIONS USED

ACCP	American College of Chest Physicians
AIDS	Acquired Immune Deficiency Syndrome
CACF	Carleton Animal Care Facility
CARS	Compensatory anti-inflammatory response syndrome
CASP	Colon ascendens stent peritonitis
CASP-I	Colon ascendens stent peritonitis with intervention
CBC	Complete blood count
CFU	Colony forming units
CLP	Caecum ligation puncture
CON	Control
CPI	Chelation Partners Inc
CRP	C-reactive protein
DAMP	Damage-associated molecular pattern
DFO	Deferoxamine
DFP	Deferiprone
DFX	Deferasirox
DMT1	Divalent metal transporter 1
DNA	Deoxyribonucleic Acid

EDTA	Ethylene diamine tetra-acetic acid
ETC	Electron transport chain
FCD	Functional Capillary Density
FDA	Food and Drug Administration
FITC-BSA	Fluorescein isothiocyanate - bovine serum albumin
H&E	Hematoxylin and Eosin
H_2O_2	Hydrogen peroxide
HIV	Human Immunodeficiency Virus
HMGB1	High mobility group box 1
HOCl	Hypochlorous acid
i.p.	Intraperitoneal
i.v.	Intravenous
ICAM-1	Intercellular adhesion molecule 1
ICU	Intensive care unit
IFN-γ	Interferon-gamma
IL-10	Interleukin-10
IL-1β	Interleukin-1 beta
IL-6	Interleukin-6
IMI	Imipenem

IVM	Intravital microscopy
LEI	Leukocyte endothelial interaction
LPS	Lipopolysaccharide
LTA	Lipoteichoic acid
MAHMP	3-hydroxy-1-(β-methacrylamidoethyl)-2-methyl-4(1 H)-pyridinone
MODS	Multiple organ dysfunction syndrome
NaCl	Sodium chloride
NETs	Neutrophil extracellular traps
NF-κB	Nuclear factor kappa B
NLR	NOD-like receptors
NO	Nitric oxide
NOS	Nitric oxide synthase
NS	Nova Scotia
O_2	Superoxyde
OH	Hydroxyl radical
ONOO-	Peroxynitrite
PAMP	Pathogen-associated molecular pattern
PBS	Phosphate buffered saline
PLF	Peritoneal lavage fluid

PRR	Pattern-recognition receptor
PSGL-1	P-selectin Glycoprotein Ligand 1
PVP	Polyvinylpyrrolidone
qSOFA	Quick sequential (sepsis-related) organ failure assessment
RLR	Retinoic acid-inducible gene-I-Like Receptors
ROS	Reactive oxygen species
s.c.	Subcutaneous
SCCM	Society of Critical Care Medicine
SEM	Standard error mean
SIRS	Systemic inflammatory response syndrome
SOD	Superoxide dismutase
SOFA	Sequential (sepsis-related) organ failure assessment
TLR	Toll-like receptor
TNF-α	Tumor necrosis factor alpha
TSA	Tryptic soy agar
UCLA	University Committee on Laboratory Animals
V1	Submucosal collecting venules
V3	Post capillary venules
VCAM-1	Vascular cell adhesion molecule-1

ACKNOWLEDGEMENTS

I would like to start this part with words from the philosopher Alfred North Whitehead: “No one who achieves success does so without the help of others. The wise and confident acknowledge this help with gratitude.”. I could not have done this work without the help of those I will mention:

Dr. Christian Lehmann, my supervisor: Thank you for believing in me and for giving me the opportunity to expand my knowledge. You have pushed me to my full potential and taught me that we can achieve everything with hard work and organization. Your assistance and guidance were essential for the development of this thesis. Thank you for the sleepless nights that I know you have spent revising my work. I have learned a lot thanks to you and I do not regret any second of this wonderful experience!

Dr. Juan Zhou: You have always been there when I needed it, whether for scientific or personal advice. Many thanks for your constant help during these years.

My supervisory committee members, Dr. Alex Quinn and Dr. Xianping Dong, for their expertise and guidance throughout my degree.

Chelation Partners Inc.: for providing DIBI.

Dr. Stueck/ Pat Colp: for training and helping me with the histological part of the project.

Jean Marshall lab: for training and helping me with cytokine measurements.

Members of the Lehmann Lab: Cassidy, Kiyanna, Geraint, Gaurav, Mariane, Nazli, Bashir, Hajer, Tanya, and Taylor. Your help has made my work much easier and fun. Special thanks to Kayle Dickson for her help with the Klebsiella experiments. To Maral Aali and Ian Burkovskiy, no word is strong enough to express my gratitude. You have been with me since the beginning, first as labmates, today as friends. Thank you for all the advice, but also for all the good moments we spend together.

To Dr. Freddy Fokam, my dear big brother. You gave me more love and support than most people get in a lifetime. I am very lucky to have you. Thank you to my wonderful parents for their endless encouragement. I also thank my only sister Viviane; my brothers Thierry and Serge; Adam, Chelsea, Jessica, Lyna, Eugene, and the rest of my family.

To Setche Cedric, my gratitude will never equal your big heart. You supported me when I needed it the most. You are a blessing in my life.

To my lovely friends, Leila, Barbara, Dominique, Anna, Meagan, Flora, Olivier, Kaitlyn, Antonio, and all the rest, MANY THANKS!

Last but not least, to all the mice sacrificed for this work. They are more than “just a tool for research”, they are a part of novel findings regarding sepsis.

CHAPTER 1: INTRODUCTION

1.1 Sepsis

1.1.1 Definition, Epidemiology and Symptoms

Sepsis is defined as a life threatening organ dysfunction due to a dysregulated host immune response to infection (1). Worldwide, sepsis affects more than 30 million people every year and represents one of the leading causes of death (2–5). The high incidence and mortality of sepsis is often underestimated in the health statistics. The main reason is that sepsis is still often considered as pathway to death from a general infection rather than as a dysregulated host immune response (6)(7). Infections represent a common health problem in people of all ages. However, elderly and infants are at higher risk of developing sepsis from an infection. The risk of sepsis increases with age and with comorbidities (such as diabetes, HIV/AIDS, cancer, or liver disease), as well as underlying immunosuppression (organ transplants, immunosuppressant drugs, etc.) (8, 9). Additionally, men seem to be slightly more affected than women and tend to have higher mortality (8, 10). Increasing incidence, remaining high mortality and enormous costs burden, make sepsis a real public health problem, especially in low and lower-middle income countries (11, 12).

In the US, nearly 2 million adults are affected by sepsis each year and more than 250,000 of them die from the condition (13). Furthermore, not only adults but children are also concerned. According to a 2019 report of the U.S. Department Of Health And Human Services, sepsis is 7th in the list of 10 leading causes of 2017 infant death in the US (14). Sepsis is one of the leading causes of death in American hospitals, accounting for 50% of hospital death (15). The prevalence and the incidence of sepsis in hospitalized patients is increasing by approximatively 9% every year (15). The more severe and complicated the sepsis, the higher the mortality.

A recently published report showed that sepsis was the most expensive condition in the US in 2013 with hospital expenses of approximately $23 billion (nearly $16 000 per hospitalization) over the $381 billion aggregate hospital costs. Sepsis is far more costly than osteoarthritis, the second most expensive condition, accounting for $16 billion in hospital expenses (16). In Canada as in the US, sepsis is also a leading cause of death and a significant financial burden on the Canadian health care system. In Canada (Quebec excluded), there are approximately 30 000 cases of sepsis recorded each year with a mortality of 35% (17). Sepsis was the 12th leading cause of death in 2011 in Canada (8). Unlike the US, there is only a small amount information available in the literature on sepsis costs for the Canadian health system. A study conducted in Quebec estimates that the mean sepsis cost for the Quebec health care system varied from $11 474 to $16 228 per hospitalization when the patient finally died and $27 481/ year if the patient survived (18). The costs associated with sepsis are not only due to the initial hospitalization but are also due to long-term consequences of sepsis survivors. Initial hospitalization expenses represent only 30% of sepsis survivors total costs (19). The remaining 70% being the result of productivity loss and indirect medical costs. Patients surviving sepsis usually have long-term physical, psychological, and cognitive disabilities, lower quality of life, often lose independence and seek help on a daily basis, miss workdays or can no longer work at all, and many times require hospital re-admission (19).

The first known reference to septic syndrome comes from ancient Egypt. It was mentioned in the oldest surgical text called the Edwin Smith Papyrus, written in the 1600 BC, a copy of a text from 3000 BC (20). For the vocabulary, the ancient Greeks seems to be the first ones to attribute a name to this condition. Sepsis comes from the ancient Greek "sepo" which means “putrefaction” or “rot”. The word "sepo" has been widely used in Greek classic literature from the 8th century BC by the poet Homer (20). In the 4th century BC, “sepo” was referred as “sepidon” first by the physician Hippocrates to describe structure dissolution, then by authors like Aristotle, Plutarch, Galen, and others (21). The term and its meaning remained unchanged for several centuries. In 1700-1800 AC, when the clinical signs of sepsis were attributed to an ongoing infection, the British surgeon George James Guthrie exposed the difference between immediate inflammation and signs of sepsis developing the following days (20).

In the 1990s, because of controversies between health care professionals about the definition and management of sepsis, the American College of Chest Physicians (ACCP) and Society of Critical Care Medicine (SCCM) consensus conference in Northbrook, Illinois, United States, suggested some definitions and criteria: sepsis-1 (22). According to the conference, 4 stages should be considered (Figure 1). First, the systemic inflammatory response syndrome (SIRS) characterized by at least 2 of the following criteria: Increased heart rate: >90 beats/min, increased respiratory rate: >20 breaths/min, high or low temperature: >38 or <36 °C, high or low level of white blood cells in the blood: >12000 cells/mm^3 or <4000 cells/mm^3 (or >10% immature cells). Second, SIRS associated with suspected or confirmed infection was defined as sepsis. Third, severe sepsis characterized by sepsis complicated by organ dysfunction and lastly, sepsis-induced persisting hypotension despite adequate fluid resuscitation called septic shock. Ten years after the 1^{st} conference, ACCP and SCCM held a 2^{nd} consensus conference (23). The definitions of sepsis-1 were considered not specific, but due to lack of evidence and data, and limited knowledge at that time, no major change has been made. The 4 stages remained the same with the only difference that SIRS criteria have been expanded in order to define it slightly more precisely.

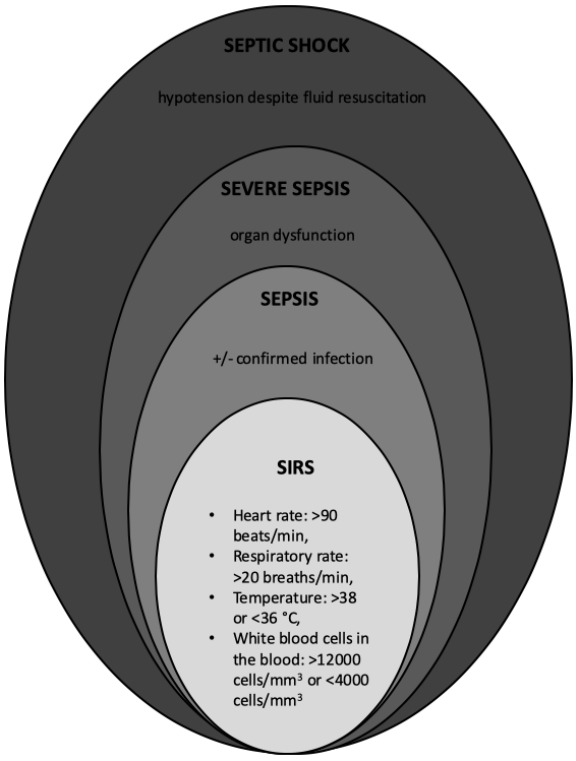

Figure 1 From Systemic Inflammatory Response Syndrome (SIRS) to septic shock: 1991 Northbrook consensus conference

A major change came with sepsis-3, the 3rd consensus conference (1). Briefly, the decision has been made to abandon the term SIRS because of low specificity and sensitivity in the discrimination of sepsis and uncomplicated infection. Moreover, sepsis has been defined as “life-threatening organ dysfunction caused by a dysregulated host response to infection”. The term sepsis was clearly separated from an infection and the immune dysregulation highlighted. Furthermore, since organ dysfunction was already part of the definition of sepsis, the term severe sepsis was no longer necessary. Finally, strict criteria for septic shock were established: “patients with septic shock can be clinically identified by a vasopressor requirement to maintain a mean arterial pressure of 65 mm Hg or greater and serum lactate level greater than 2 mmol/L (>18 mg/dL) in the absence of hypovolemia.” (1). Clinically, sepsis varies depending on patient characteristics, severity of the condition, type of infection, and can be very general. Therefore, sepsis is suspected in presence of signs of infection (or confirmation of infection) associated with organ failure.

Because sepsis is a complex clinical syndrome and not a specific disease, there is not one validated diagnostic test for confirmation. Many different tests (like white blood cell count, blood C-reactive protein or procalcitonin, lactate level in blood, blood culture, X-ray etc.) are used to guide physicians (24, 25). The Third International Consensus Conference mentioned the lack of standardized diagnostic method to identify sepsis contributing to incomplete data regarding incidence and outcomes. The recommendation for identifying both sepsis and septic shock is to use a scoring system to evaluate organ failure of suspected sepsis patients and quickly assess how likely a patient is to have sepsis or septic shock. The score is named Sequential Organ Failure Assessment (SOFA) score (26). It evaluates from 0 to 4 (0 being normal and 4 severe alteration) each of the respiratory, neurological, cardiovascular, hepatic, renal and coagulation systems for a maximum of 25 points. A score greater than or equal to two is associated with a 10% mortality risk in patients suspected of sepsis (1). The SOFA score is very useful but includes blood tests which take some time for results. A faster but still effective version of the SOFA score utilizable at patient's bedside was also recommended. The quick SOFA (qSOFA) score consists of 3 parameters that will be scored 1 if present (Table 1): low blood pressure (SBP ≤ 100 mmHg), respiratory rate ≥ 22 breaths / min, and change in mental status (Glasgow score ≤ 14). A qSOFA score greater than 2 points indicates organ dysfunction (21) and has been suggested to have a similar predictive power to the original SOFA score (1).

qSOFA criteria

Increased respiratory rate ≥ 22/min
Altered mental status (Glasgow Coma Scale Score ≤ 14)
Systolic Blood Pressure ≤ 100 mmH

Table 1 Quick Sequential Organ Failure Assessment (qSOFA) scoring system parameters.
A qSOFA score greater than 2 points indicates organ dysfunction

Studies have shown that in term of sepsis treatment, the earlier the better. Although no approved treatment is available at the moment for the immune dysregulation, some therapies are used in sepsis (27). The main goal of sepsis treatment is the control of the source of infection, surgically and/or by using appropriate antimicrobial therapy. Therefore, antibiotics should start as soon as possible with broad-spectrum antibiotics followed by more specific antibiotics once the type of bacteria involved in known after blood culture. Other treatments for sepsis include for example intravenous fluids and vasopressors in case of low blood pressure, low doses of corticosteroids or insulin to stabilize blood sugar levels, painkillers in case of pain, antipyretics in case of high temperature. Early detection of sepsis with quick appropriate initiation of treatment increases survival of patients with sepsis (24, 28–32). In order to better diagnose sepsis, the understanding of sepsis pathophysiology is crucial.

1.1.2 Pathophysiology

Sepsis is an inappropriate immune response to an infection. The words infection and inflammation are sometimes used interchangeably, but their meaning is very different. Infection is the invasion and multiplication of pathogens such as bacteria, viruses, fungi, and parasites into sterile tissues, while inflammation is the body's response to harmful stimuli, including non-infectious triggers i.e. burn, muscle strain, auto-immune disease, mechanical trauma, and infectious triggers (33). However, humans are colonized by a large number of (not harmful) bacteria. Studies have shown that these bacteria are essential and that a change in their composition or number can affect health (34). On the other hand, when these pathogens invade sterile tissues, the immune system is activated and an inflammatory process is triggered. The immune system can be broadly divided in innate and adaptive immunity (35). The innate immunity is the first line of defense against pathogens.

1.1.2.1 Immune Response

1.1.2.1.1 Innate Immune Response

When infection occurs, there is a release of pathogen products (pathogen-associated molecular patterns - PAMPs). In addition, endogenous stress signaling molecules of the body, called danger-associated molecular patterns (DAMPs) are released. PAMPs include bacterial components like peptidoglycan (PGN) and lipoteichoic acids (LTA) from Gram-positive bacteria, as well as lipopolysaccharide (LPS) from Gram-negative bacteria. They also include molecules from fungi (zymosan), parasites (profillin), etc (36). DAMPs are cellular components from damaged tissues or cells - such as high-mobility group box 1 (HMGB1), mitochondrial DNA and metabolic molecules such as ATP, uric acid, and others - that are externalized (37).

PAMPs and DAMPs are recognized by the pattern recognition receptors (PRRs) of cells of the innate immunity - such as dendritic cells, macrophages, neutrophils (38). Pattern recognition receptors include Toll-like receptors (TLRs), NOD receptors (NLRs) and RIG-I receptors (RLRs) with Toll-like receptors being the most studied (39). TLRs are transmembrane proteins. There are 10 TLRs so far identified in humans and 12 in mice (TLRs 1–9 common to both species) (40). Bacterial components like peptidoglycan (PGN) and lipoteichoic acids (LTA) from Gram-positive bacteria generally activate TLR-2 whereas lipopolysaccharide (LPS) from Gram-negative bacteria usually activates TLR-4 (41–43). Recognition of those PAMPs by TLRs is a critical initiator of inflammation in sepsis, resulting in activation of intracellular transcription factors such as NF-κB. NF-κB then induces transcription, translation and extracellular release of cytokines and adhesion molecules (Intercellular Adhesion Molecule-1, Vascular Cell Adhesion Molecule-1) (44). A well-coordinated innate immune response is important in order to resolve the infection by participating in leukocyte chemotaxis, boosted phagocytic activity, reactive oxygen species (ROS) production, activation of adaptive immune response, and initiation of the coagulation system.

1.1.2.1.2 Adaptive Immune Response

The response of the innate immune system is very immediate but non-specific unlike the second line of defense, the adaptive immune response, which takes time to start but is highly specific and long-lasting (35). Immature dendritic cells, long-lived phagocytic cells, are the main inducer of the adaptive immune response. PAMPs and DAMPs are recognized by dendritic cells pattern recognition receptors (PRRs) that activate them to engulf and degrade pathogens. The now activated dendritic cells become highly effective antigen-presenting cells and carry antigen (part of the degraded pathogen) to immature T and B lymphocytes in peripheral lymphoid organs (45). Activated B and T cells proliferate, and while some of them produce antibodies highly specific to the antigen and destroy pathogens, others become memory cells and live for many years remembering the insult. In case of re-infection by a known pathogen, the adaptive immune response is very quickly activated, and the pathogen eradicated.

1.1.2.1.3 Cytokines release

Cytokines are important signaling and regulating molecule of the immune response. There are two types of cytokines. First, pro-inflammatory cytokines (IL-1β, IL-6, TNF-α, IL-8, IL-11, and a variety of chemokines that attract immune cells) to support the inflammatory process (46). After being activated by either PAMPS or DAMPS, several types of cells from the innate and adaptive immune response start releasing cytokines (macrophages, neutrophils, dendritic cells, lymphocytes, helper T cells) to initiate diverse processes. The most important cytokines and the first to be release by macrophages, monocytes and endothelial cells are TNF-α and IL-1, followed by IL-6 (47). These pro-inflammatory cytokines have diverse effects. They induce the activation of immune cells to the site of inflammation, the degradation of glycocalyx - a coat that protect endothelial cells – and trigger the synthesis of adhesions molecules such as ICAM1 or VCAM1 that will allow activated immune cells to adhere to the vascular endothelium and facilitate transmigration in the inflamed tissues (48). TNF-α, IL-1 and IL-6 stimulate the production of mediators of inflammation - acute phase proteins - by the liver cells i.e. hepatocytes (46).

These acute phase proteins are plasma molecules (such as C-reactive protein, serum amyloid A, α1-acid glycoprotein, haptoglobin, mannose-binding protein, α1-antitrypsin, complement components C3 and C4, and coagulation proteins as fibrinogen and prothrombin) that participate in the activation of immune cells, in the destruction of bacteria and also in platelets activation. Interferon gamma, IL-3, and granulocyte-macrophage colony-stimulating factor (GM-CSF), amplify IL-1 and TNF macrophages production. IL-8 and macrophage chemoattractant protein-1 are cytokines contributing to the chemotaxis of leucocytes to the site of injury. Because they stimulate the expression of tissue factor on mononuclear and endothelial cells that trigger coagulation cascade, IL-1 and IL-6, are considered powerful inducers of coagulation (whereas the anti-inflammatory molecule IL-10 down regulates coagulation by inhibiting the expression of tissue factor) (45).

Second, there is anti-inflammatory cytokines that inhibit inflammation and induce a healing process (46). They are specific cytokine inhibitors and soluble cytokine receptors. As pro-inflammatory ones, several types of cells can release anti-inflammatory cytokines (monocytes, macrophages, fibroblasts, lymphocytes, dendritic cells). Major anti-inflammatory cytokines are IL-10, interleukin-1 receptor antagonist, and Tumor necrosis factor receptor. They are potent inhibitors of pro-inflammatory cytokines production as IL-1 and TNF-α (49). Cytokines released at the appropriate levels and time lead to a controlled mechanism of inflammation.

1.1.2.1.4 Immune Dysregulation in Sepsis

The most common sites of infection leading to sepsis include the lungs, urinary tract and abdomen (50). The actors of the innate immune response try locally to control this infection and when they fail, infection becomes generalized. The pathogens then disseminated in the bloodstream and systemically activate immune cells to control the infection. Sepsis starts when, for an incompletely known reason, the initial appropriate host response to an infection becomes excessively amplified, i.e. dysregulated (45).

NF-κB induces release of huge amounts of cytokines called cytokine storm responsible for oxidative stress, tissue damage, sepsis-associated coagulopathy, and ultimately multiorgan dysfunction (46). The exact mechanism of sepsis immune dysregulation is multifactorial and still poorly understood. For the moment, studies agree that sepsis starts with a hyperactivation phase marked by the overactivation of immune response. Then, a compensatory mechanism called Compensatory Anti-Inflammatory Response Syndrome (CARS) emerges. The goal of CARS is to induce a systemic inactivation of the overactive immune system in order to restore a certain homeostasis (51). This phenomenon leads to a stage of immunosuppression. Even though it can be hard to conceive, CARS does not mark the ending of the hyperactivation phase. Both phases happen at the same time, with mediators of one phase being sometimes more present than the other (Figure 2) (51, 52).

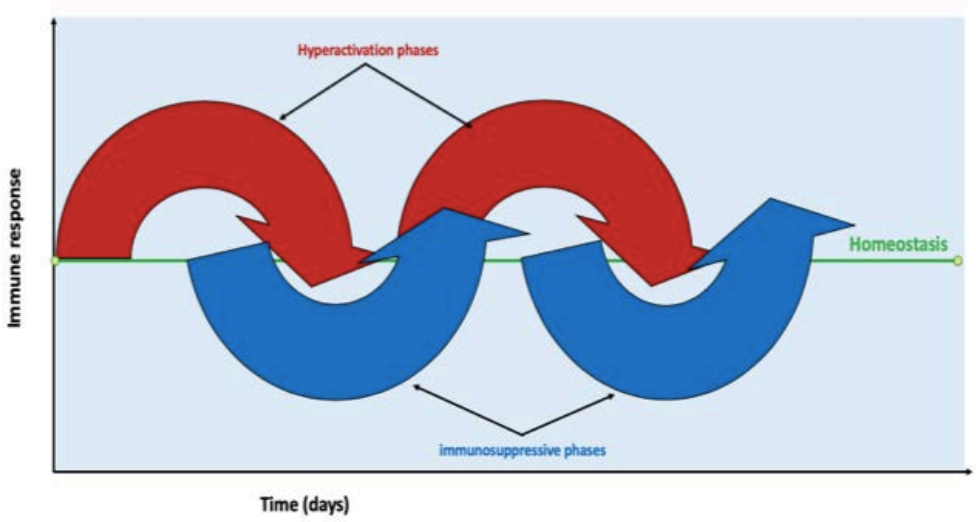

Figure 2 Clinical course of sepsis

1.1.2.1.5 Leukocyte Endothelial Interactions in Systemic Inflammation

Leukocytes move freely in the bloodstream. During an infection, they are attracted to the inflammation site by chemotaxis. As mentioned above, PAMPs recognition by cells of the innate immune system activate pro-inflammatory pathways, dominated by NF-κB activation, which lead to cytokine release responsible for endothelial cell activation.

The pathogens can, at a lesser extent, directly activate endothelial cells via their pattern recognition receptors (PRRs) (53). Consequently, endothelial cells start expressing adhesion molecules (L-, P-, and E-selectins, Intercellular Adhesion Molecule-1 or ICAM-1, Vascular Cell Adhesion Molecule-1 or VCAM-1, etc.). Leukocyte-endothelial Interaction starts with rolling of leukocytes on the endothelium. The P-Selectin Glycoprotein Ligand-1 (PSGL-1) of leukocytes can bind to both P-selectin and E-selectin presented on the endothelial cells surface (54). The first and main binding is PSGL-1 and P-selectin. At this point, the binding is quite fragile, therefore instead of stopping completely their course, leukocytes rather slow down and roll. Meanwhile, the closer contact between endothelial cells and leukocytes associated with the interaction of leukocytes PSGL-1 and endothelial E-selectin activates molecules on leukocytes called integrins (54). Leukocyte integrins bind to ICAM-1 and VCAM-1 to develop a very firm adherence. This process ends with leukocytes finally transmigrating to the inflammatory site.

During the early septic hyperactivation phase, cytokines are overexpressed (cytokine storm) leading to overexpression of adhesion molecules on endothelial cells. All this, combined with the fact that an excessive quantity of leukocytes is mobilized, contributes to the increased endothelial adhesion of leukocytes. The oxidative stress and tissue damage due to sepsis increases the release of DAMPs, which worsen the cytokine storm and feed the vicious sepsis circle.

1.1.2.2 Microcirculation Disorder in Sepsis

Macrocirculation parameters such as blood pressure and cardiac output are commonly used to assess clinical patients with sepsis. Although those parameters are critical, microcirculatory changes precede those changes. Many studies have established the fact that macrocirculation may appear normal while the microcirculation is impaired early during sepsis (55–58). Several studies have shown that the microcirculation is mainly responsible for the occurrence of organ failure and represents a prognostic parameter for survival of patients with sepsis (59–61). Persistent altered microcirculation is associated with high mortality in septic patients (60).

Microcirculation includes arterioles, capillaries and venules consisting of endothelial cells, smooth muscle cells, red blood cells, leukocytes, and platelets (62). During sepsis, there is an increase in leukocytes adherence to the endothelium. Cytokine storm due to activation of NF-KB and other inflammatory pathways induces the release of inflammatory mediators including reactive oxygen species and nitric oxide leading to loss of integrity and increased permeability of the endothelium, oxidative damage of surrounding tissues, coagulopathy, redistribution of blood, and physical obstruction of capillaries by activated leukocytes (46, 63). The ultimate damage is tissue hypoxia leading to multiorgan dysfunction then death (62, 64).

1.2 Iron

1.2.1 Iron Homeostasis

Iron is one of the most abundant elements on our planet (65). This molecule is essential for physiological processes of most forms of life. Many ancient civilizations in Egypt, India, Greece, and others, during their time, were already aware of the crucial role of iron in health and disease (66). One of the reasons why iron is so widely involved in biological processes is because of its electron transferring properties. By switching between different states (ferrous Fe^{2+} and ferric Fe^{3+}) iron catalyzes chemical reactions by accepting or donating electrons. In vertebrates in general and humans in particular, one of the main roles of iron is its involvement in the oxygen-carrying capacity of hemoglobin and myoglobin (67). Iron metabolism include intestinal absorption, erythroid iron uptake, reutilization of senescent red blood cells by macrophages, hepatic iron storage, and systemic regulation (Figure 3).

The human body does not produce iron, it recycles the iron that it already contains and absorbs by the diet the additional iron necessary to compensate losses (blood loss by hemorrhage or menses for example) (67).

Iron ability to exchange its electrons is a powerful advantage, but also a potential major threat. Iron is as useful as toxic, therefore, its tightly regulation by the organism is very important for the maintenance of homeostasis. Depending on the need, only 15 - 30% of the iron from the diet is absorbed by intestinal enterocytes through carriers such as Heme Carrier Protein-1 or Divalent Metal Transporter-1 (68, 69). Once in the enterocytes, iron is added to the systemic circulation via the metal transporter, Ferroportin-1. Since iron is highly reactive and thus potentially harmful, it is always linked to a protein under normal conditions. In the blood iron is bound to transferrin. Transferrin bound iron in the circulation is then moved to where it is needed (essentially to the bone marrow for erythropoiesis - formation of red blood cells) (67).

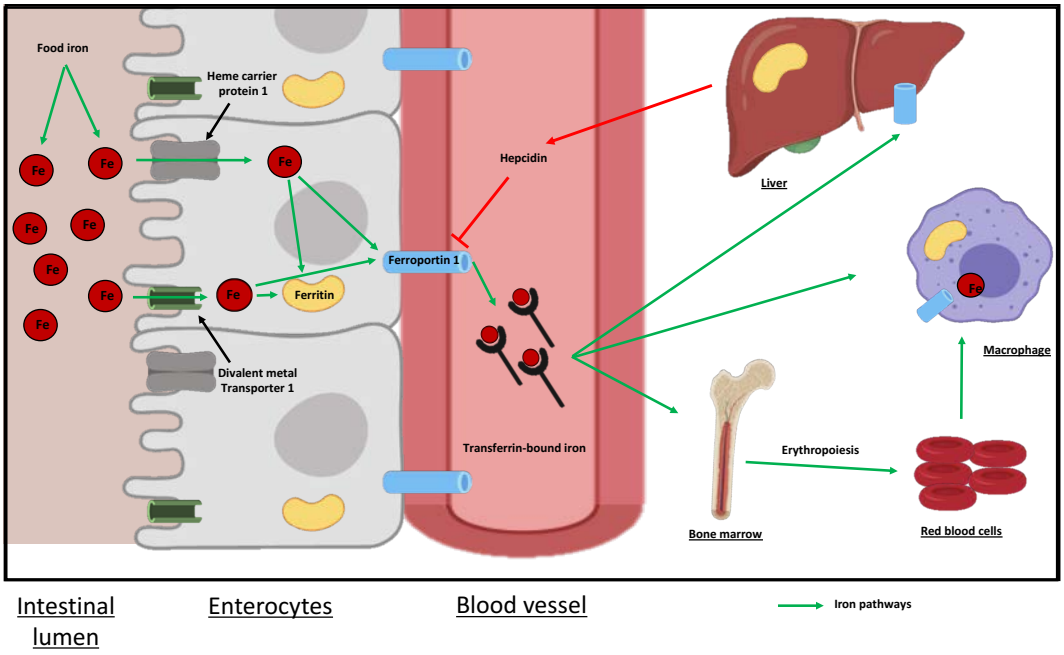

Figure 3 Summary of iron metabolism
Iron is absorbed from the diet by intestinal enterocytes through carriers such as Heme Carrier Protein-1 or Divalent Metal Transporter-1. It is then spilled, through a carrier called Ferroportin-1, in the bloodstream where it is bound to Transferrin then moved to bone marrow where it is used for erythropoiesis, formation of red blood cells. Iron from senescent red blood cells is recycled by macrophages and all excess systemic iron is stored in liver and other tissues. Systemic regulation of iron is done by Hepcidin, capable of stopping iron release by Ferroportin-1 in case of overload.

Senescent red blood cells are eliminated by macrophages and their iron recycled and released into the systemic iron pool or stored. The liver is the major organ of iron storage, excess systemic iron is stored as ferritin and hemosiderin. To a lesser extent, iron is stored in other cells as a labile iron pool. The labile iron is biologically active because it can participate in intracellular metabolism like oxidation–reduction reactions, and cell signaling (68). The body does not possess iron excretion mechanisms but regulates systemic iron level by stimulating the release of hepcidin, an iron regulatory protein in the liver. In case of iron overload, hepcidin is released and binds to ferroportin on the cell surface leading to direct inhibition of intestinal absorption of iron, and promotion of iron storage by down-regulating expression of ferroportin by cells. Without ferroportin, iron is trapped in cells. Studies have shown that hepcidin release increase during inflammation and infection, highlighting the role of this molecule in sepsis (70–72).

1.2.2 Iron and sepsis

1.2.2.1 Iron and systemic inflammation

To better understand the role of iron in inflammation, an understanding of the inflammatory actions of reactive oxygen species (ROS) is needed. ROS, such as hydrogen peroxide - H_2O_2, superoxide - $O_2{\cdot}-$ and hydroxyl radical - HO· are unstable and highly reactive molecules due to unpaired electrons in their outermost shell. They are mainly produced in the mitochondrial electron transport chain (73). As previously mentioned, phagocytic cells such as macrophages are critical payers in innate immune response to inflammation. Two types of macrophages have been described: M1 and M2. It is important to have the right type of macrophage at the right time. M1 macrophages are useful in the acute phase of inflammation (strong microbicidal function and secrete large amounts of proinflammatory molecules) when M2 are needed in the late phase for wound healing and tissue repair (produce high levels of anti-inflammatory mediators) (74).

The differentiation of macrophage into M1 or M2 is complex and not yet fully understood; nevertheless, studies have shown that ROS are instrumental in this process (75, 76). Briefly, "high level" of ROS leads to the differentiation of M1 macrophages whereas “low level” of ROS results in M2 macrophages. Furthermore, ROS promote the phagocytic process by aiding the degradation of engulfed pathogens (77).

Iron participates in each of these processes by catalyzing oxidation reactions through the Fenton reaction: $O_2 \cdot -$ leads to the highly reactive HO· in the presence of free iron ($Fe^{2+} + H_2O_2 \rightarrow Fe^{3+} +$ OH− + HO·) (78). Studies have shown that high intracellular iron levels stimulate the secretion of pro-inflammatory cytokines (79, 80). Moreover, iron-overloaded macrophages differentiate more into M1 than M2 type, leading to delayed wound healing and continuous tissue damage (81). This happens because high iron level induces high ROS level. A very large cohort study even showed that high iron levels are associated with increased mortality of patients with sepsis (82). All this information put together shows the pro-inflammatory effect of iron via ROS. In a context like sepsis where there is a hyperinflammatory phase, iron act as a catalyst to perpetuate inflammation.

1.2.2.2 Iron and Bacteria

Iron is essential to nearly all life forms on Earth including bacteria. Hepcidin has a negative feedback role crucial during inflammation and infection. Its ability to down-regulate ferroportin expression by cells is an important physiological response during infection called hypoferremia of inflammation (83). Increased cytokine levels (e.g. interleukin-6) in patients with sepsis induces an increased synthesis of hepcidin causing quick decrease in plasma iron (83). The purpose of the hypoferremia is to lower iron bioavailability for harmful reactions with ROS, but also to have iron, bacteria’s nutrient, away from pathogens and potentially reduce microbial growth. Such a reaction has a biological cost. The hypoferremia of inflammation induce at some point anemia by restriction of iron supply for red blood cell production in the bone marrow (84).

Hepcidin-reduced iron levels place bacteria in survival mode. They subsequently develop ways to acquire iron and survive. Different bacteria have different methods of acquiring iron (85, 86). They can extract and capture heme-iron from host hemoproteins or acquire transferrin-bound iron through specific binding proteins or the secretion of siderophores - molecules capable of chelating iron. Some bacteria produce their own siderophores, when others have siderophore transporters used to obtain iron from siderophores produced by other organisms. Another way of acquiring iron by bacteria is to catalyze the oxidation of cytoplasmic molecules and reduce iron using electrons produced by that oxidation.

1.2.3 Iron Chelators and Sepsis

Iron chelators are molecules that bind to iron with high affinity. The main FDA approved iron chelators are deferoxamine (DFO), deferiprone (DFP), and deferasirox (DFX). They are used clinically for iron overload syndromes, e.g. hemochromatosis, thalassemia, and sickle cells disease (87). The aforementioned implications of iron-related ROS production in sepsis make iron an interesting drug target in this deadly condition. The use of the FDA approved iron chelators in sepsis represents an innovative treatment approach. Pilot studies have shown some improvements in experimental models of inflammation and sepsis (88–91).

DIBI is a novel highly selective synthetic iron chelator (developed by Chelation Partners Inc. - CPI, Halifax, NS) (Figure 4). It is a molecule with a large polyvinylpyrrolidone backbone and nine 3-hydroxy-1-(β-methacrylamidoethyl)-2-methyl-4(1 H)pyridinone (MAHMP) residues (92). Compared to the other iron chelators, DIBI has many advantages. Unlike DIBI, the three mentioned FDA-approved iron chelators can induce some toxicity: ototoxicity, allergic reactions, pain, gastrointestinal disorders, neurodegeneration, ophthalmological toxicity, etc (93, 94). DIBI's corneal toxicity and tolerability was evaluated in mice for both acute and chronic dosages. Through gross ocular examination, intraocular pressure measurements and Hematoxylin-Eosin staining of ocular tissue, no adverse effects due to the administration of DIBI has been seen (95).

Moreover, according to unpublished data, DIBI has been shown to be not toxic to both human and murine fibroblasts and epithelial cells. Repeated systemic and oral administration of DIBI (respectively 500 mg/kg/day intravenously and 1000 mg/kg/day orally) during 14 days in rat did not show toxicity: no weight gain or loss, no tissue damages (histology), no hematology disorders. DIBI and deferiprone have the strongest iron affinity comparing to the two others: one molecule of deferoxamine and deferasirox bind to respectively one and two molecules of iron, when one molecule of DIBI or deferiprone bind to 3 molecules of iron. However, unlike deferiprone, DIBI keep iron in a redox-inactive state once bound. With deferiprone, bacteria can still utilize the iron. The major goal of this research project was to evaluate the potential role of iron chelation, using DIBI, in different experimental sepsis models.

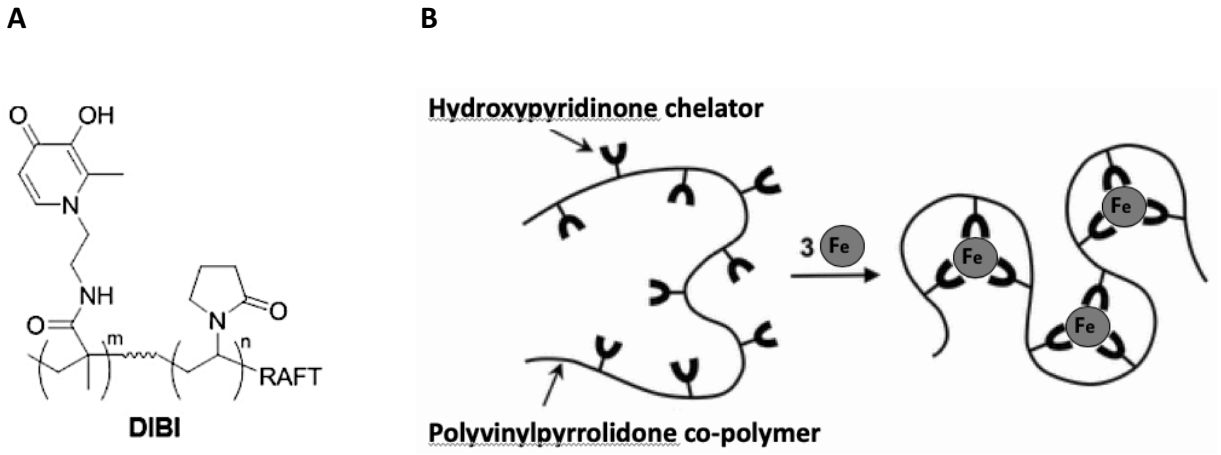

Figure 4 Structure of DIBI polymer.
(A) chemical structure of DIBI; nine 3-hydroxy-1-(β-methacrylamidoethyl)-2-methyl-4(1 H)-pyridinone (MAHMP) residues on a PVP backbone; (B) representation of iron molecules arrangement by DIBI.

1.3 Hypothesis

Iron chelation in the acute phase of hyperinflammation reduces inflammation and bacterial growth in experimental sepsis. More precisely, DIBI, a novel iron chelator, improves outcomes by reducing (iron-related) inflammatory damages, diminishing immune cells recruitment, preventing capillary blood flow impairment, and increasing the physiological hypoferremia in order to attenuate Gram-positive and Gram-negative bacterial growth in murine models of sepsis.

1.4 Study Objectives

This study aimed to assess the impact of the novel iron chelator, DIBI, on microcirculation using three experimental models: LPS-induced cystitis, experimental toxemia and Colon Ascendens Stent Peritonitis (CASP).

First, a pilot study has been done to evaluate, how early systemic activation of the immune response starts in a murine model of local inflammation (LPS-induced cystitis). Leukocyte-endothelial interactions and capillary blood flow in the intestinal microcirculation has been studied using intravital microscopy, plasma cytokines levels were measured, and intestinal tissue damage was examined by H&E staining. The goal was to better understand sepsis and also to have an idea of how early a possible treatment targeting the hyper-activated immune response phase should start.

Second, the toxemia model was used to assess potential anti-inflammatory effects of the novel iron chelator, DIBI, on the immune response to systemic inflammation induced by Gram-positive and negative bacterial toxins on intestinal leukocyte-endothelial interactions and capillary blood flow using intravital microscopy, plasma cytokines analysis, and evaluation of intestinal tissue damage histologically.

The focus here being the immune response, the well-established murine model of toxin-induced systemic pro-inflammatory immune response has been used to assess immune hyperactivation. This model simulates a systemic inflammation due to the intravenous administration of bacterial components. DIBI showed some effect in previous experimental studies using E. coli LPS in the same murine model. Therefore, it was aimed to first confirm DIBI impact on E. coli toxin, then on other gram-negative toxins, and finally on different gram-positive toxins.

For the last experimental sepsis model, a clinically relevant model of poly-bacterial sepsis has been chosen. The CASP model is more clinically relevant than the toxemia model because CASP mimics the clinical course of human abdominal sepsis and also the pathophysiology due to the presence of living pathogens (gram-positive and negative) and their inflammatory mediators. Unlike the toxemia model, CASP allowed the assessment of the possible anti-microbial effect of DIBI. The goal here was to study the possible effect of DIBI on the immune response to CASP-induced abdominal sepsis, on intestinal leukocyte-endothelial interactions, intestinal capillary blood flow, and bacterial burden. DIBI's effect was assess using intravital microscopy, plasma cytokines analysis, evaluation of intestinal tissue damage histologically, and bacterial count in peritoneal lavage fluid and blood.

CHAPTER 2: MATERIALS AND METHODS

2.1 Animal Models and Ethics Statement

Female CD1 mice (used for LPS-induced cystitis model) and male C57BL/6 mice (used for endotoxemia and Colon Ascendens Stent Peritonitis model) were purchased from Charles River Laboratories International Inc. (Saint-Constant, QC, Canada). All mice were wild type, 8-10 weeks-old, 20 to 30g, housed in ventilated plastic cage racks in a pathogen free room (room tested for pathogens every 3 months) of the Carleton Animal Care Facility (CACF) in the Faculty of Medicine at Dalhousie University, Halifax, NS, Canada. Animals were kept on a 12-hour light/dark cycle in a 21°C room. Prior to the experiments, animals were acclimatized for 1 week in the CACF. Mice received a standard diet of rodent chow and filtered city water ad libitum.

All experimental procedures were approved by the University Committee on Laboratory Animals at Dalhousie University under protocols No. 17-070 and 18-057, and were performed following the guidelines and standards of the Canadian Council on Animal Care.

2.2 Bacterial Toxins

Toxins from different species of Gram-negative and -positive bacteria were purchased from Sigma-Aldrich (Oakville, ON, Canada) and used without further purification. Toxins were stored at 4° and prepared (diluted in 0.9% NaCl solution) as suggested by the supplier.

A Gram-negative endotoxin (lipopolysaccharide), from *Escherichia coli,* serotype O26:B6 (LPS_e) was used in cystitis and in toxemia experiments. *Klebsiella pneumoniae* (L4268) lipoplysaccharide (LPS_k), a separate Gram-negative toxin, was used in the toxemia model only. As Gram-positive toxins, lipoteichoic acid (LTA, L2515) and Peptidoglycan (PGN, 77140) from *Staphylococcus aureus* were used in the toxemia experimental model.

2.3 Experimental Models

2.3.1 LPS-Induced Cystitis

2.3.1.1 Anesthesia

The animal was weighed prior to anesthesia using a commercially available weighing scale. Induction of anesthesia was accomplished by first manually restraining the mouse, as per trained technique, followed by an intraperitoneal (i.p.) injection of sodium pentobarbital (90 mg/kg; 54 mg/ml; Ceva Sainte Animale, Montreal, QC, Canada) using 25 gauge 5/8 needles. The injection site was checked to ensure no bleeding and mouse was placed back in the cage on the heating pad until fully anesthetized. Continuous observation was done to ensure the animal had clear airways and was able to breathe. Depth of anesthesia was assessed by the pedal withdrawal reflex (any animals' response to toe pinch) every 15 minutes throughout the procedure. Additional diluted doses of pentobarbital sodium (9 mg/kg; 5.4mg/ml) were administered as needed.

2.3.1.2 Surgical procedure

Prior to the experiment, a 5cm catheter was made by placing non-radiopaque polyethylene tubing (PE10, Clay Adams, Sparks, MD, USA) over a 30-gauge needle. The catheter was tested for any obstructions or leakages by flushing a small amount of sterile saline (0.9% sodium chloride) and observing that no fluid leaked out. The catheter was then secured with waterproof glue. The fully anesthetized animal was moved from the cage to a clean heated surgical station, positioned and taped in supine position. A Vaseline-lubricated thermometer was then inserted rectally to continuously monitor the animal temperature (TCAT-2LV Controller; Physitemp Instruments Inc. New Jersey, USA). Supplementary oxygen was provided in cases of irregular breathing.

The abdominal skin of the animal was lifted up around the umbilical region and a small cut was made using straight scissors (Figure 5). To limit bleeding, the abdominal wall was cut following the linea alba (Figure 6). Afterwards, cotton tips wet with warm normal saline were used to expose the bladder. Any visible excess fat was not cut, but gently moved aside. The bladder was gently squeezed manually for emptying. After lubricating the urethral orifice with warm saline, the previously made catheter was smoothly inserted transurethrally by using two forceps (curved and straight forceps). Then, LPS was carefully instilled intravesically for 2 hours. To avoid backflow or leakage, the urethral opening was clamped with forceps. The catheter was retracted upon effective instillation. For comparative experiments with systemic inflammation, LPS was injected i.p.; while healthy controls received i.p. injection of normal saline.

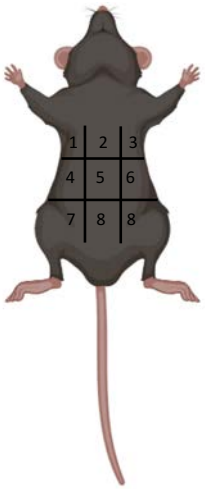

Figure 5 Abdominal regions.

1. Right hypochondriac region
2. Epigastric region
3. Left hypochondriac region
4. Right lumbar region
5. Umbilical region
6. Left lumbar region
7. Right iliac region
8. Hypogastric region
9. Left iliac region

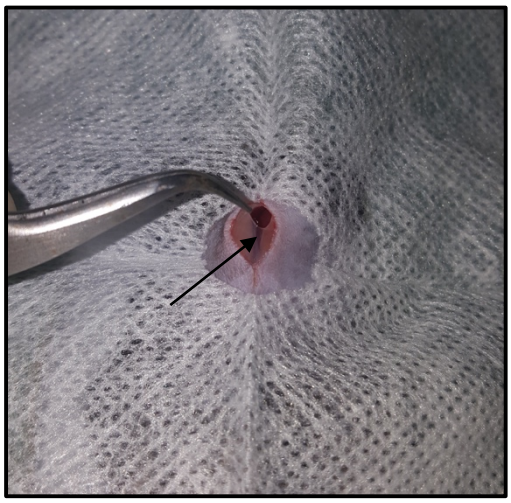

Figure 6 Opening of abdominal wall following the linea alba.
The black arrow identifies the linea alba, a “white” line in the middle of the abdomen mostly made of connective tissue and lacking of nerves and blood vessels.

2.3.1.3 Experimental Timeline

The induction of anesthesia marks the beginning of the cystitis protocol timeline (time T-45 min; Figure 7). Once a surgical plane of anesthesia is confirmed, a laparotomy was performed to confidently empty and catheterize the bladder. Cystitis was then induced by slow and gentle intravesical administration of 0.2 mg/kg LPS dissolved in sterile saline (0.1 mg/ml). LPS administration represents time = 0 min (T0) in the experimental timeline. The control group received vehicle (saline) intravesically instead of LPS. For systemic inflammation, either the same dose of LPS (0.2 mg/kg; 0.04 mg/ml), a standard high LPS dose to induce sepsis (5 mg/kg; 1mg/ml) or vehicle were injected intraperitoneally. The rationale for the timing and dosage of LPS was based on the literature (96, 97) and successful cystitis induction in previous experiments in the lab (unpublished data). Cystitis was carried out for 2 hours before IVM. Fluorescencent dyes, Fluorescein Isothiocyanate-Bovine Serum Albumin (FITC-BSA) and Rhodamine-6G, were administered intravenously (i.v.) via tail vein injection fifteen minutes prior to IVM procedures. At the end of the IVM, blood was collected by cardiac puncture and terminal neck dislocation was performed (T 160 min). Additionally, samples of the small intestine were collected. For cytokine measurements, plasma was separated from the blood samples (see section 2.5 for full details).

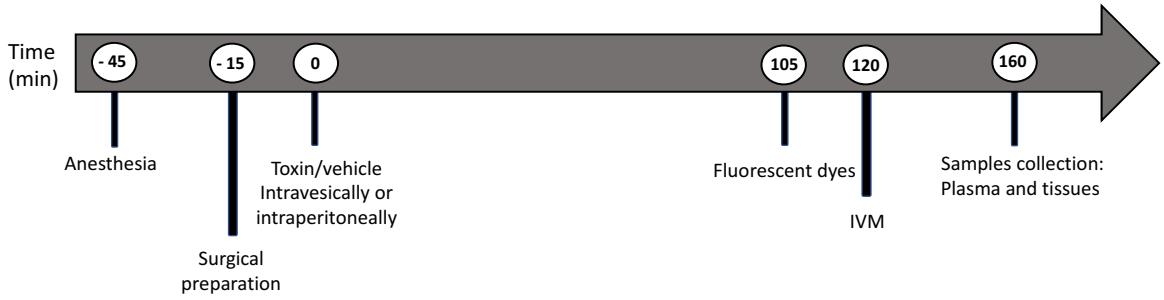

Figure 7 Experimental timeline for the LPS-induced cystitis model.

2.3.1.4 Experimental Groups

In the LPS-induced cystitis model, there were 5 experimental cohorts tested with 5-6 animals per group (Table 2). Group 1 (CON_B) represented a healthy control group where saline was administered intravesically into the bladder. Cystitis was induced by intravesical administration of LPS (0.2 mg/kg) in group 2 (LPS_B). Group 3 (CON_S), a healthy control group received i.p. injections of saline into the abdominal cavity; while group 4 ($LPS_{S\text{-}Low}$) represented the cohort in which systemic inflammation was induced by an i.p. administration of a low dose of LPS (0.2 mg/kg). Systemic inflammation (sepsis) was induced in the fifth and final group ($LPS_{S\text{-}High}$) by i.p. administration of a high dose of LPS (5 mg/kg).

Model	**Groups**	**Intervention**
LPS-INDUCED CYSTITIS	CON_B	Saline intravesically
	LPS_B	LPS (0.2 mg/kg) intravesically
	CON_S	Saline i.p.
	$LPS_{S\text{-}Low}$	LPS (0.2 mg/kg) i.p.
	$LPS_{S\text{-}High}$	LPS (5 mg/kg) i.p.

Table 2 Experimental groups for LPS-induced cystitis experiments.

2.3.2 Experimental Toxemia

2.3.2.1 Anesthesia

The animal was weighed prior to anesthesia using a commercially available weighing scale. Induction of anesthesia was accomplished by first manually restraining the mouse, as per trained technique, followed by an intraperitoneal (i.p.) injection of sodium pentobarbital (90 mg/kg; 54 mg/ml; Ceva Sainte Animale, Montreal, QC, Canada) using 25 gauge 5/8 needles. The injection site was checked to ensure no bleeding and mouse was placed back in the cage on the heating pad until fully anesthetized. Continuous observation was done to ensure the animal had clear airways and was able to breathe. Depth of anesthesia was assessed by the pedal withdrawal reflex (any animals' response to toe pinch) every 15 minutes throughout the procedure. Additional diluted doses of pentobarbital sodium (9 mg/kg; 5.4mg/ml) were administered as needed.

2.3.2.2 Surgical Procedures

Prior to theexperiment, a 5 cm catheter was made by placing non-radiopaque polyethylene tubing (PE10, Clay Adams, Sparks, MD, USA) over a 30-gauge needle. The catheter was tested for any obstructions or leakages by flushing a small amount of sterile saline (0.9% sodium chloride) and observing that no fluid leaked out. The catheter was then secured with waterproof glue. In addition, it was verified that all the tools and materials needed for the surgery were clean and ready to use. The fully anesthetized animal was moved from the cage to a clean heated surgical station, positioned and taped in supine position. A thermometer was lubricated with Vaseline then inserted rectally to continuously monitor the animal's internal body temperature (TCAT-2LV Controller; Physitemp Instruments Inc. New Jersey, USA).

The induction of toxemia was performed following a standard procedure previously described in the literature (98). The anterior region of the neck area was shaved and disinfected using isopropyl alcohol swabs. Prior to incision, a subcutaneous injection of 0.04 ml of lidocaine 1% (1 mg/ml) was administered to the incision area. A small incision was made using scissors on the right side of the neck. Underlying tissues were then dissected with curved hemostats until 5-10 mm of jugular vein was clearly visible and free of connective tissue, fat and muscle. Fine-tip forceps were placed underneath the well-exposed vein in order to position 2 pieces of silk thread. At the distal end of the vessel section, a surgical knot was made using one of the threads to tie off the vessel and avoid any bleeding. At the proximal end of the vessel, a loose knot was made using the other thread. A small incision was subsequently made using micro-dissecting scissors at the distal end of the vessel just below the surgical knot. A catheter was inserted roughly 1 cm into the vessel through the incision site. To secure the catheter, the proximal knot was tightened three times followed by an additional double knot tightened over the distal end of the vessel. Cannulation was successful when saline was injected through the catheter without leakage. The cannulation of the jugular vein allowed for intravenous administration of toxins, treatment drugs, fluorochromes, anesthetics and 0.9% NaCl depending on the group. Toxemia was carried out for 2 hours.

2.3.2.3 Experimental Timeline

The anesthesia induction marks the beginning of the toxemia protocol timeline (time T-45 min; Figure 8). After surgical preparation during which cannulation was performed in order to be able to administered intravenously the products, systemic inflammation was induced by slow and gentle administration of LPS dissolved in sterile saline (5 mg/kg; 1mg/ml). LPS administration represents time = 0 min (T0) in the experimental timeline. The treatment group received DIBI (10 mg/kg; 5mg/ml) 15 min after LPS induction; untreated animals received saline instead of DIBI. DIBI was provided by Chelation Partners Inc., Halifax, NS, Canada. The control group of this procedure received vehicle (saline) intravenously instead of LPS and/or DIBI. The rationale for the timing and dosage of LPS and DIBI was based on previous experiments in the lab (3).

Systemic inflammation was carried out for 2 hours before performing IVM. Fifteen minutes prior to IVM, fluorescent dyes, Fluorescein Isothiocyanate-Bovine Serum Albumin (FITC-BSA) and Rhodamine-6G were slowly administered i.v. through the jugular vein. At the end of the IVM procedure, blood was collected by cardiac puncture and terminal neck dislocation was performed (T160 min). In addition, samples of the small intestine were collected. For cytokine measurements, plasma was separated from the blood samples and frozen (see section 2.5 for an in-depth protocol).

Figure 8 Experimental timeline for the toxemia model.

2.3.2.4 Experimental Groups

Nine groups of animals (n = 5-10/group) were tested for this study (Table 3). Toxemia was induced by 5mg/kg of LPS_e, LPS_k, LTA or PGN. Treatment groups received 10 mg/kg DIBI (LPS_e+DIBI, LPS_k+DIBI, LTA+DIBI, PGN+DIBI). Control animals received vehicle (normal saline, 0.9% Sodium Chloride). Pilot experiments did not show any DIBI toxicity, therefore a DIBI only group (without toxins) was not included.

Model	Groups	Intervention
TOXEMIA	CON	Saline i.v.
	LPS_e	LPS_e (5mg/kg) + saline i.v.
	LPS_e + DIBI	LPS_e (5mg/kg) + DIBI (10mg/kg) i.v.
	LPS_k	LPS_k (5mg/kg) i.v. + saline i.v.
	LPS_k + DIBI	LPS_k (5 mg/kg) + saline i.v.
	LTA	LTA (5 mg/kg) + saline i.v.
	LTA + DIBI	LTA (5mg/kg) + DIBI (10mg/kg) i.v.
	PGN	PGN (5 mg/kg) + saline i.v.
	PGN + DIBI	PGN (5mg/kg) + DIBI (10mg/kg) i.v.

Table 3 Experimental groups for toxemia experiments.

2.3.3 Colon Ascendens Stent Peritonitis

2.3.3.1 Anesthesia

Anesthesia was induced by placing the mouse in an induction chamber with 4% isoflurane in oxygen (flow rate of 1 L/hour). When the animal was fully anesthetized (unresponsive to the toe pinch test), depth of anesthesia was maintained by providing a continuous flow of 1-2% isoflurane at an oxygen flow rate of 0.8 L/hour through a ventilation tube securely placed over the nose of the mouse. The animal then received a subcutaneous injection of buprenorphine (0.1 mg/kg, 0.03 mg/ml) as pre-emptive analgesia. Eye lubricant gel was also applied to prevent irritation and dryness of the eyes.

2.3.3.2 Surgical Procedures

Pre-surgery: Fully anesthetized animals were taped in a supine position on a heating pad. The abdominal area was shaved with an electric shaver and surgical scrub was performed. First, a cotton ball soaked with hibitane (chlorhexidine gluconate) was applied to the skin in a circular motion, starting at the incision site and working out toward the periphery. Second, isopropyl alcohol 70% solution and povidone-iodine were applied three times in the same manner as hibitane to further disinfect the mouse. The surgeon wore a clean lab coat, a surgical cap, a mask, and sterile gloves in accordance with Dalhousie University CACF guidelines.

Surgery: A sterile drape and a sterile gauze pad were placed on the animal with an opening over the incision area. This allowed access to the incision site while providing the surgeon with a sterile field. The abdominal skin of the animal was lifted up around the umbilical region and a midline skin incision was made using a No. 15 scalpel. The abdominal wall was cut following the linea alba to avoid bleeding. Afterwards, wet cotton tips were used to carefully expose the caecum, followed by the ascending colon in the abdominal cavity (Figure 9). Sterile saline was regularly applied on the intestine to keep it moist. At approximately 1 cm from the caecum, 5 mm of a 20G 1-1/4 transparent catheter (Jelco, Smiths Medical, Kent, UK) was inserted and fixed on the ascending colon by three knots of a blue 7/0, non-absorbable polypropylene monofilament (3304H, Pronova ETHICON® Silk Sutures, Johnson & Johnson, USA) (Figure 10). The intestine was gently squeezed using wet cotton tips to fill the catheter with fecal matter and ensure the stent was not obstructed. After that, the catheter was then cut to leave 2-3 mm of the tube projecting from the ascending colon. The ascending colon was then gently placed back in the abdominal cavity and the abdominal muscle layer sutured using a 5/0 non-absorbable polypropylene monofilament (7740G, Prolene ETHICON® Silk Sutures, Johnson & Johnson, USA). Treatment drugs or vehicle were administered i.p. post-surgical intervention. The abdominal skin layer was sutured using the same 5/0 non-absorbable polypropylene monofilament. Throughout the surgical procedure, the animal was closely monitored for anesthetic depth. SHAM surgery was carried out using the identical surgical procedures, however the stent was sutured on top of the outer-layer of the intestinal wall without perforation of the colon.

Post-operative care in a quiet room for recovery: at the end of the surgical procedure, the mouse was placed in a new clean cage with water and easy-to-chow mash ad libitum. The animal was then closely monitored until fully awake and mobile (5-15 min). Monitoring of the animal was performed every 2h for a total of 6h. The animal was then brought to the laboratory for the remaining experimental time.

Figure 9 Localization of ascending colon during CASP surgery.
The black arrow shows the caecum

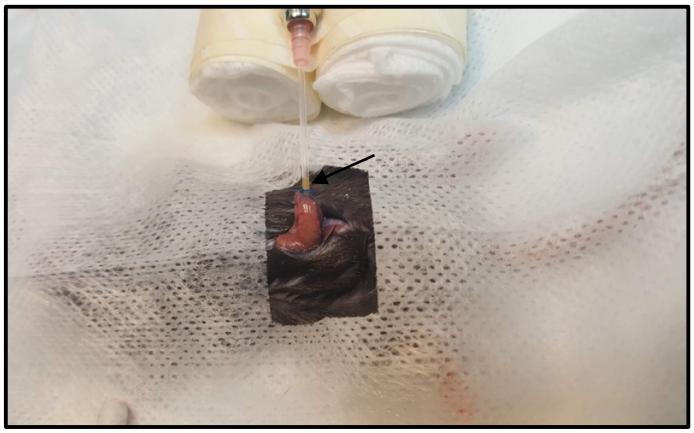

Figure 10 Stent placed and fixed in ascending colon during CASP surgery.
Stent is cut approximatively 5 mm above the sutured area. The black arrow shows fecal matter inside the stent.

2.3.3.3 Experimental Timeline

As per previous experiments, the CASP timeline was initiated by the animal's anesthesia induction (time t-0.5 hours). This was followed by the surgical procedure during which a stent is either inserted through the ascending colon or sutured on top of it (Figure 11). The treatment groups received intraperitoneal injection of 80 mg/kg DIBI and/or 25 mg/kg imipenem immediately following surgery, marked as T = 0h in the experimental timeline. "Healthy" surgical control (SHAM) and untreated CASP groups received the vehicle (saline) intraperitoneally instead of DIBI/imipenem. DIBI was provided by Chelation Partners Inc., Halifax, NS, Canada; and imipenem was purchased from Ranbaxy Pharmaceuticals Canada Inc., Mississauga, ON, Canada. The rationale for the timing and dosage of DIBI and imipenem was based on previous experiments in the lab (99). The observation time preceding IVM procedures was 8 hours.

Seven hours after treatment/vehicle administration, the animals were anesthetized again with diluted doses of pentobarbital sodium (9 mg/kg; 5.4 mg/ml) in preparation for IVM. Thirty minutes later (T=7.5h), the previously closed abdomen after the CASP surgery was re-opened and peritoneal lavage fluid (PLF) collected to assess bacterial counts and microbiome composition. This was done by administering 2 ml pre-warmed saline into the abdominal cavity; this saline solution was therefore mixed with the peritoneal content and about 1.6 ml of PLF was collected. After this procedure, fluorescence dyes, Fluorescein Isothiocyanate-Bovine Serum Albumin (FITC-BSA) and Rhodamine-6G, were slowly administered intravenously via tail vein injection. At the end of the IVM, blood was collected by cardiac puncture and terminal neck dislocation was performed (T=8.5h). In addition, samples of the small intestine were collected. For further cytokine measurements, plasma was separated from the blood samples and frozen (section 2.5).

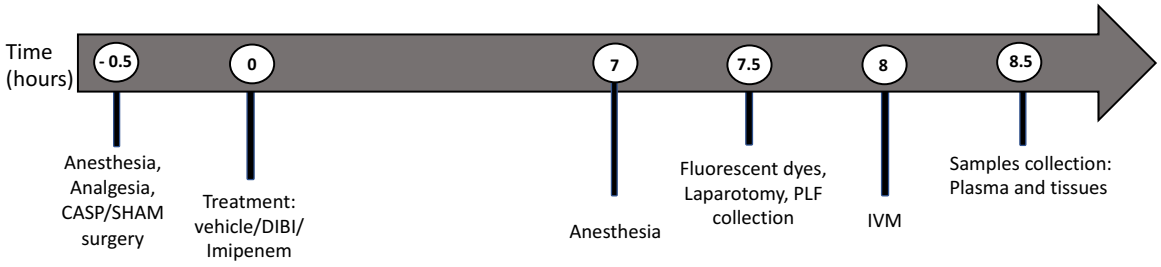

Figure 11 Experimental timeline of CASP model.

2.3.3.4 Experimental Groups

Five groups of animals (n = 5-12/group) were tested during this study (Table 4). Group 1 was the surgical control group (SHAM). Animals from this group underwent the same surgery as the CASP group, but the stent was placed on top of the ascending colon and did not perforate the intestine; therefore, mice did not have active leakage of feces into the peritoneum. Group 2 was untreated sepsis (CASP): mice underwent CASP surgical procedure and did not receive any treatment. They received saline instead. Group 3 was DIBI treated septic animals (CASP+DIBI): animals underwent CASP surgical procedure and received 80 mg/kg of DIBI i.p. Group 4 was septic animals treated with antibiotic (CASP+IMI): animals underwent CASP surgery and received 25 mg/kg of imipenem i.p. as treatment. Group 5 was septic animals treated with DIBI and imipenem (CASP+IMI+DIBI): animals underwent CASP surgical procedure and received both 80 mg/kg of DIBI i.p. and 25 mg/kg of imipenem. All treatments were administered immediately after CASP surgery at T=0h.

Model	Groups	Intervention
CASP	SHAM	SHAM + saline
	CASP	CASP (20 G) + saline i.p.
	CASP+DIBI	CASP (20 G) + DIBI 80 mg/kg i.p.
	CASP+IMI	CASP (20 G) + Imipenem 25mg/kg i.p.
	CASP+IMI+DIBI	CASP (20 G) + Imipenem 25mg/kg + DIBI 80 mg/kg i.p.

Table 4 Experimental groups for Colon Ascendens Stent Peritonitis (CASP) experiments.

2.4 Intravital Microscopy

2.4.1 Preparation Before Microscopy

IVM of the terminal ileum was performed on anesthetized mice, as previously described (98, 100–102), 2 hours post-cystitis and -toxemia induction, and 8 hours after CASP surgery. Briefly, 15 minutes after injection of fluorescence dyes (1.5 ml/kg 0.05% Rhodamine 6G used to stain leukocytes; 1 ml/kg 5% fluorescein isothiocyanate albumin used to observe capillary perfusion; Sigma-Aldrich, Oakville, ON, Canada), the mouse was positioned in left lateral position, with a loop of the terminal ileum exteriorized from the abdominal cavity and placed on a customized stage (100). The exposed loop of intestine was moisturized by a continuous flow of warm saline (37°C; 50 ml/hour) during the entire in vivo microscopic procedure to keep the intestine moist and to mimic physiological conditions. Isoproterenol (1:25000 dilution in 0.9% NaCl; Sandoz Canada Inc, Boucherville, QC, Canada) was given drop-wise as needed to reduce peristaltic movements of the intestine. A thin glass cover was placed over the intestine and the stage with the animal on top was positioned under the microscope for IVM (Figure 12).

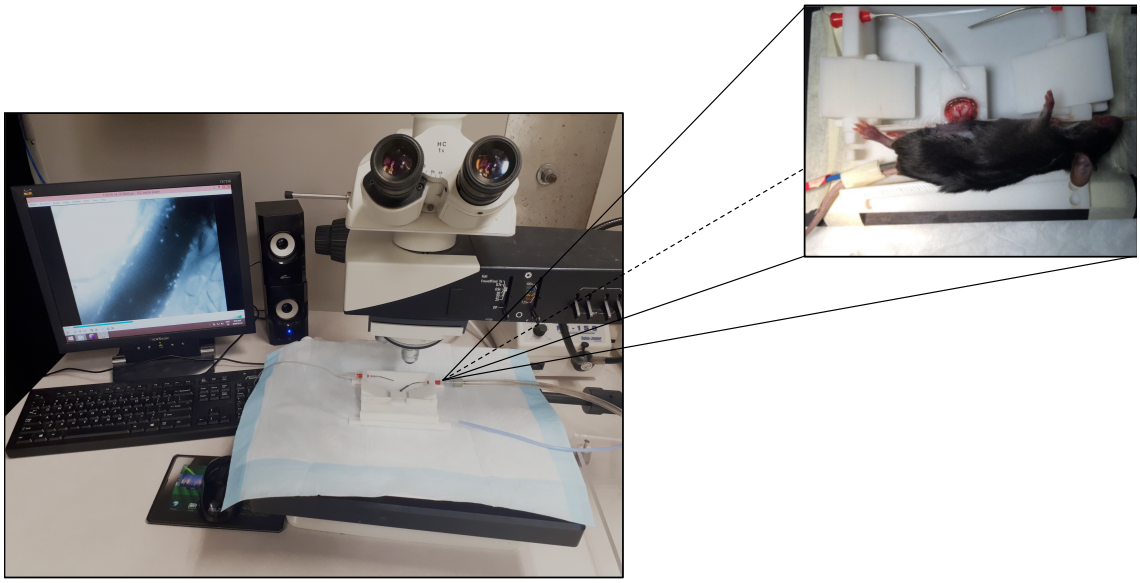

Figure 12 Animal set up for intravital microscopy.

2.4.2 Microscopy

In vivo imaging was performed using an epifluorescent microscope (Leica DMLM, Wetzlar, Germany) and a light source (LEJ EBQ 100; Carl Zeiss, Jena, Germany) allowing visualization of the intestinal microcirculation. Black and white videos were captured in real time using a CCD video camera (BC-71; AVT Horn, Aalen, Germany). The images were recorded using WinDV software (version 1.2.3, Czech Republic) and transferred to a Windows desktop computer.

Rhodamine-6G labeled leukocytes were visualized using a green light filter. Leukocyte adhesion was assessed in submucosal collecting venules (V1, diameter > 40 µm) and post capillary venules (V3, diameter < 40 µm). Six videos of V1 venules and six videos of V3 venules were recorded and analyzed offline. Capillary blood flow was evaluated in intestinal muscle and mucosa layers. Capillary perfusion was visualized using FITC-BSA as fluorescence dye and a blue light filter. Mucosal villi were exposed by opening part of the intestine using an electric cauterizer and micro-scissors.

2.4.3 Offline Videos Analysis

Video analysis was performed offline in a blinded manner using ImageJ software (Version 2.0.0-rc-69/1.52p, National Institute of Health, USA). Leukocyte adhesion (V1 and V3), muscle and mucosal capillary perfusion were the three parameters assessed per animal. Adherent leukocytes were defined as immobile leukocytes within a pre-defined vessel area for the duration of the recording (30 seconds) and quantified as number of cells/mm^2. To quantify capillary perfusion, all perfused capillaries in an area were added together to calculate the functional capillary density (FCD; in cm/cm^2) in the intestinal muscle and mucosal layers.

A **B**

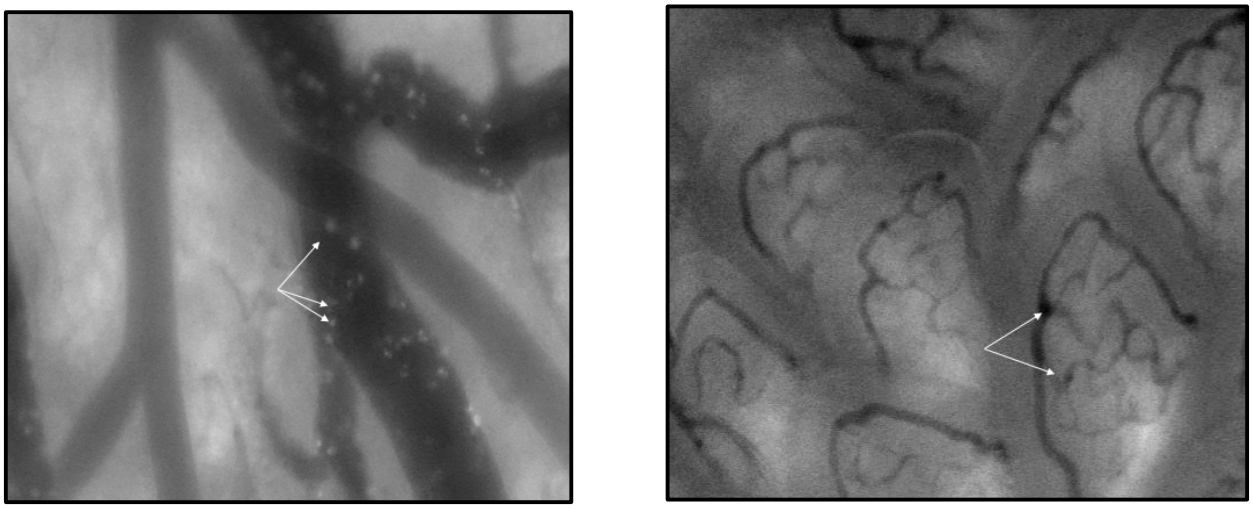

Figure 13 Screenshots of Intestinal intravital microscopy videos of leukocytes in submucosal collecting venules (A) and capillary blood flow of the mucosa layer(B).
The arrows indicate leukocytes in the vessels (A) and capillaries in the villi (B).

2.5 Blood and Tissue Collection Analysis

At the end of the IVM procedures, the chest cavity of the mouse was opened using straight scissors and the heart was exposed. A blood sample was collected using cardiac puncture (0.5 – 0.9 ml of whole blood) using a syringe connected to a 26G needle containing 20 µl of heparin as anti-coagulant (1000 USP units/ml; Sandoz Canada Inc. Boucherville, QC, Canada). Additionally, samples of the small intestine were collected and fixed in 10% neutral buffered formalin (EK Industries, Joliet, IL) for histological analysis. After the aforementioned procedures, cervical dislocation was performed to ensure euthanization of the animal.

2.5.1 Plasma cytokines and adhesion molecules measurements

Analysis was performed in Dr. Jean Marshall's lab (Department of Microbiology and Immunology, Dalhousie University). Whole blood samples taken by cardiac puncture were centrifuged at 3000 rpm for 10 minutes. Following centrifugation, plasma was placed in a 1 ml Eppendorf tube and stored in a -80°C freezer until analysis. Plasma levels of selected inflammatory cytokines and adhesion molecules were analyzed using a custom made 6-plex Mouse Magnetic bead-based multiplex assay obtained from Bio-Rad (Mississauga, ON, Canada). Bio-Plex instruments containing Bio-Plex software (Bio-Rad, Mississauga, ON, Canada) were used according to protocols provided by the manufacturer. The principle of these assays is similar to the sandwich ELISA. Six cytokines were chosen to be measured: TNF-α, IL-6, IL-10, IL-1β, soluble ICAM-1 (s ICAM-1) and P-selectin. Briefly, all plasma samples were thawed and prepared following the manufacturer's instructions. Samples were run in duplicate and prepared in three-fold dilutions using the Bio-Plex® sample diluent (50 µl of plasma mixed with 100 µl of diluent). Each diluted sample was added to a well of a flat-bottom 96 well plate. Standards were prepared in three-fold serial dilutions and added to the plate along with the samples.

First, 50 µl of detection antibody magnetic beads was added to each well and incubated for 2 hours in the dark on a shaker at 800 rpm and then washed (with buffer) 3 times using the Bio-Plex Pro wash station.

Second, 100 µl of biotinylated antibodies was added to each well, incubated in the dark for 1 hours, then washed 3 times to wash away any unbound substances and allow the antibodies to bind the analytes of interest. Thirdly, streptavidin-PE, which binds to the biotinylated antibody, is added to each well, incubated in the dark for 30 minutes and washed 3 additional times to remove any unbound substances. At this point, the complex is formed as follows: detection antibody magnetic bead + biomarker of interest + biotinylated antibodies + streptavidin-PE. Finally, the plate was read using the Bio-Rad 200 luminometer with Bio-Plex manager software. Analysis with the Bio-Rad machine uses two lasers: one to excite the dyes inside each magnetic bead and identify the bead region; another one to excite the PE to measure the amount of analyte bound to the beads.

2.5.2 Histology

Directly after euthanasia, samples from the small intestine not exposed during IVM were collected from the mice. The intestine was separated from the mesentery, quickly emptied of its contents (stool) by a gentle wash using saline solution and fixed in 10% phosphate-buffered formalin for 7 days. Samples were then stored in 70% ethanol prior to processing. The process continued with blinded histological preparation and staining (hematoxylin and eosin). Briefly, samples were embedded in paraffin using an automated tissue processor (Leica Microsystems Inc., Richmond Hill, ON, Canada). Embedded tissues were then sliced into 5 µm sections using a microtome (Jung AG, Heidelberg, Germany) and a tissue float water bath (Lipshaw MFG Co., Detroit, MI, USA). Tissue samples were dried for at least two days (56-76ºC) in an oven on glass microscope slides. Once dry, hematoxylin and eosin staining was performed. Slides were deparaffinized using sequential washes with xylene (3x), 100% ethanol (3x), 95% ethanol (2x) and 70% ethanol (2x) then put in a container with running tap water. Deparaffinized slides were then stained with filtered hematoxylin and eosin. Slides were rinsed under running tap water and assessed for color quality before moving to the following step.

Well stained slides were then dehydrated by sequential washes in 70% ethanol (2x), 95% ethanol (2x), 100% ethanol (2x) and xylene (3x). Each wash consisted of 20 dips. Cover slips were then mounted on slides using Cytoseal (Electron Microscopy Sciences, Fort Washington, PA, USA) and dried overnight. Finally, stained intestinal tissues on slides were examined in a blinded manner and the degree of histological injury assessed using a scoring system as described by Chiu et al. (103). Damage was scored from 0 to 5 (Table 5).

Score	Histopathological findings
0	Normal mucosal villi
1	Development of subepithelial space and capillary congestion at the apex
2	Extension of the subepithelial space with moderate lifting of the epithelial layer
3	Massive epithelial lifting with some denuded tips
4	Denuded villi with lamina propria and exposed dilated capillaries; increased cellularity of lamina propria
5	Digestion of lamina propria, hemorrhage and/or ulceration

Table 5 Assessment of intestinal damage histologically using Chiu score (103).

2.8 Bacterial Count

Seven hours after treatment/vehicle administration, the previously closed abdomen from animals that underwent the CASP intervention was re-opened and peritoneal lavage fluid was collected to assess bacterial burden. This was done by administering 2 ml of sterile pre-warmed saline into the abdominal cavity (peritoneum); this saline solution was therefore mixed with the peritoneum content and 1.5-1.8 ml of PLF and was collected using a sterile syringe. At the end of the IVM, 50 µl of the blood collected by cardiac puncture was saved for bacterial counts. Aseptic technique was used to maintain the integrity of all bacterial data during the following steps. As samples were obtained, serial dilutions began. The bacterial suspension was mixed for a minimum of 10 seconds between all steps to ensure even mixing.

Next, 50 µl of PLF or blood was transferred to the first tube containing 450 µl of Phosphate-Buffered Saline to make a 1:10 dilution. The transfer was repeated from tube 1 to tube 2, and then each subsequent tube until a 1:100000 dilution was achieved (tube 5). A new tip was used between each transfer. Each dilution of PLF or blood was then plated out using a triplicate spot method. Two sets of Tryptic Soy Agar plates (TSA; Millipore Sigma, Etobicoke, Ontario, Canada) and two sets of MacConkey plates (Millipore Sigma, Etobicoke, Ontario, Canada) were prepared (Figure 14). One set of TSA and MacConkey plates were incubated at 37ºC under aerobic conditions. The other set of TSA and MacConkey were incubated using a jar and GasPak (BD®, Franklin Lakes, NJ, USA) under anaerobic conditions. The plates were then enumerated after 16-24h hours to determine the number of colony-forming units (CFU) per milliliter. A row of spots was only enumerated if distinct colonies could be observed. Calculations were based on the mean value obtained from the triplicate spots and the dilution factor:

$$\text{CFU/ml}=\frac{\#colonies \times dilution}{0.02ml}$$

The rationale for the timing, the dilution of samples (PLF and blood), and the appropriate range of spots selected, were based on pilot experiments.

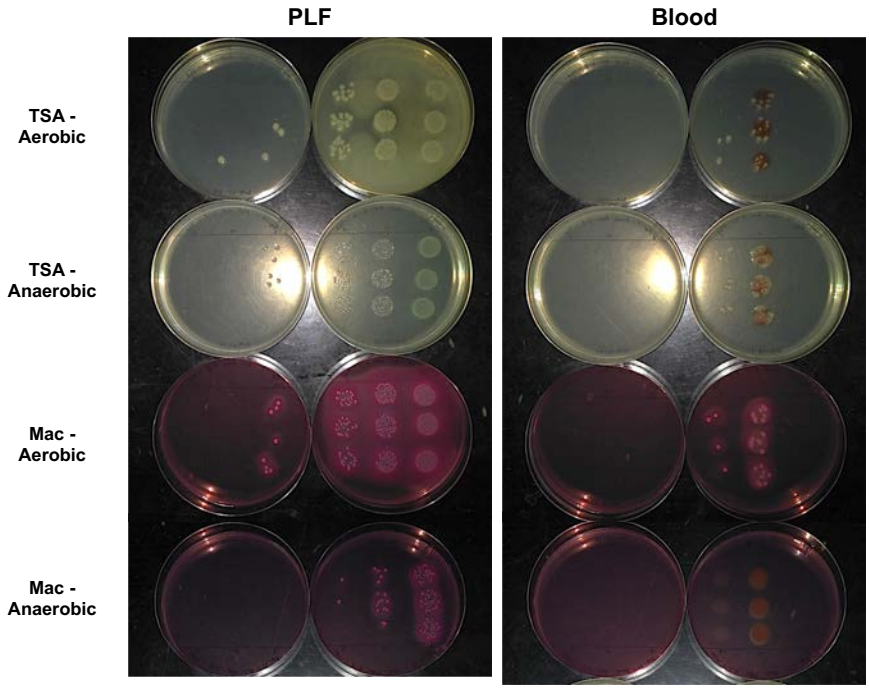

Figure 14 Prepared sets of tryptic soy agar plates (TSA) and MacConkey (Mac) plates in the CASP model
Triplicate spots of 10-fold dilutions 16-24h after plating to allow count of Colony Forming Unit bacteria. Samples are from a CASP group animal

2.10 Statistical analysis

All data were analyzed using the software Prism 8 version 8.2.0 272 (GraphPad Software, La Jolla, CA, USA) and expressed as mean ± standard error of mean (SEM). The Kolmogorov-Smirnov Test was used to confirm normal distribution of data. Pairwise comparisons were performed using Student's t-test. One-way ANOVA followed by Newman Keuls' test for multiple comparison was used to analyze normally distributed data for 3 or more groups. When the distribution was not normal, Kruskal-Wallis test was used. We considered differences at $P<0.05$ statistically significant.

CHAPTER 3: RESULTS

3.1 LPS-Induced Cystitis

The systemic immune response was evaluated by intestinal IVM, measurement of inflammatory cytokines levels in plasma, and histological analysis of morphological intestinal tissue damage using H&E staining.

3.1.1 IVM

3.1.1.1 Leukocyte Adhesion

The control groups showed low levels of leukocyte adhesion and no significant difference was observed between all control groups ($P>0.05$). Two hours following LPS administration into the bladder (LPS_B) or systemically ($LPS_{S\text{-}low}$, $LPS_{S\text{-}high}$), leukocyte adhesion increased significantly ($P<0.05$) compared to their respective control groups. Furthermore, systemically administered LPS ($LPS_{S\text{-}low}$ and $LPS_{S\text{-}high}$) induced similar increases in leukocyte adhesion ($P>0.05$) in both the collecting and post-capillary venules of the intestinal submucosa despite the high LPS dose being twenty times higher than the low dose (5mg/kg vs 0.2 mg/kg) (figure 15 and 16).

There was no significant difference in terms of leukocyte adhesion between the low, the high and the intravesical LPS groups (figure 16A) in the collecting venules two hours after LPS challenge. In the post-capillary venules, mice that received LPS into the bladder had a significantly lower number of adhering leukocytes compared to the groups that received LPS intraperitoneally ($LPS_{S\text{-}low}$ and $LPS_{S\text{-}high}$) ($P<0.05$) (figure 16B).

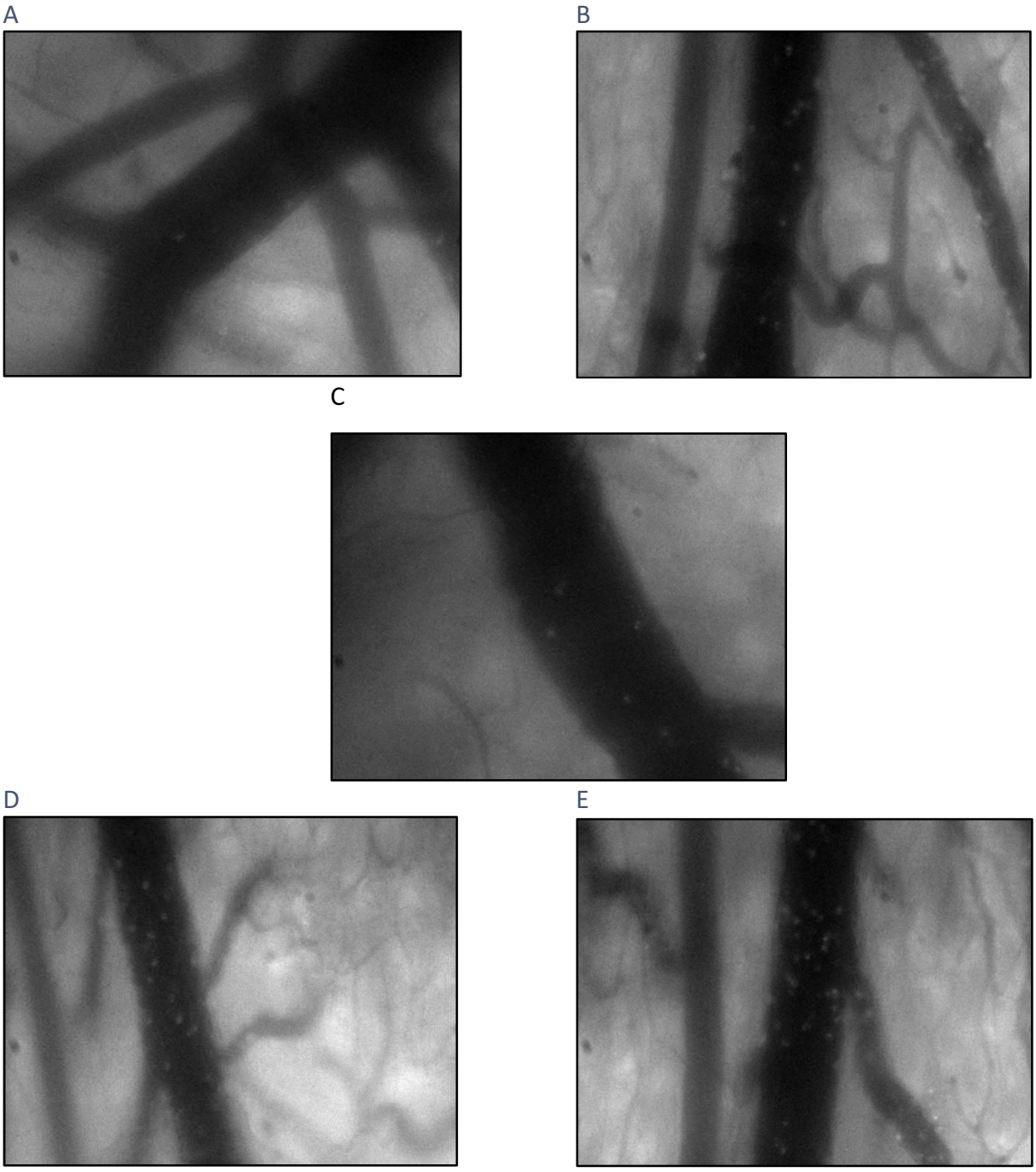

Figure 15 Pictures from IVM videos representing the effects of LPS-induced cystitis and systemic inflammation on leukocyte adhesion in intestinal submucosal collecting venules.
The white spots represent leukocytes. The LPS_B group (B) represents mice that received 0.2 mg/kg of LPS in the bladder and CON_B is the matching control group (A). $LPS_{S\text{-}low}$ (D)and $LPS_{S\text{-}high}$ (E)groups represent mice that received 0.2 mg/kg or 5 mg/kg LPS intraperitoneally, respectively, and CON_S is their matching control group (C).

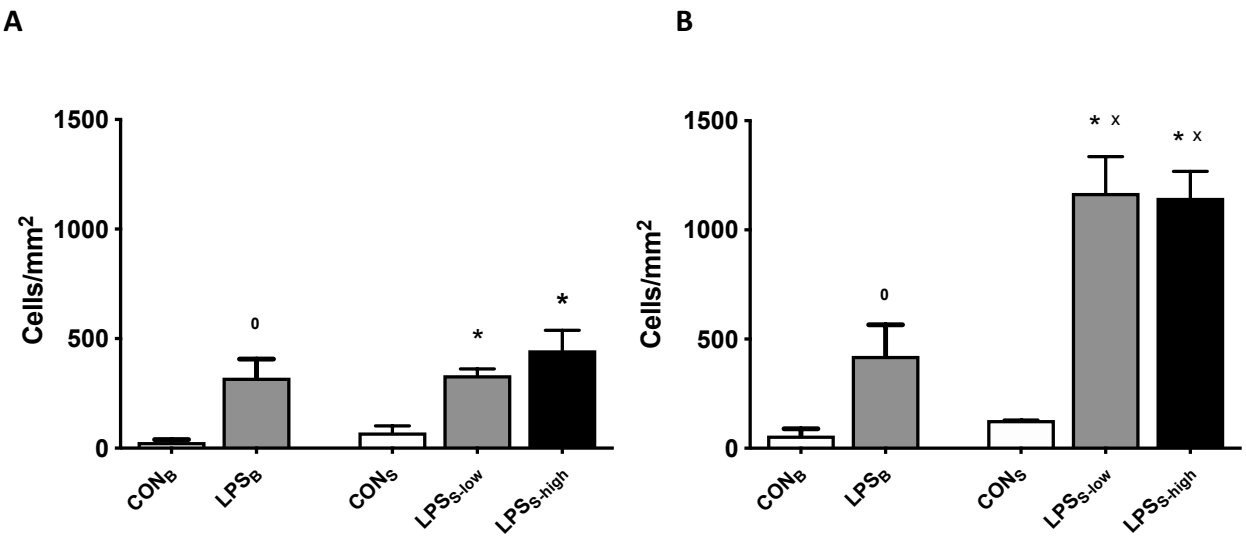

Figure 16 Effects of LPS-induced cystitis and systemic inflammation on leukocyte adhesion in intestinal submucosal collecting (A) and postcapillary (B) venules (cells/mm^2)

Each bar graph represents mean values ± SEM (n = 3-6 per group). The white bars represent control groups, the gray bars represent administration of 0.2 mg/kg LPS, and black bars represent administration of 5 mg/kg LPS. The LPS_B group represents mice that received 0.2 mg/kg of LPS in the bladder and CON_B is the matching control group. $LPS_{S\text{-}low}$ and $LPS_{S\text{-}high}$ groups represent mice that received 0.2 mg/kg or 5 mg/kg LPS intraperitoneally, respectively, and CON_S is their matching control group. ^{0} $P<0.05$ compared to CON_B group; * $P<0.05$ compared to CON_S group; x $P<0.05$ compared to LPS_B group. CON=control; LPS= lipopolysaccharide.

3.1.1.2 Capillary Perfusion

The FCD of the intestinal muscle and mucosa layers were unchanged two hours after low dose LPS administration into the bladder (LPS_B) or systemic low dose LPS administration ($LPS_{S\text{-}low}$). In the muscle layer, only the challenge with 5mg/kg LPS intraperitoneally decreased the FCD significantly ($P<0.05$) compared to the control group and the low LPS dose in the bladder and systemically (LPS_B and $LPS_{S\text{-}low}$) (figure 18A). This effect was not completely present in the mucosa layer. The only significant difference in that layer was between the high 5mg/kg LPS administered intraperitoneally ($LPS_{S\text{-}high}$) and its matching control CON_s ($P<0.05$) (figure 18B). The high LPS dose seems to have reduced FCD of the mucosa layer comparing to the lower doses (LPS_B, $LPS_{S\text{-}low}$), but that difference was not statistically significant ($P>0.05$).

A

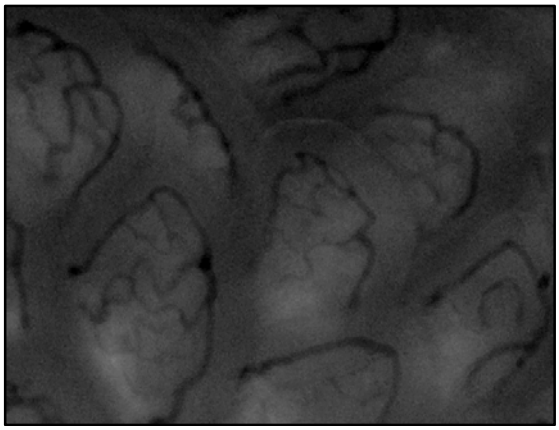

B

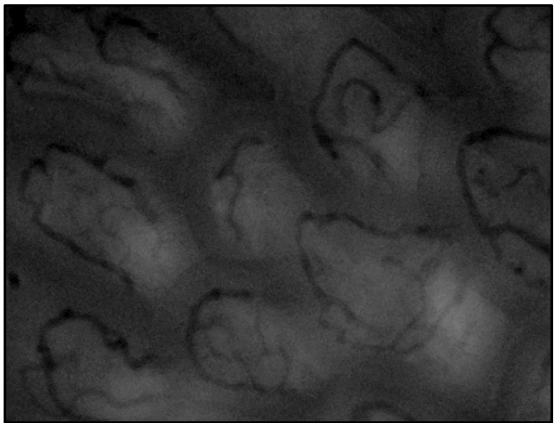

C

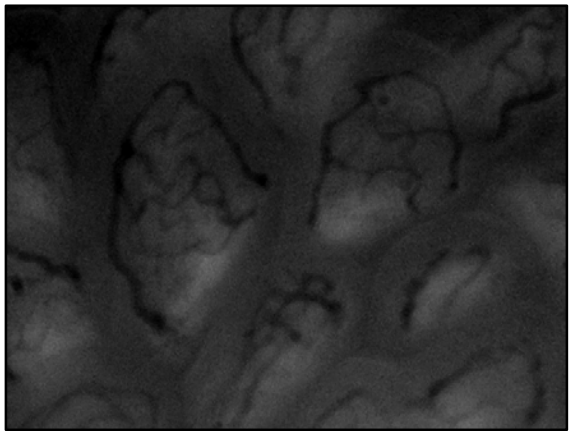

D

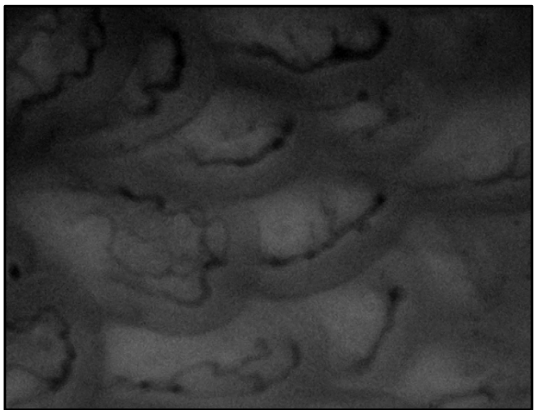

E

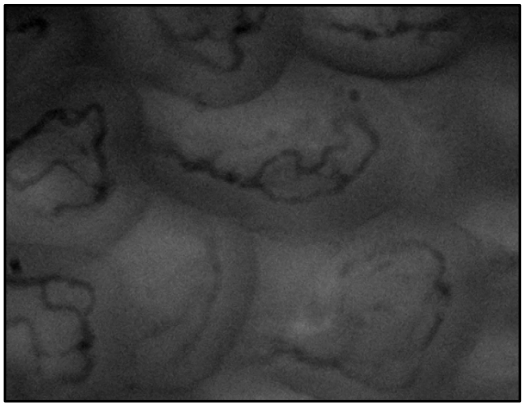

Figure 17 Pictures from IVM videos representing the effects of LPS-induced cystitis and systemic inflammation on leukocyte adhesion in intestinal mucosa layer.

The LPS_B group (B) represents mice that received 0.2 mg/kg of LPS in the bladder and CON_B is the matching control group (A). $LPS_{S\text{-}low}$ (D)and $LPS_{S\text{-}high}$ (E)groups represent mice that received 0.2 mg/kg or 5 mg/kg LPS intraperitoneally, respectively, and CON_S is their matching control group (C).

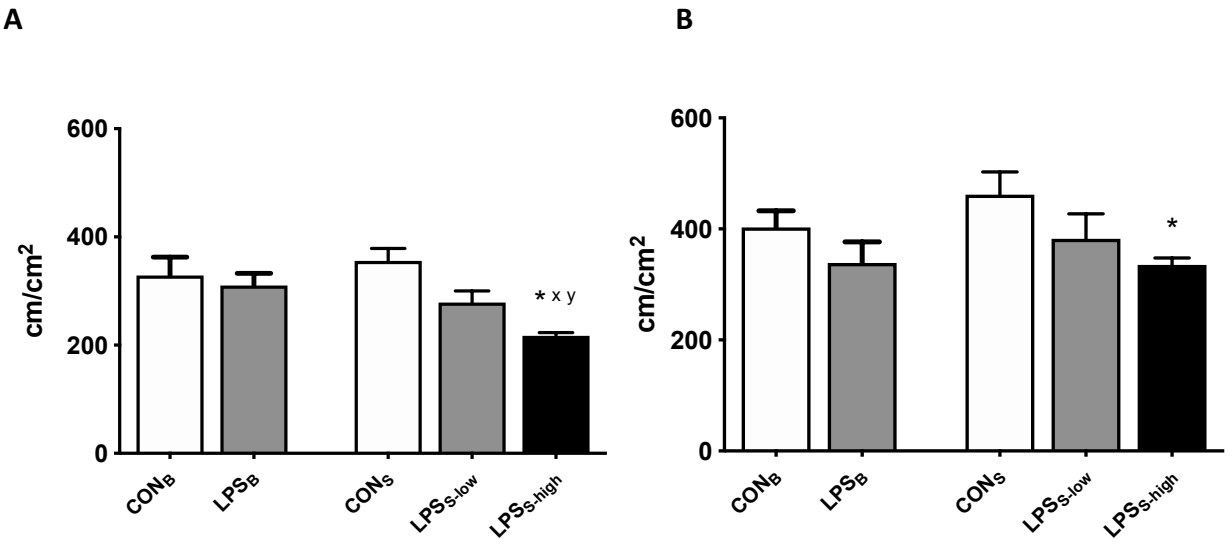

Figure 18 Effects of LPS-induced cystitis and systemic inflammation on intestinal FCD in the muscle (A) and mucosa (B) layers (cm/cm^2).

Each bar graph represents mean values ± SEM (n = 3-6 per group). The white bars represent control groups, the gray bars represent administration of 0.2 mg/kg LPS, and black bars represent administration of 5 mg/kg LPS. LPS_B group represents mice that received 0.2 mg/kg of LPS in the bladder and CON_B is the matching control group. $LPS_{S\text{-}low}$ and $LPS_{S\text{-}high}$ groups represent mice that received 0.2 mg/kg or 5 mg/kg LPS intraperitoneally, respectively, and CON_S is their matching control group. *P<0.05 compared to CON_S; x P<0.05 compared to LPS_B group; y P<0.05 compared to $LPS_{S\text{-}Low}$ group. CON=control; LPS= lipopolysaccharide.

3.1.2 Cytokines

3.1.2.1 Tumor Necrosis Factor-Alpha

Three hours after LPS bladder instillation (LPS_B) or systemic LPS challenge ($LPS_{S\text{-}low}$ and $LPS_{S\text{-}high}$) there was a significant increase of TNF-α plasma levels compared to the matching control groups (Figure 19). LPS instillation in the bladder (LPS_B) induced similar levels of plasma TNF-α compared to the same dose administered systemically ($LPS_{S\text{-}low}$). Animals that received the high systemic dose of LPS had significantly higher levels of TNF-α in the plasma ($P<0.05$) than those receiving the low dose.

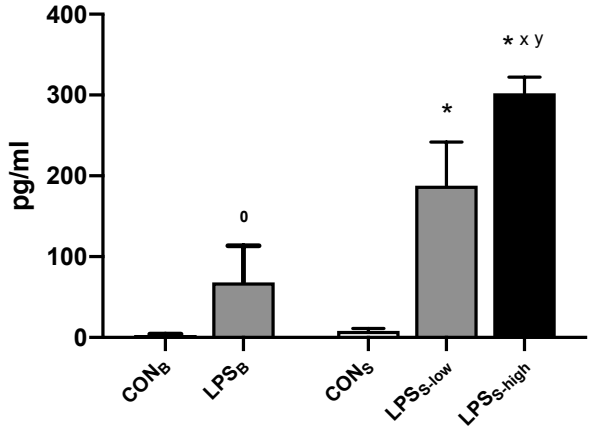

Figure 19 Effects of LPS-induced cystitis and systemic inflammation on TNF-α plasma levels (pg/ml).

TNF-α plasma levels three hours after challenge with LPS from *E. coli*. Each bar of the graph represents mean values ± SEM (n = 3-6 per group). The white bars represent control groups, the gray bars represent administration of 0.2 mg/kg LPS, and black bar represents administration of 5 mg/kg LPS. LPS_B group represents mice that received 0.2 mg/kg of LPS in the bladder and CON_B is the matching control group. $LPS_{S\text{-}low}$ and $LPS_{S\text{-}high}$ groups represent mice that received 0.2 mg/kg or 5 mg/kg LPS intraperitoneally, respectively, and CON_S is their matching control group. ^{0} $P<0.05$ compared to CON_B group; * $P<0.05$ compared to CON_S group; x $P<0.05$ compared to LPS_B group; y $P<0.05$ compared to $LPS_{S\text{-}Low}$ group. CON=control; LPS= lipopolysaccharide.

3.1.2.2 Interleukin-6

Plasma levels of IL-6 were significantly increased in groups receiving three hours post-LPS instillation into the bladder (LPS_B) and the high systemic LPS dose ($LPS_{S\text{-}high}$) compared to their matching control groups (Figure 20). The low systemic LPS dose ($LPS_{S\text{-}low}$) did not significantly increase plasma IL-6 levels compared to the control group. For animals that received the high LPS dose systemically, plasma IL-6 levels were significantly higher ($P<0.05$) compared to those receiving the low doses.

3.1.2.3 Interleukin-10

LPS instillation into the bladder (LPS_B) and systemic delivery of LPS ($LPS_{S\text{-}low}$ and $LPS_{S\text{-}high}$) induced a significant rise in IL-10 plasma levels compared to their matching control groups (Figure 21) three hours post-challenge. LPS instillation in the bladder (LPS_B) induced similar levels of plasma IL-10 compared to the same dose administered systemically ($LPS_{S\text{-}low}$). Animals that received the systemic high LPS dose had significantly higher ($P<0.05$) plasma IL-10 levels compared to those receiving the low doses of LPS.

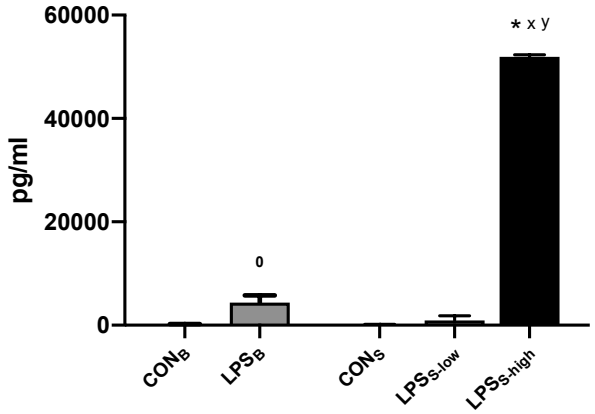

Figure 20 Effects of LPS-induced cystitis and systemic inflammation on IL-6 plasma levels (pg/ml). IL-6 plasma levels three hours after challenge with LPS from *E. coli*. Each bar graph represents mean values ± SEM (n = 3-6 per group). The white bars represent control groups, the gray bars represent administration of 0.2 mg/kg LPS, and black bar represents administration of 5 mg/kg LPS. LPS_B group represents mice that received 0.2 mg/kg of LPS in the bladder and CON_B is the matching control group. $LPS_{S\text{-}low}$ and $LPS_{S\text{-}high}$ groups represent mice that received 0.2 mg/kg or 5 mg/kg LPS intraperitoneally, respectively, and CON_S is their matching control group. ^{0} P<0.05 compared to CON_B group; * P<0.05 compared to CON_S group; x P<0.05 compared to LPS_B group; y P<0.05 compared to $LPS_{S\text{-}Low}$ group. CON=control; LPS= lipopolysaccharide.

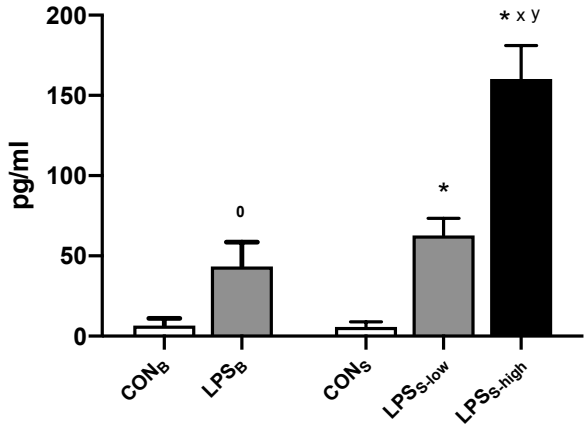

Figure 21 Effects of LPS-induced cystitis and systemic inflammation on IL-10 plasma levels (pg/ml).

IL-10 plasma levels three hours after challenge with LPS from *E. coli*. Each bar graph represents mean values ± SEM (n = 3-6 per group). The white bars represent control groups, the gray bars represent administration of 0.2 mg/kg LPS, and black bar represents administration of 5 mg/kg LPS. LPS_B group represents mice that received 0.2 mg/kg of LPS in the bladder and CON_B is the matching control group. $LPS_{S\text{-}low}$ and $LPS_{S\text{-}high}$ groups represent mice that received 0.2 mg/kg or 5 mg/kg LPS intraperitoneally, respectively, and CON_S is their matching control group. ^{0} P<0.05 compared to CON_B group. ^{0} P<0.05 compared to CON_B group; * P<0.05 compared to CON_S group; x P<0.05 compared to LPS_B group; y P<0.05 compared to $LPS_{S\text{-}Low}$ group. CON=control; LPS= lipopolysaccharide.

3.1.2.4 Interleukin-1 beta

After two hours LPS instillation into the bladder (LPS_B) and the same dose administered systemically ($LPS_{S\text{-}low}$) did not have a significant impact on IL-1β plasma levels compared to their matching control groups (Figure 22). Only animals that received the high LPS dose systemically showed significantly higher IL-1β plasma levels ($P<0.05$) compared to the matching control group and to those receiving the low LPS dose.

3.1.2.5 Soluble Intercellular Adhesion Molecule-1

LPS instillation into the bladder (LPS_B) did not have a significant impact on sICAM-1 plasma levels compared to its control (CON_B) (Figure 23). Only animals that received the systemic LPS delivery had a significantly higher ICAM-1 plasma levels ($P<0.05$) compared to the control (CON_S). There was no significant difference between the two systemic doses of LPS doses even though $LPS_{S\text{-}high}$ group received 20 times more LPS than the low dose LPS group (0.2 mg/kg vs 5 mg/kg).

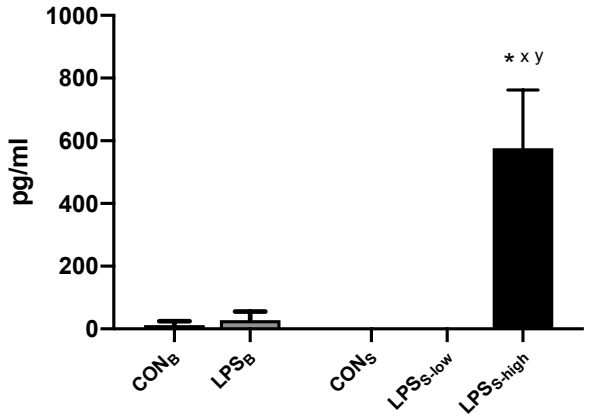

Figure 22 Effects of LPS-induced cystitis and systemic inflammation on IL- 1β plasma levels (pg/ml).

IL-1β plasma levels three hours after challenge with LPS from *E. coli*. Each bar graph represents mean values ± SEM (n = 3-6 per group). The white bars represent control groups, the gray bars represent administration of 0.2 mg/kg LPS, and black bar represents administration of 5 mg/kg LPS. LPS_B group represents mice that received 0.2 mg/kg of LPS in the bladder and CON_B is the matching control group. $LPS_{S\text{-}low}$ and $LPS_{S\text{-}high}$ groups represent mice that received 0.2 mg/kg or 5 mg/kg LPS intraperitoneally, respectively, and CON_S is their matching control group. ^{0} P<0.05 compared to CON_B group. ^{0} P<0.05 compared to CON_B group; * P<0.05 compared to CON_S group; x P<0.05 compared to LPS_B group; y P<0.05 compared to $LPS_{S\text{-}Low}$ group. CON=control; LPS= lipopolysaccharide.

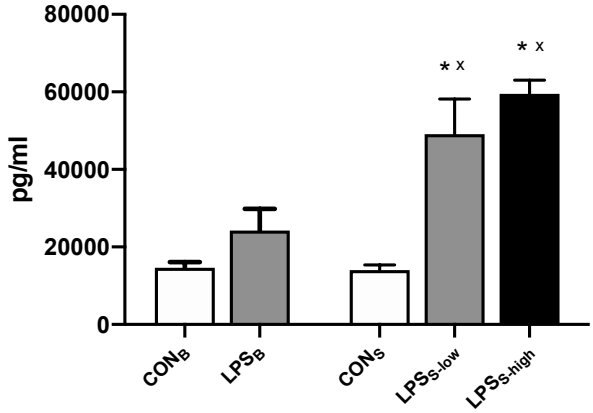

Figure 23 Effects of LPS-induced cystitis and systemic inflammation on sICAM-1 plasma levels (pg/ml).

sICAM-1 plasma levels three hours after challenge with LPS from *E. coli*. Each bar graph represents mean values ± SEM (n = 3-6 per group). The white bars represent control groups, the gray bars represent administration of 0.2 mg/kg LPS, and black bar represents administration of 5 mg/kg LPS. LPS_B group represents mice that received 0.2 mg/kg of LPS in the bladder and CON_B is the matching control group. $LPS_{S\text{-}low}$ and $LPS_{S\text{-}high}$ groups represent mice that received 0.2 mg/kg or 5 mg/kg LPS intraperitoneally, respectively, and CON_S is their matching control group. ^{0} P<0.05 compared to CON_B group. * P<0.05 compared to CON_S group; x P<0.05 compared to LPS_B group. CON=control; LPS= lipopolysaccharide.

3.1.3 Histology

Instillation of LPS for the duration of three hours into the bladder (LPS_B) or the same LPS dose administered systemically ($LPS_{S\text{-}low}$) did not have a morphological impact on intestinal tissue (Figure 25). Only animals that received systemic delivery of the high LPS dose showed significant intestinal damage ($P<0.05$) when compared to their respective control and those receiving the lower LPS doses (increase from grade 0 to grade 2 on the Chiu score).

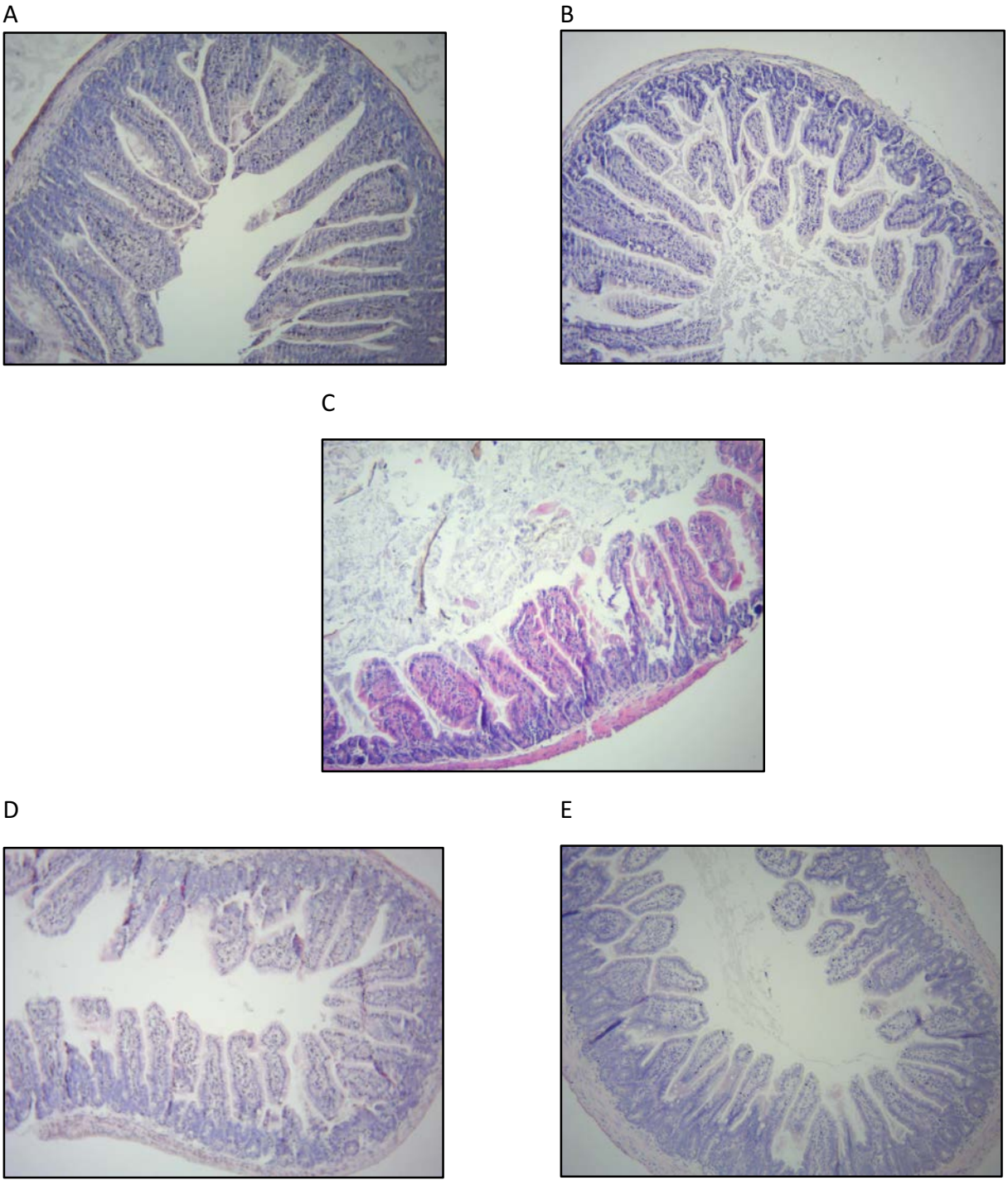

Figure 24 Effects of LPS-induced cystitis and systemic inflammation on intestinal tissue
H&E staining of cross-sectional samples from the terminal ileum under 40X magnification. A. CON_B; B. LPS_B; C. CON_S; D. $LPS_{S\text{-}low}$; E. $LPS_{S\text{-}high}$

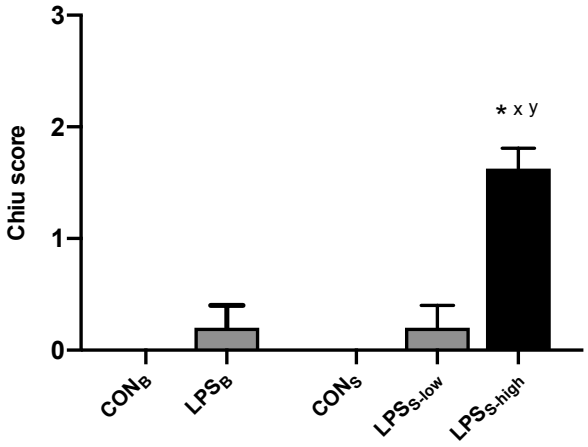

Figure 25 Effects of LPS-induced cystitis and systemic inflammation on intestinal tissue (Chiu score (103).

Each bar graphs represents mean values ± SEM (n = 3-6 per group). The white bars represent control groups, the gray bars represent administration of 0.2 mg/kg LPS, and black bar represents administration of 5 mg/kg LPS. The LPS_B group represents mice that received 0.2 mg/kg of LPS in the bladder and CON_B is the matching control group. $LPS_{S\text{-}low}$ and $LPS_{S\text{-}high}$ groups represent mice that received 0.2 mg/kg or 5 mg/kg LPS intraperitoneally, respectively, and CON_S is their matching control group. ^{0} $P<0.05$ compared to CON_B group. * $P<0.05$ compared to CON_S group; x $P<0.05$ compared to LPS_B group; y $P<0.05$ compared to $LPS_{S\text{-}Low}$ group. CON=control; LPS= lipopolysaccharide.

3.2 Experimental Toxemia

3.2.1 IVM

3.2.1.1 Leukocyte Adhesion

All toxins induced inflammation as shown by the significant increase in leukocyte adhesion ($P<0.05$) in both collecting and post-capillary venules two hours after toxin-challenge.

In collecting venules, the administration of 10 mg/kg DIBI significantly reduced ($P<0.05$) leukocyte adhesion for all four toxins (LPS_e, LPS_k, LTA, and PGN), but not back to control levels (figure 27). When comparing Gram-negative toxins data together in collecting venules, it was noticed that 5 mg/kg LPS from *E. coli* ($LPS_{e)}$ induced a significantly higher number of adhering leukocytes than the same dose of LPS from *K. pneumoniae* ($LPS_{k)}$ (figure 27A). Such difference was not seen with the Gram-positive toxins from *S. aureus*. Even though the LTA-induced adhesion of leukocyte seems higher than PGN-induced leukocyte adhesion, this difference was not statistically significant ($P>0.05$) (figure 27B)

As in the collecting venules, 10 mg/kg DIBI significantly reduced ($P<0.05$) leukocyte adhesion for all four toxins (LPS_e, LPS_k, LTA, and PGN) in post-capillary venules (figure 28). Similarly, the reduced level of adhesion by DIBI remained significantly higher than the controls ($p<0.05$) except for LPS from *K. pneumoniae* (LPS_k+DIBI) (figure 28A). When comparing Gram-negative toxins data together in post-capillary venules, it was observed that LPS from *E. coli* ($LPS_{e)}$ induced a significantly higher number of adhering leukocytes than LPS from *K. pneumoniae* ($LPS_{k)}$ (figure 28A). The same difference was seen when comparing Gram-positive toxins from *S. aureus*. LTA induced significantly more adhesion of leukocytes than PGN ($P<0.05$) (figure 28B)

A

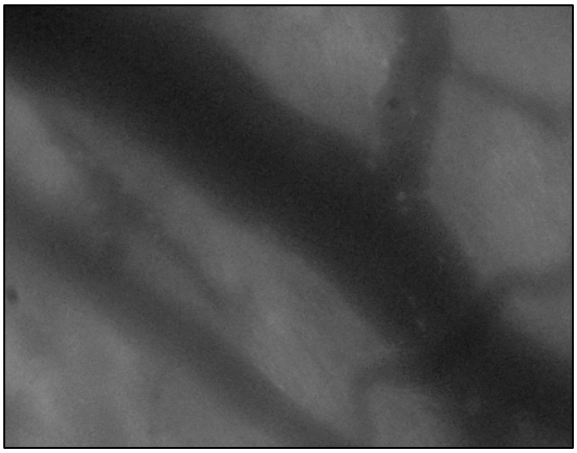

B

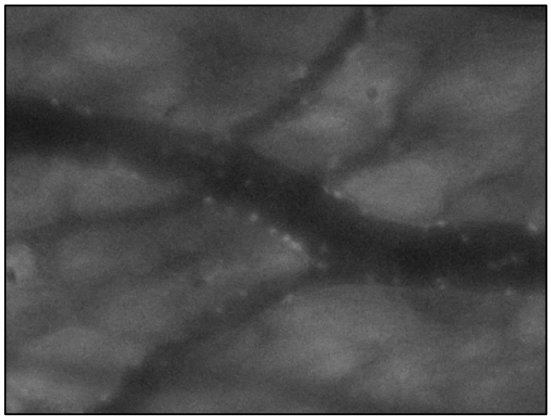

C

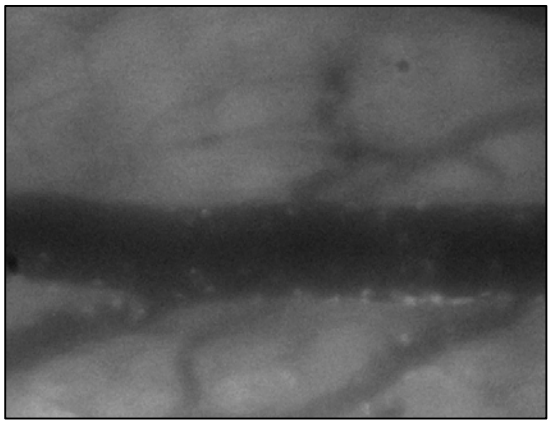

D

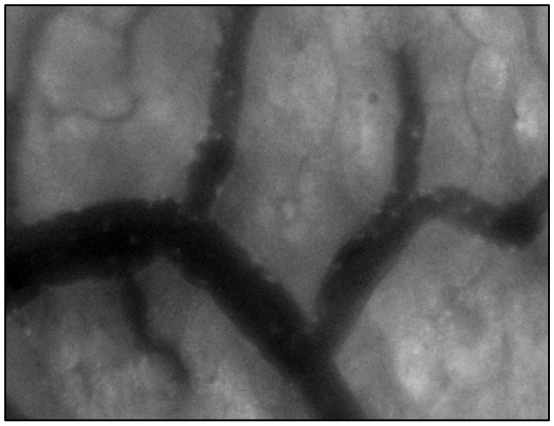

E

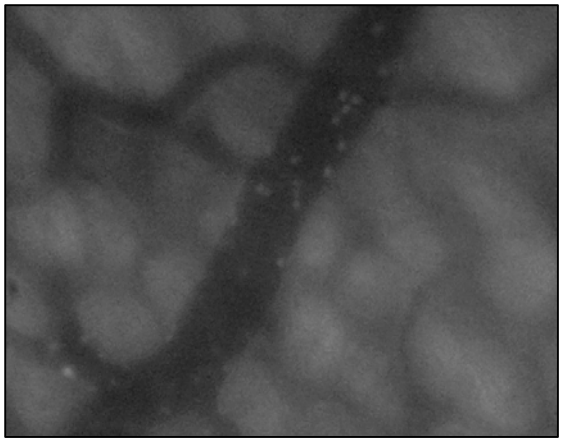

F

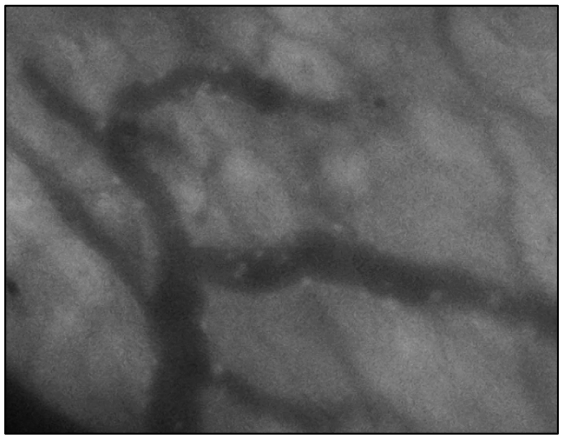

G

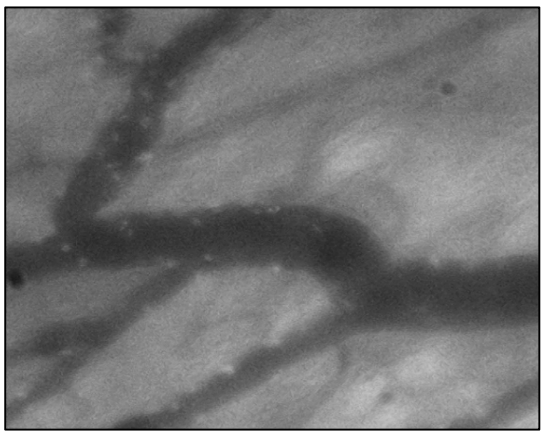

H

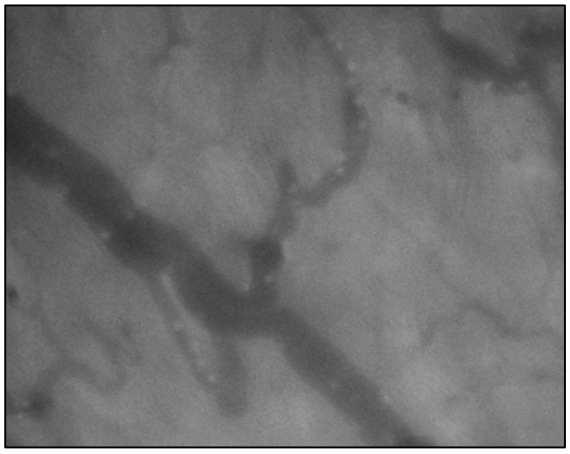

I

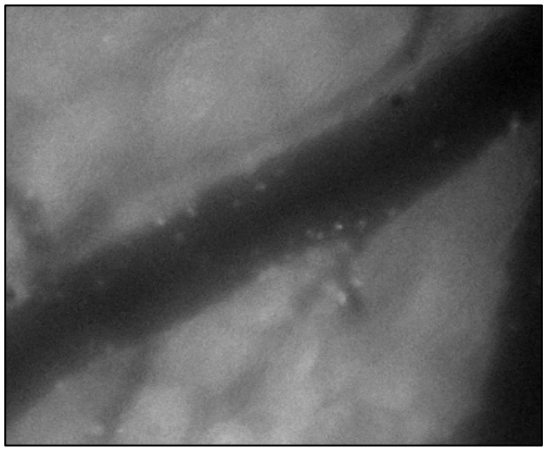

Figure 26 Pictures from IVM videos representing DIBI effects on leukocyte adhesion in intestinal collecting venules two hours after challenge with toxins from Gram-negative (A) and Gram-positive (B) bacteria

(A)Represents control group; (B and C) represent administration of 5 mg/kg of toxins (LPS_e from *E. coli)* and the same toxin + 10 mg/kg of DIBI; (D and E) represent administration of 5 mg/kg of toxins (LPS_k from *K. pneumoniae)* and the same toxin + 10 mg/kg of DIBI; (F and G) represent administration of 5 mg/kg of toxins (LTA from *S. aureus)* and the same toxin + 10 mg/kg of DIBI; (H and I) represent administration of 5 mg/kg of toxins (LTA from *S. aureus)* and the same toxin + 10 mg/kg of DIBI;

CON=control; LPS= lipopolysaccharide; LTA=lipoteichoic acid; PGN= peptidoglycan.

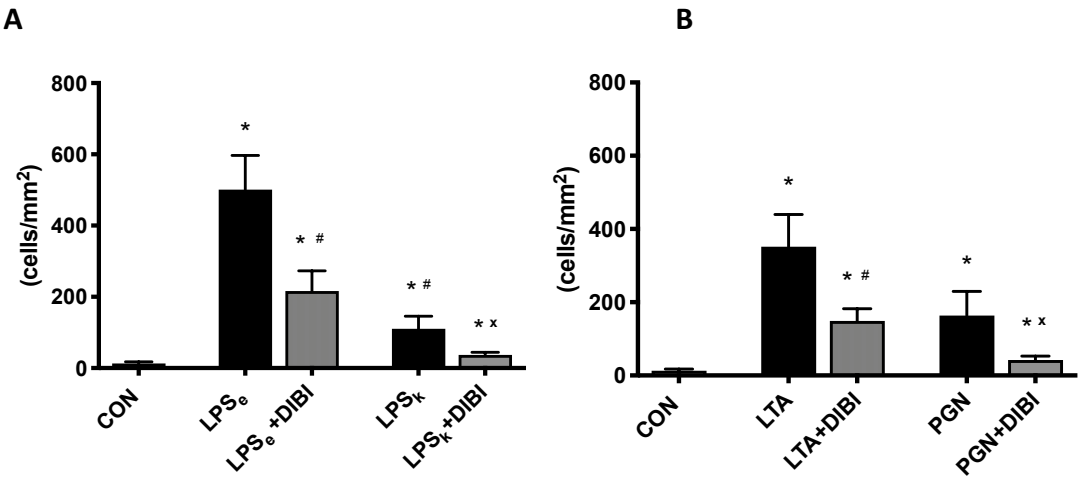

Figure 27 DIBI effects on leukocyte adhesion in intestinal collecting venules two hours after challenge with toxins from Gram-negative (A) and Gram-positive (B) bacteria (cells/mm^2).
Each bar shows mean ± SEM (n = 5 - 10 mice per group). The white bars represent control groups, the black bars represent administration of 5 mg/kg of toxins (LPS_e from *E. coli*; LPS_k from *K. pneumoniae*; LTA and PGN from *S. aureus*), and the gray bars represent administration of 5 mg/kg of toxin + 10 mg/kg of DIBI. (A)* P<0.05 compared to CON group; # P<0.05 compared to LPS_e; x P<0.05 compared to LPS_k; (B)* P<0.05 compared to CON group; # P<0.05 compared to LTA group; x P<0.05 compared to PGN group. CON=control; LPS= lipopolysaccharide; LTA=lipoteichoic acid; PGN= peptidoglycan.

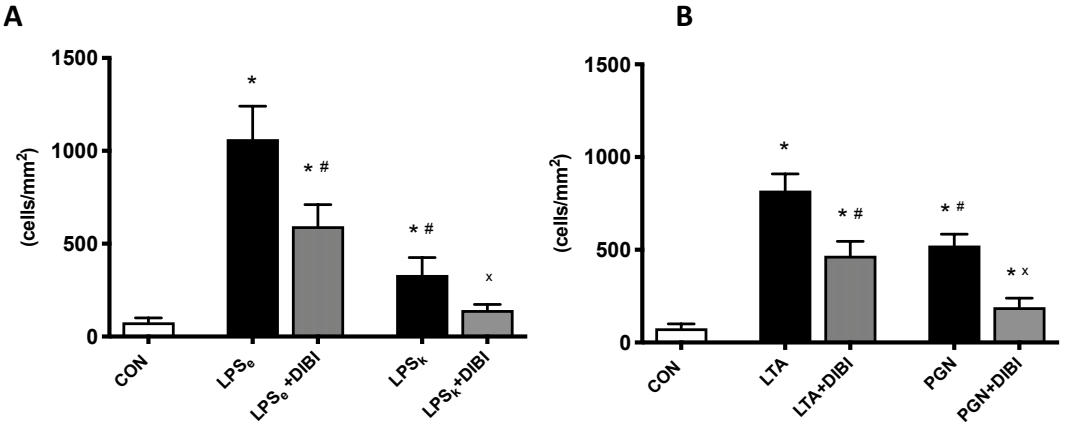

Figure 28 DIBI effects on leukocyte adhesion in intestinal post-capillary venules two hours after challenge with toxins from Gram-negative (A) and Gram-positive (B) bacteria (cells/mm^2).
Each bar shows mean ± SEM (n = 5 - 10 mice per group). The white bars represent control groups, the black bars represent administration of 5 mg/kg of toxins (LPS_e from *E. coli*; LPS_k from *K. pneumoniae*; LTA and PGN from *S. aureus*), and the gray bars represent administration of 5 mg/kg of toxin + 10 mg/kg of DIBI. (A) * P<0.05 compared to CON group; # P<0.05 compared to LPS_e; x P<0.05 compared to LPS_k; (B) * P<0.05 compared to CON group; # P<0.05 compared to LTA group; x P<0.05 compared to PGN group. CON=control; LPS= lipopolysaccharide; LTA=lipoteichoic acid; PGN= peptidoglycan.

3.2.1.2 Capillary Perfusion

The second parameter used to assess inflammation was the functional capillary density (FCD) in the intestinal muscle and mucosa layers (figure 30 and 31).

Compared to the control group (CON), 5mg/kg of all Gram-negative and -positive toxins induced a significant decrease of the FCD in the intestinal muscle layer (figure 30) measured two hours after induction of toxemia ($P<0.05$). DIBI at the dose of 10 mg/kg significantly improved the intestinal muscle layer FCD in the LPS_e+DIBI and the PGN+DIBI group. There was no significant effect of DIBI at the dosage of 10 mg/kg in the intestinal muscle layer FCD two hours after challenge with 5 mg/kg LPS from *K. pneumoniae* and 5 mg/kg *S. aureus* LTA.

In the intestinal mucosa layer, 5 mg/kg of all toxins induced a significant decrease of FCD measured two hours after toxin administration ($P<0.05$) comparing to the baseline (CON) (Figure 31). Here, DIBI at the dose of 10 mg/kg significantly improved the intestinal mucosa layer FCD in the LPS_e+DIBI group only. When using DIBI, mucosal FCD of LPS_e+DIBI group was not significantly different from control levels. DIBI did not improve the FCD of the intestinal mucosa layer two hours after animals received LPS from *K. pneumoniae* or *S. aureus* LTA/PGN, respectively.

A

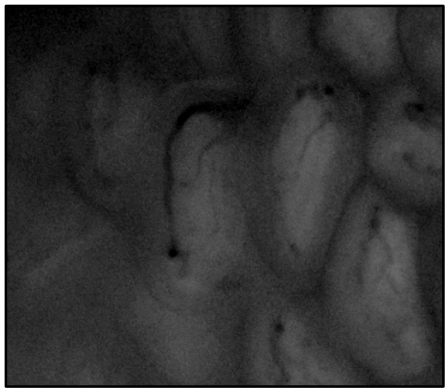

B

C

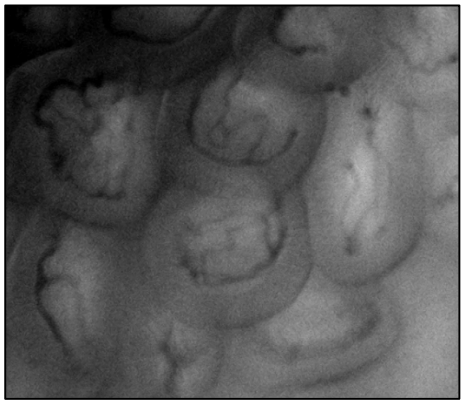

D

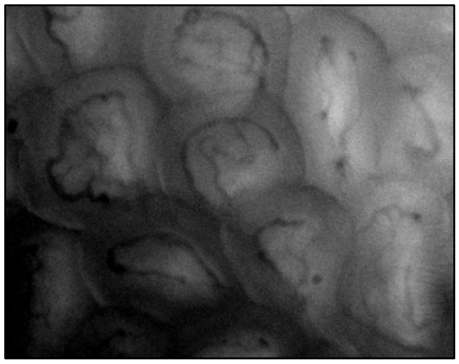

E

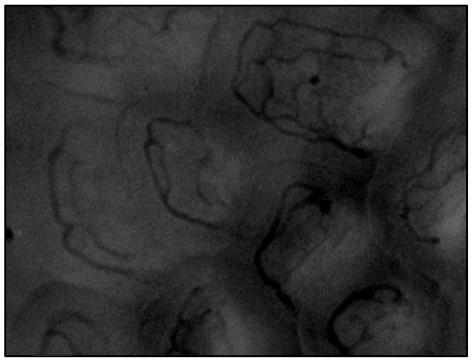

F

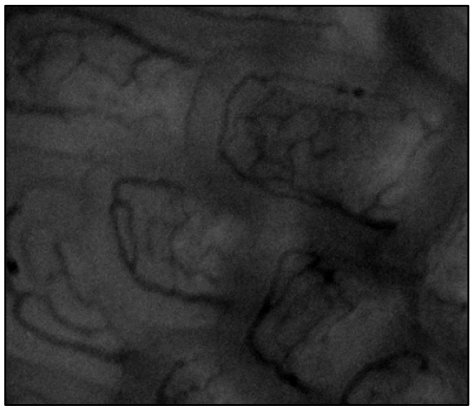

G

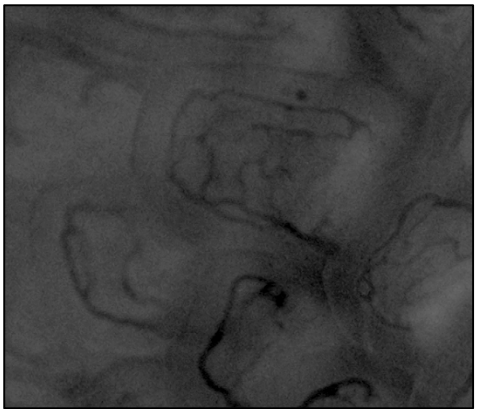

H

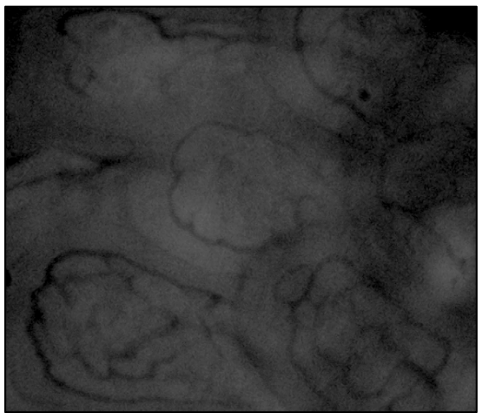

I

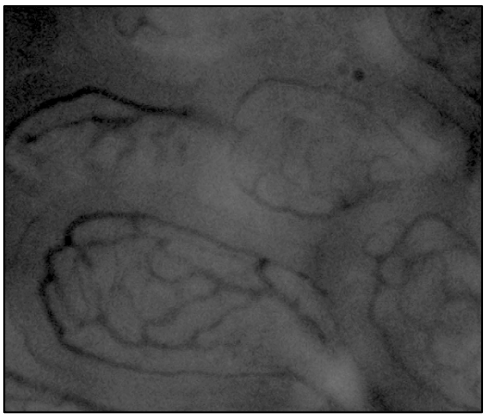

Figure 29 Pictures from IVM videos representing DIBI effects on capillary perfusion in intestinal mucosa layer two hours after challenge with toxins from Gram-negative and Gram-positive bacteria

(A)Represents control group; (B and C) represent administration of 5 mg/kg of toxins (LPS_e from *E. coli)* and the same toxin + 10 mg/kg of DIBI; (D and E) represent administration of 5 mg/kg of toxins (LPS_k from *K. pneumoniae)* and the same toxin + 10 mg/kg of DIBI; (F and G) represent administration of 5 mg/kg of toxins (LTA from *S. aureus)* and the same toxin + 10 mg/kg of DIBI; (H and I) represent administration of 5 mg/kg of toxins (LTA from *S. aureus)* and the same toxin + 10 mg/kg of DIBI;

CON=control; LPS= lipopolysaccharide; LTA=lipoteichoic acid; PGN= peptidoglycan.

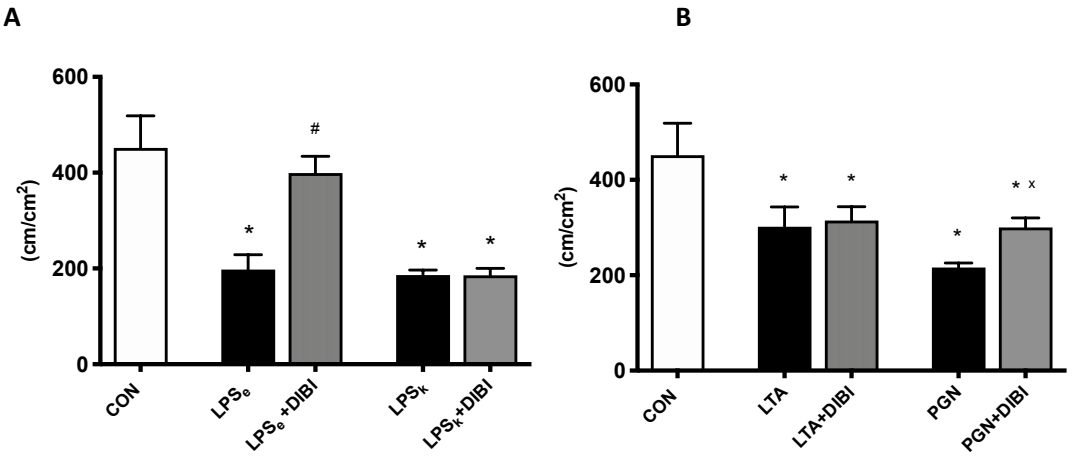

Figure 30 DIBI effects on FCD in the intestinal muscle layer two hours after challenge with toxins from Gram-negative (A) and Gram-positive (B) bacteria (cm/cm^2).
Each bar shows mean ± SEM (n = 5 - 10 mice per group). The white bars represent control groups, the black bars represent administration of 5 mg/kg of toxins (LPS_e from *E. coli*; LPS_k from *K. pneumoniae*; LTA and PGN from *S. aureus*), and the gray bars represent administration of 5 mg/kg of toxin + 10 mg/kg of DIBI. (A) * P<0.05 compared to CON group; # P<0.05 compared to LPS_e; (B) * P<0.05 compared to CON group; x P<0.05 compared to PGN group. CON=control; LPS= lipopolysaccharide; LTA=lipoteichoic acid; PGN= peptidoglycan.

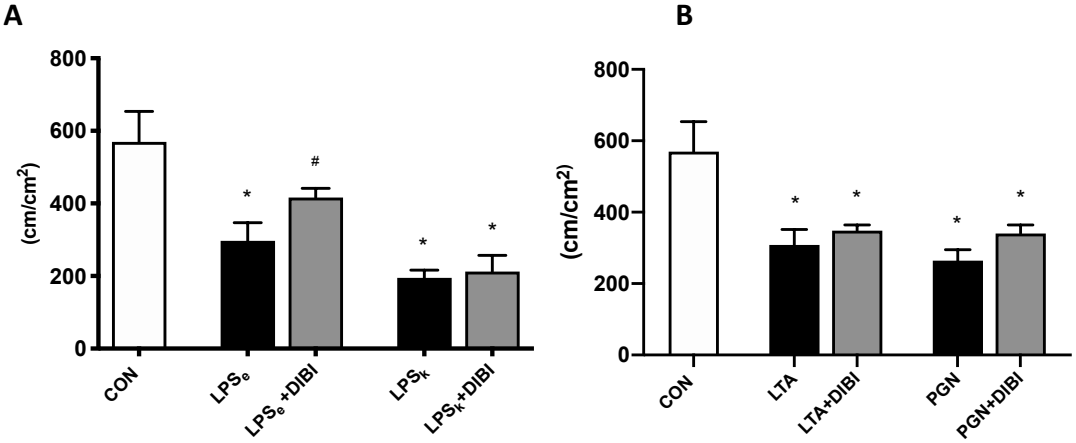

Figure 31 DIBI effects on intestinal FCD in the mucosa layer two hours after challenge with toxins from Gram-negative (A) and Gram-positive (B) bacteria (cm/cm^2).
Each bar shows mean ± SEM (n = 5 - 10 mice per group). The white bars represent control groups, the black bars represent administration of 5 mg/kg of toxins (LPS_e from *E. coli*; LPS_k from *K. pneumoniae*; LTA and PGN from *S. aureus*), and the gray bars represent administration of 5 mg/kg of toxin + 10 mg/kg of DIBI. (A) * P<0.05 compared to CON group; # P<0.05 compared to LPS_e; (B) * P<0.05 compared to CON group. CON=control; LPS= lipopolysaccharide; LTA=lipoteichoic acid; PGN= peptidoglycan.

3.2.2 Cytokines

3.2.2.1 Tumor Necrosis Factor-Alpha

Three hours after administering 5mg/kg of Gram-negative toxins (LPS_e or LPS_k respectively), a significant increase ($P<0.05$) of TNF-α plasma levels was observed relative to the control group (CON) (figure 32A). DIBI at the dose of 10 mg/kg significantly increased TNF-α plasma levels in animals that received LPS from *K. pneumoniae* (LPS_k+DIBI) ($P<0.05$).

For the Gram-positive toxins, *S. aureus* PGN did not significantly increase TNF-α plasma levels whereas *S. aureus* LTA induced a significant increase. DIBI administration significantly reduced the LTA-induced increases of TNF-α release to baseline levels (figure 32B) ($P<0.05$).

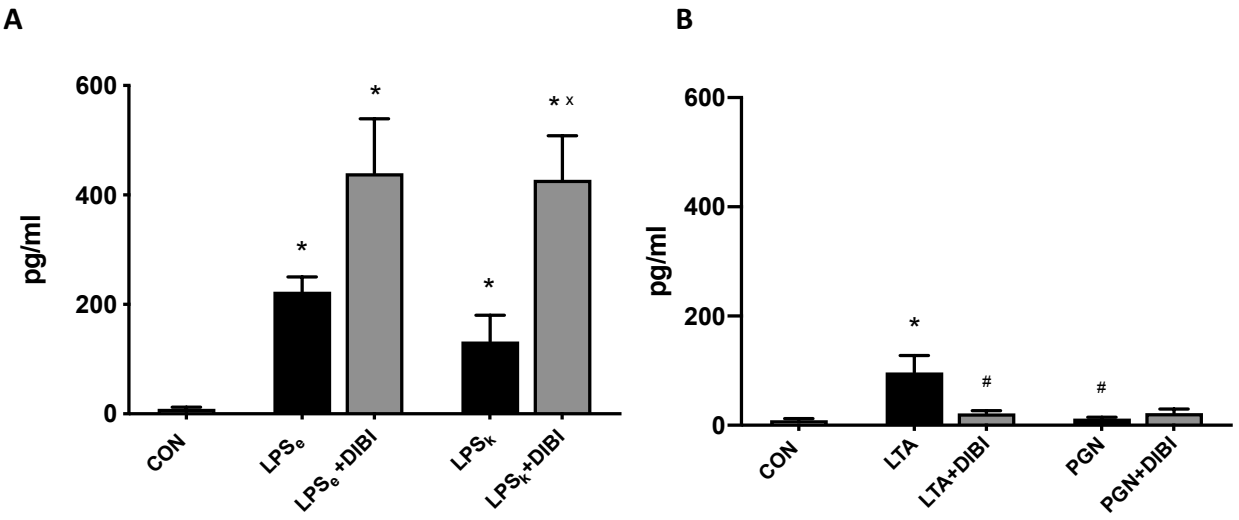

Figure 32 DIBI effects on TNF-α plasma levels three hours after challenge with toxins from Gram-negative (A) and Gram-positive (B) bacteria (pg/ml).

Each bar represents mean values ± SEM (n = 5-13 per group). The white bars represent control groups, the black bars represent administration of 5 mg/kg of toxins (LPS_e from *E. coli*; LPS_k from *K. pneumoniae*; LTA and PGN from *S. aureus*), and the gray bars represent administration of 5 mg/kg of toxin + 10 mg/kg of DIBI. (A)* $P<0.05$ compared to CON group; # $P<0.05$ compared to LPS_e; x $P<0.05$ compared to LPS_k group. (B) * $P<0.05$ compared to CON group; # $P<0.05$ compared to LTA group. CON=control; LPS= lipopolysaccharide; LTA=lipoteichoic acid; PGN= peptidoglycan.

3.2.2.2 Interleukin-6

There was a significant increase ($P<0.05$) in IL-6 plasma levels compared to the control group (CON) three hours after the administration of Gram-negative toxins at 5mg/kg (figure 33A). Moreover, *E. coli* LPS (LPS_e) challenge demonstrated significantly higher levels of IL-6 than *K. pneumoniae* LPS (LPS_k). For the Gram-positive toxins, *S. aureus* PGN did not induce a significant change in IL-6 plasma levels whereas *S. aureus* LTA induced a significant increase ($P<0.05$) (figure 33B). Administration of DIBI significantly reduced the IL-6 plasma levels in the LTA+DIBI group ($P<0.05$).

3.2.2.3 Interleukin-10

Three hours after administration of 5 mg/kg of Gram-negative or -positive toxins, a significant increase ($P<0.05$) of IL-10 plasma levels relative to the control group (CON) was observed (figure 34). DIBI treatment significantly decreased IL-10 levels by LTA. DIBI did not have a significant effect on *E. coli* and *K. pneumoniae* LPS (LPS_e+DIBI, LPS_k+DIBI) or on *S. aureus* PGN (PGN+DIBI) induced IL-10 release.

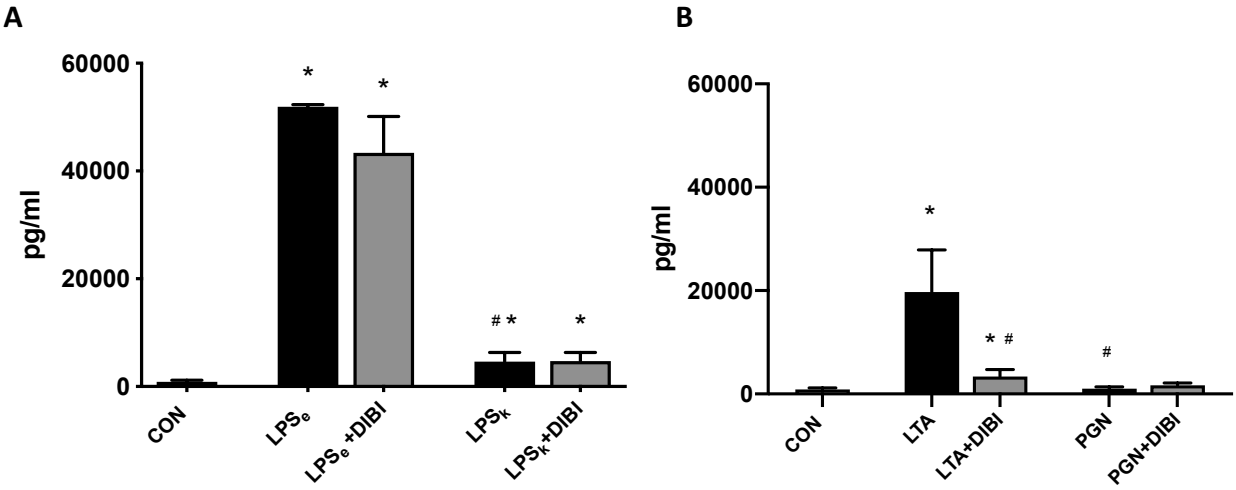

Figure 33 DIBI effects on IL-6 plasma levels three hours after challenge with toxins from Gram-negative (A) and Gram-positive (B) bacteria (pg/ml).
Each bar represents mean values ± SEM (n = 5-13 per group). The white bars represent control groups, the black bars represent administration of 5 mg/kg of toxins (LPS_e from *E. coli*; LPS_k from *K. pneumoniae*; LTA and PGN from *S. aureus*), and the gray bars represent administration of 5 mg/kg of toxin + 10 mg/kg of DIBI. (A) * P<0.05 compared to CON group; # P<0.05 compared to LPS_e; (B) * P<0.05 compared to CON group; # P<0.05 compared to LTA group. CON=control; LPS= lipopolysaccharide; LTA=lipoteichoic acid; PGN= peptidoglycan.

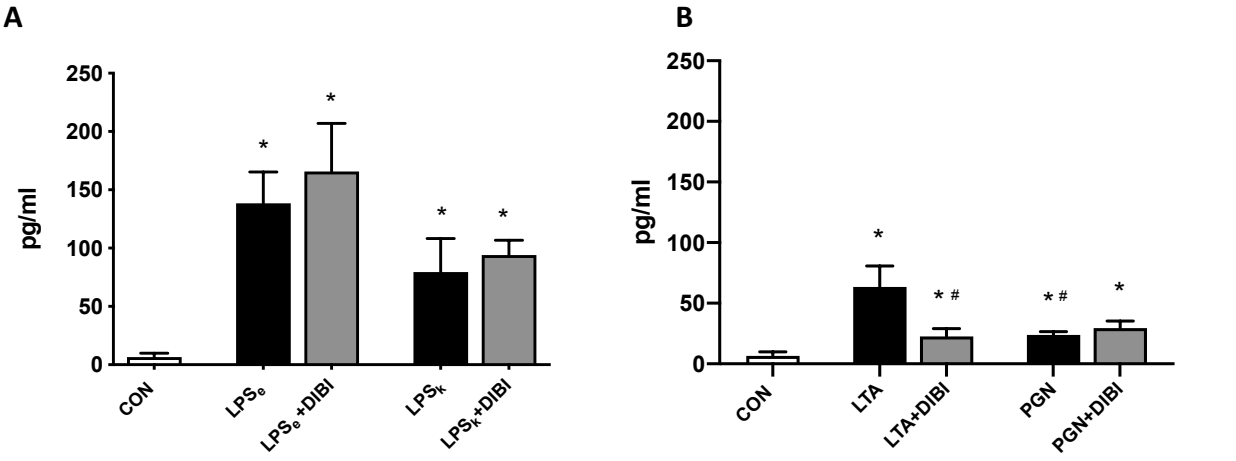

Figure 34 DIBI effects on IL-10 plasma levels three hours after challenge with toxins from Gram-negative (A) and Gram-positive (B) bacteria (pg/ml).
Each bar graphs represent mean values ± SEM (n = 5-13 per group). The white bars represent control groups, the black bars represent administration of 5 mg/kg of toxins (LPS_e from *E. coli*; LPS_k from *K. pneumoniae*; LTA and PGN from *S. aureus*), and the gray bars represent administration of 5 mg/kg of toxin + 10 mg/kg of DIBI. (A) * P<0.05 compared to CON group; (B) *P<0.05 compared to CON group; # P<0.05 compared to LTA group. CON=control; LPS= lipopolysaccharide; LTA=lipoteichoic acid; PGN= peptidoglycan.

3.2.2.4 Interleukin-1 beta

Three hours after administration of 5 mg/kg of Gram-negative or positive toxins, there was a significant increase ($P<0.05$) in IL-1 β plasma levels in groups receiving the *E. coli* LPS challenge (LPS_e) compared to controls (figure 35). DIBI, at the dose of 10 mg/kg, did not have a significant effect on the increased levels of plasma IL-1β plasma induced by *E. coli* LPS (LPS_e+DIBI).

3.2.2.5 Soluble Intercellular Adhesion Molecule-1

Three hours after administering 5mg/kg of Gram-negative or positive toxins, a significant increase ($P<0.05$) in sICAM-1 plasma levels compared to the control group (CON) (figure 36). DIBI at the dose of 10 mg/kg significantly reduced toxin-induced increases of plasma sICAM-1.

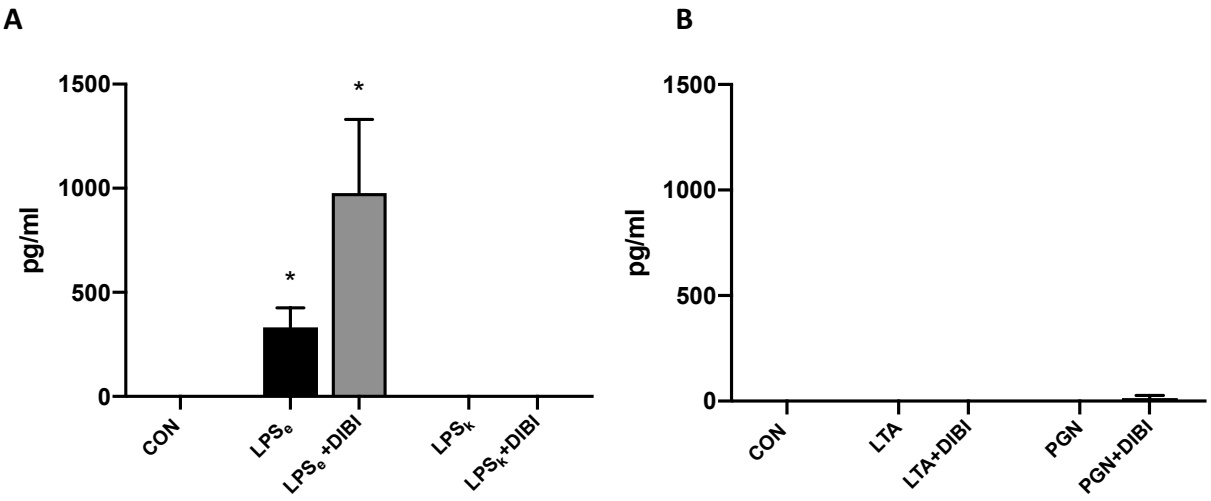

Figure 35 DIBI effects on interleukin (IL)-1β plasma levels three hours after challenge with toxins from Gram-negative (A) and Gram-positive (B) bacteria (pg/ml).
Each bar represents mean values ± SEM (n = 5-13 per group). The white bars represent control groups, the black bars represent administration of 5 mg/kg of toxins (LPS_e from *E. coli*; LPS_k from *K. pneumoniae*; LTA and PGN from *S. aureus*), and the gray bars represent administration of 5 mg/kg of toxin + 10 mg/kg of DIBI. * P<0.05 compared to CON group. CON=control; LPS= lipopolysaccharide; LTA=lipoteichoic acid; PGN= peptidoglycan.

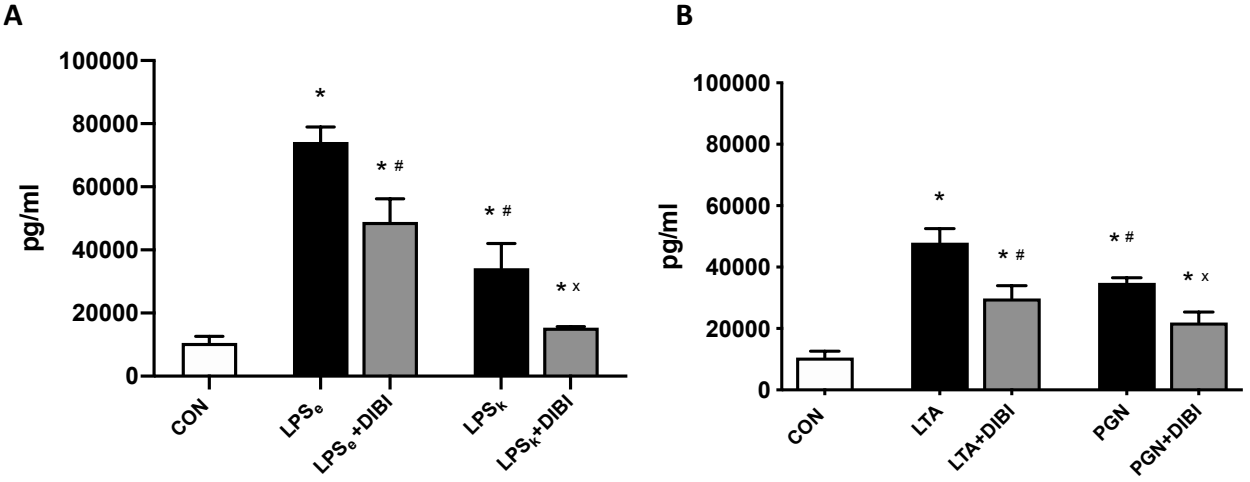

Figure 36 DIBI effects on sICAM-1 plasma levels three hours after challenge with toxins from Gram-negative (A) and Gram-positive (B) bacteria (pg/ml).
Each bar graph represents mean values ± SEM (n = 5-13 per group). The white bars represent control groups, the black bars represent administration of 5 mg/kg of toxins (LPS_e from *E. coli*; LPS_k from *K. pneumoniae*; LTA and PGN from *S. aureus*), and the gray bars represent administration of 5 mg/kg of toxin + 10 mg/kg of DIBI. (A) * P<0.05 compared to CON group; # P<0.05 compared to LPS_e; x P<0.05 compared to LPS_k; (B) * P<0.05 compared to CON group; # P<0.05 compared to LTA group; x P<0.05 compared to PGN group. CON=control; LPS= lipopolysaccharide; LTA=lipoteichoic acid; PGN= peptidoglycan.

3.2.3 Histology

The control group (CON) presented only slight morphological alterations based on the Chiu scoring method (grade 0-1).

For the Gram-negative toxins, only LPS from *E. coli* (LPS_e) challenge induced significant ($P<0.05$) damage of the intestinal tissue three hours after induction of inflammation compared to the control group (CON) (Figure 39A). The iron chelator DIBI at the dose of 10 mg/kg was able to significantly reduce the damages caused by LPS_e. LPS from *K. pneumoniae* (LPS_k) did not damage intestinal tissues significantly. When comparing the two LPS groups, LPS_k was significantly less potent than LPS_e ($P<0.05$).

For the Gram-positive toxins, the only observed significant differences were between the treated groups (LTA+DIBI and PGN+DIBI) and the control group (Figure 39B). The iron chelator DIBI at the dose of 10 mg/kg significantly increased the Chiu score ($P<0.05$) compared to the control group. There were no significant differences between treated and untreated groups and between untreated groups and control ($P<0.05$).

A

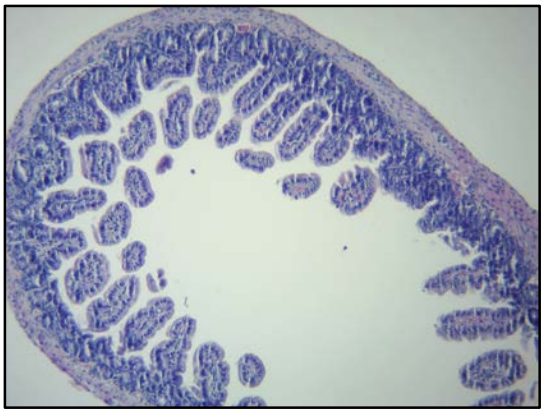

B

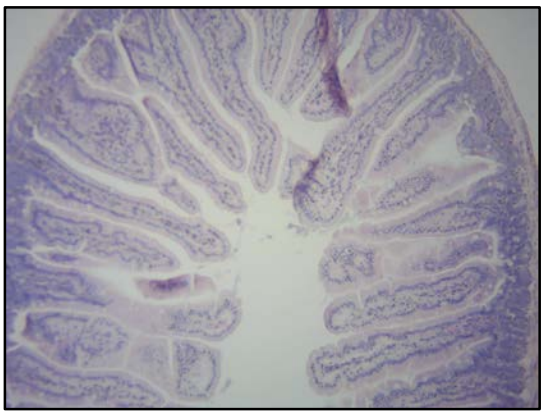

C

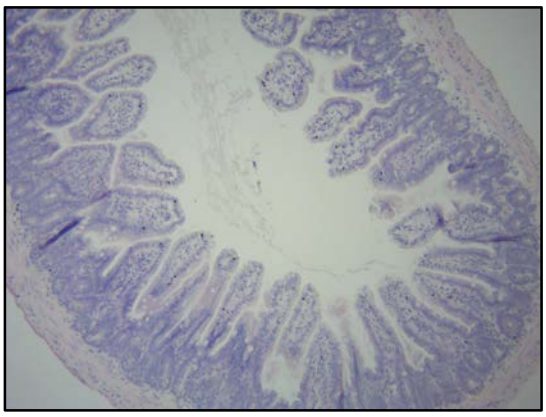

D

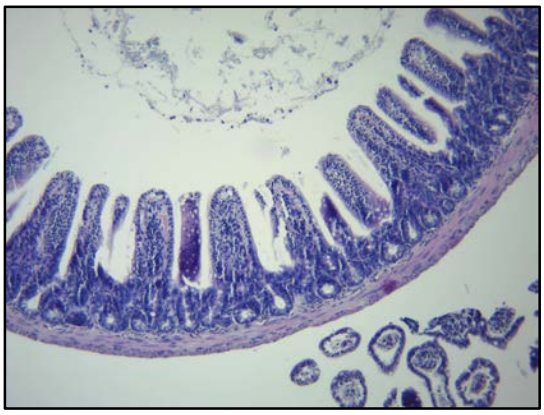

E

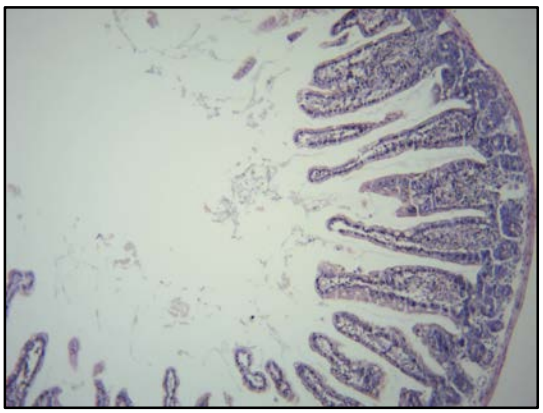

Figure 37 The effects of DIBI on morphological changes of the intestine three hours after challenge with toxins from Gram-negative bacteria
H&E staining of cross-sectional samples from the terminal ileum under 40X magnification A. Control; B. LPS_e; C. LPS_e+DIBI; D. LPS_k; E. LPS_k+DIBI

A

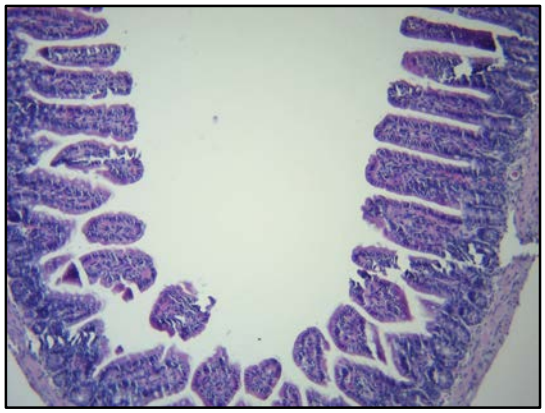

B

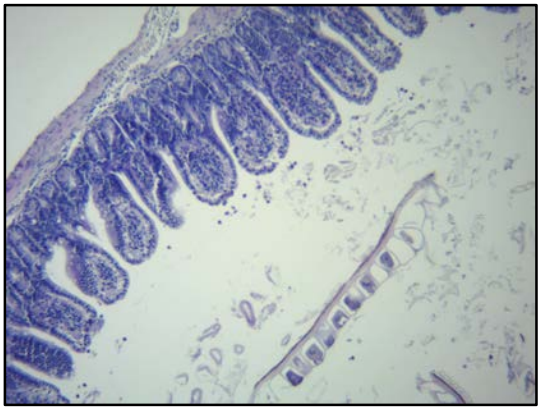

C

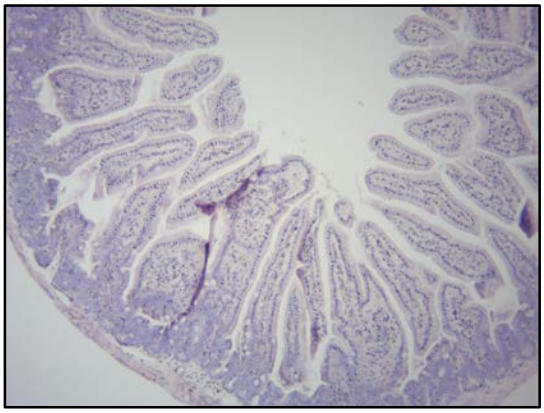

D

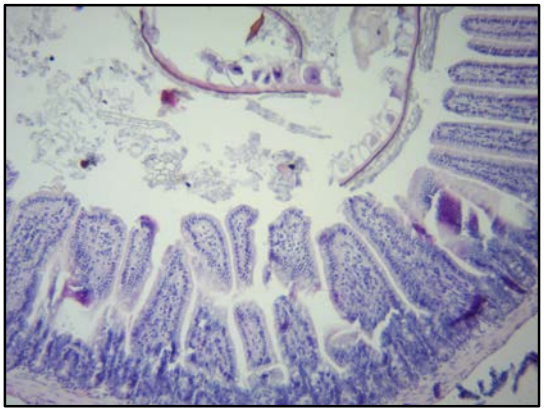

E

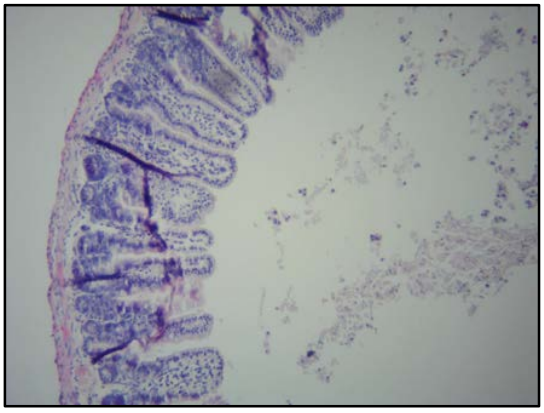

Figure 38The effects of DIBI on morphological changes of the intestine three hours after challenge with toxins from Gram-positive bacteria
H&E staining of cross-sectional samples from the terminal ileum under 40X magnification. A. Control; B. LTA; C. LTA+DIBI; D. PGN; E. PGN+DIBI

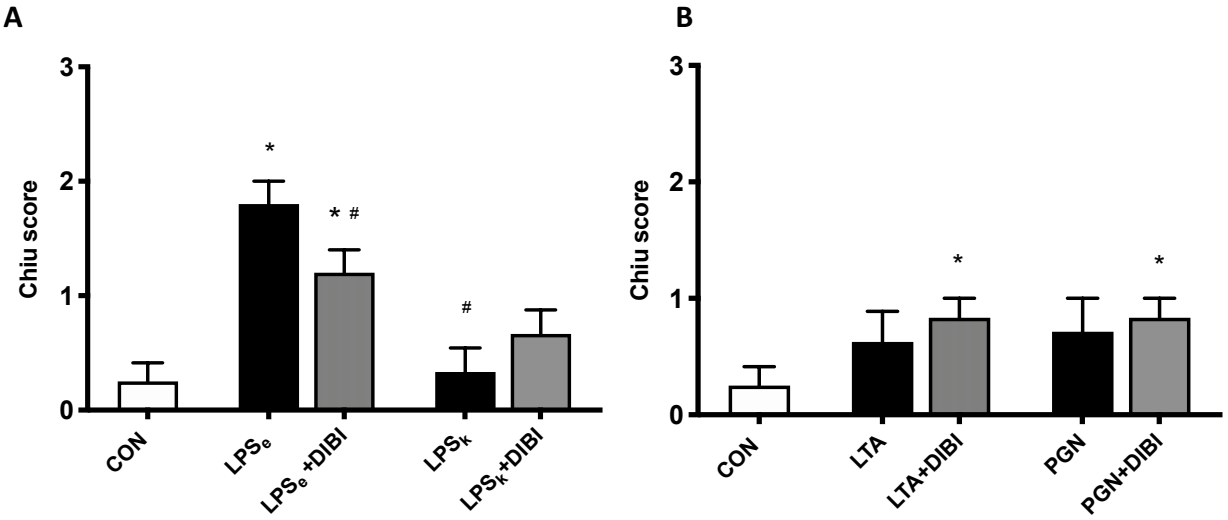

Figure 39 The effects of DIBI on morphological changes of the intestine three hours after challenge with toxins from Gram-negative (A) and Gram-positive (B) bacteria (Chi score (103)). Each bar represents mean values ± SEM (n = 5-13 per group). The white bars represent control groups, the black bars represent administration of 5 mg/kg of toxins (LPS_e from *E. coli*; LPS_k from *K. pneumoniae*; LTA and PGN from *S. aureus*), and the gray bars represent administration of 5 mg/kg of toxin + 10 mg/kg of DIBI. (A) * $P<0.05$ compared to CON group; # $P<0.05$ compared to LPS_e; (B) * $P<0.05$ compared to CON group. CON=control; LPS= lipopolysaccharide; LTA=lipoteichoic acid; PGN= peptidoglycan.

3.3 Colon Ascendens Stent Peritonitis

3.3.1 IVM

3.3.1.1 Leukocyte Adhesion

In the surgical control group (SHAM), a low level of leukocyte adhesion in collecting and post-capillary venules was observed (figure 40 and 41). The CASP group demonstrated a significant increase in the number of adhering leukocytes ($P<0.05$) compared to SHAMs in both collecting and post-capillary venules 8 hours after sepsis induction.

When administered intraperitoneally at the end of CASP surgery, 80 mg/kg of the new iron chelator DIBI and/or 25 mg/kg of the antibiotic imipenem significantly reduced the leukocyte adhesion ($p<0.05$) in collecting and post-capillary venules measured 8 hours after sepsis induction compared to the untreated CASP group. DIBI and IMI groups were not significantly different from each other but the combination of both drugs (DIBI+IMI group) resulted in significantly reduced numbers of adhering leukocytes in collecting venules compared to untreated CASP animals ($P<0.05$) (figure 41A). Post-capillary leukocyte adhesion was not significantly different amongst treated groups 8 hours after sepsis induction (figure 41B).

Leukocyte adhesion in all groups, treated and untreated, were significantly higher from SHAM group ($P<0.05$).

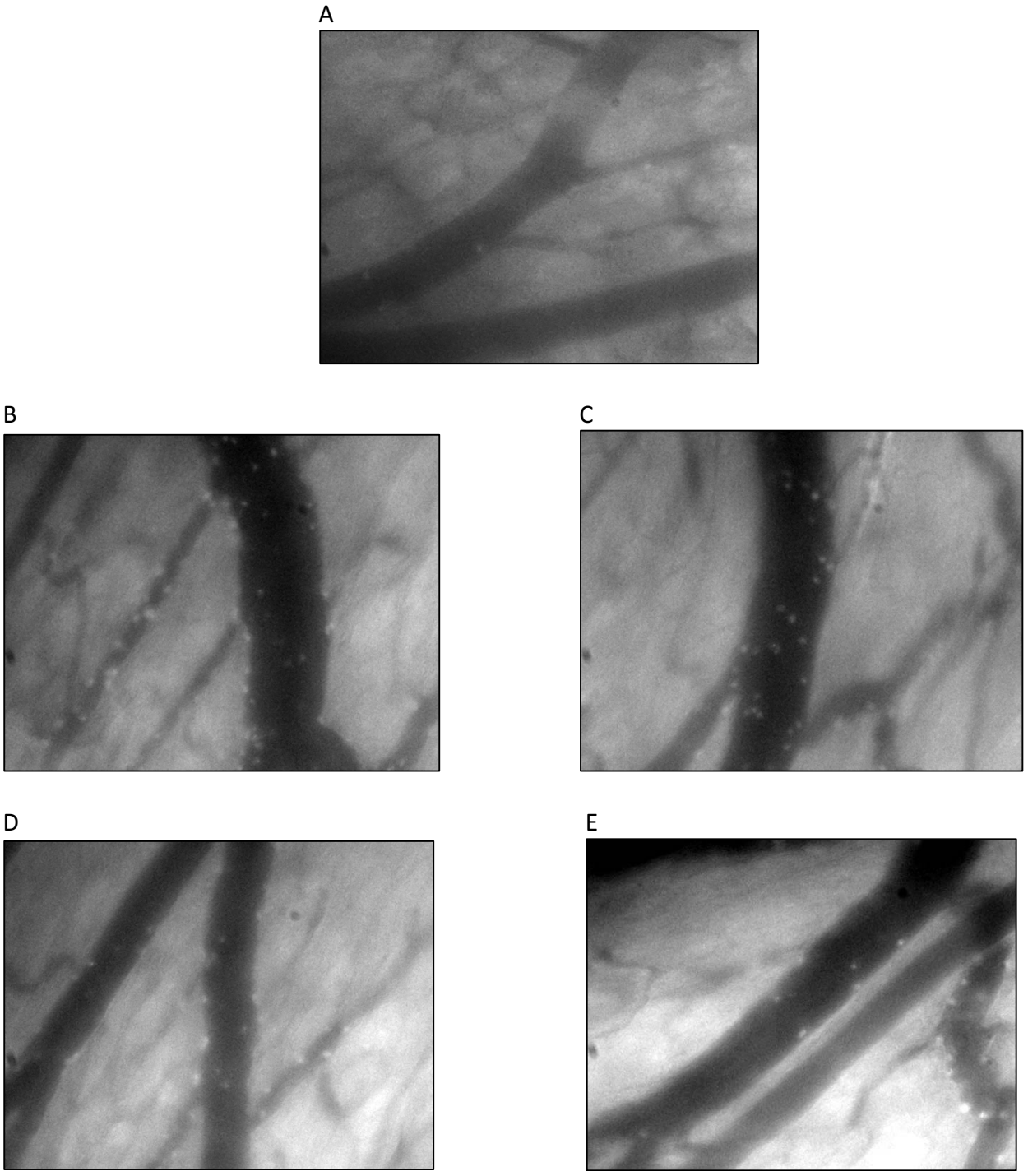

Figure 40 Pictures from IVM videos representing the effect of DIBI and/or imipenem on leukocyte adhesion in intestinal submucosal collecting venules 8 hours after sepsis induction
(A)Represents control group; (B) represents CASP group; (C) represents 10 mg/kg DIBI treated group; (D) represents 25 mg/kg IMI treated group; (E) represents DIBI+IMI treated group.

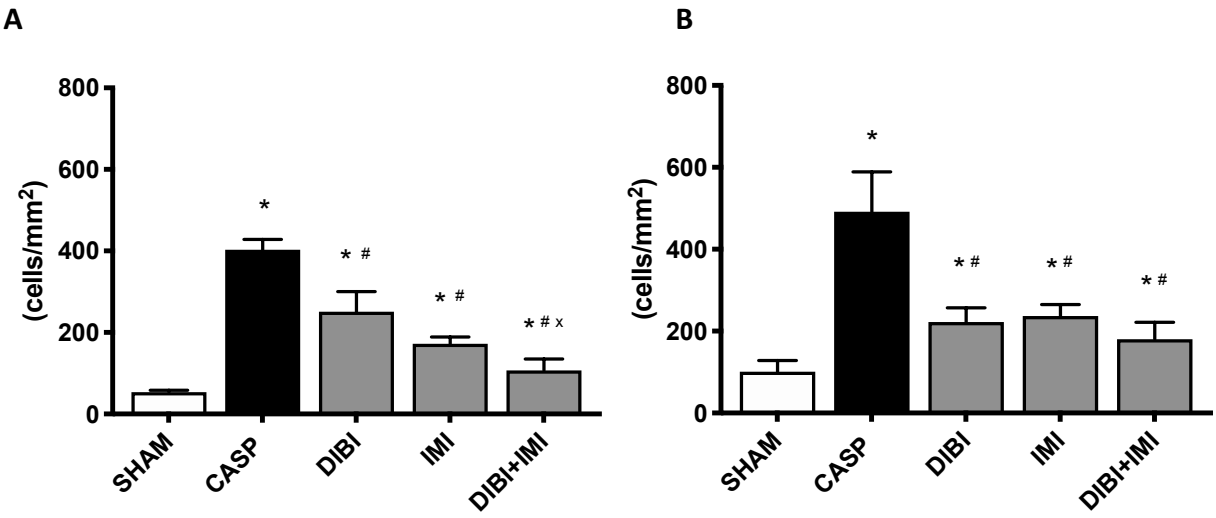

Figure 41 The effect of DIBI and/or imipenem on leukocyte adhesion in intestinal submucosal collecting (A) and postcapillary (B) venules 8 hours after sepsis induction (cells/mm^2).
Each bar graph represents mean values ± SEM (n = 7-14 per group). The white bars represent animals from the surgical control group, the black bars represent the untreated septic group, and the gray bars represent treated septic groups. * P<0.05 compared to SHAM group; # P<0.05 compared to CASP group; x P<0.05 compared to DIBI group.

3.3.1.2 Capillary Perfusion

When comparing to the baseline (SHAM), we observed a significant decrease in FCD ($P<0.05$) in the intestinal muscle and mucosa layers in the CASP group compared to the SHAM baselines 8 hours after sepsis induction (figure 42 and 43).

In the intestinal muscle layer, neither the new iron chelator DIBI at the dose of 80 mg/kg nor the antibiotic imipenem at the dose of 25 mg/kg improved the reductions of FCD. The combination of DIBI and imipenem (DIBI+IMI) significantly increased FCD compared to the imipenem only (IMI) treatment group (figure 43A). The DIBI+IMI group was not significantly different from SHAM, CASP, and DIBI only groups.

In the intestinal mucosa layer, all treatments significantly improved FCD ($P<0.05$) 8 hours after sepsis induction compared to the CASP group (figure 43B). Imipenem alone, or in combination with DIBI, showed the largest increases in FCD compared to CASP and DIBI only groups. FCD of all treated groups was still significantly lower than the control SHAM group FCD 8 hours after sepsis induction.

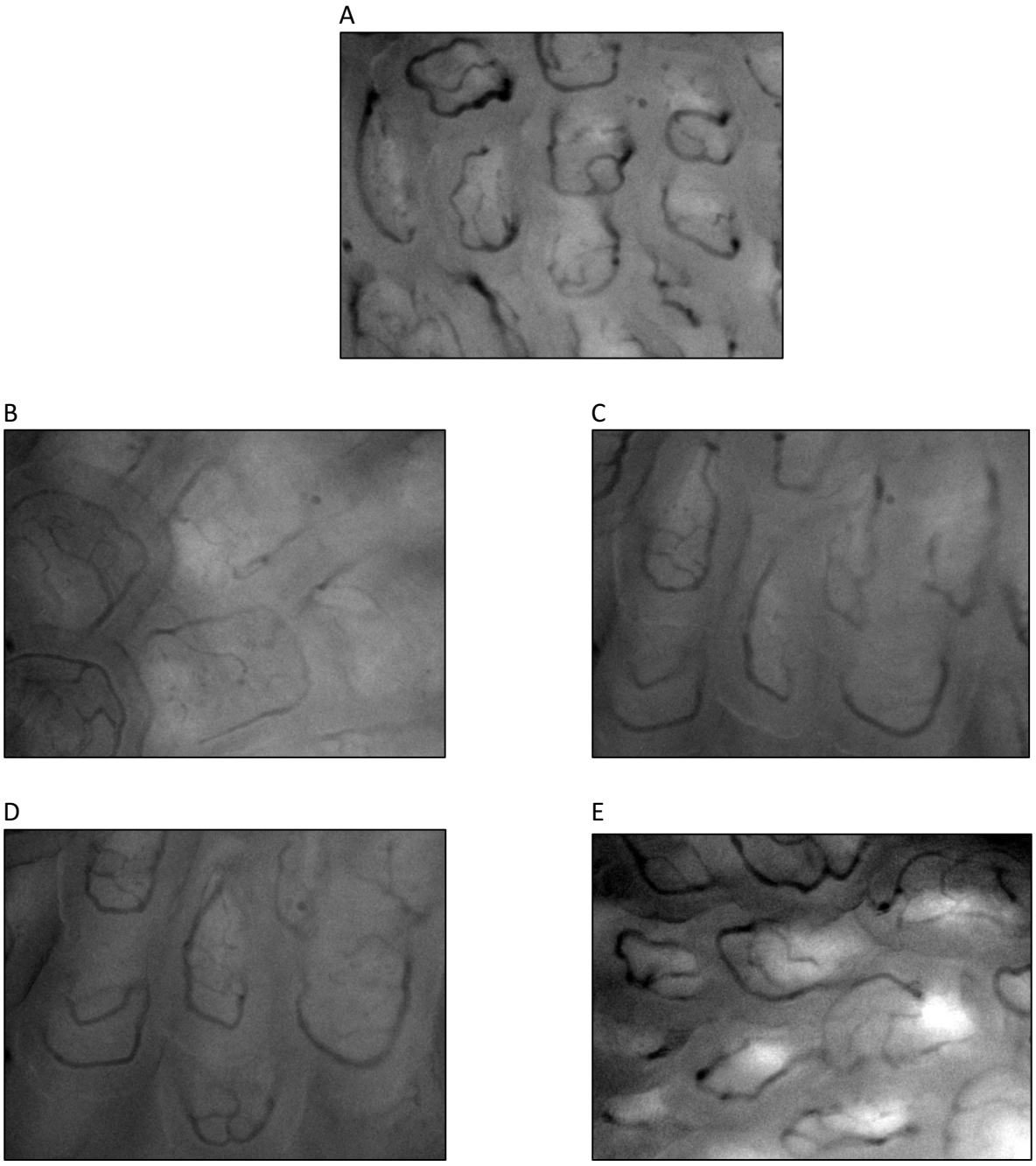

Figure 42 Pictures from IVM videos representing the effect of DIBI and/or imipenem on capillary perfusion in intestinal mucosa layer 8 hours after sepsis induction
(A)Represents control group; (B) represents CASP group; (C) represents 10 mg/kg DIBI treated group; (D) represents 25 mg/kg IMI treated group; (E) represents DIBI+IMI treated group.

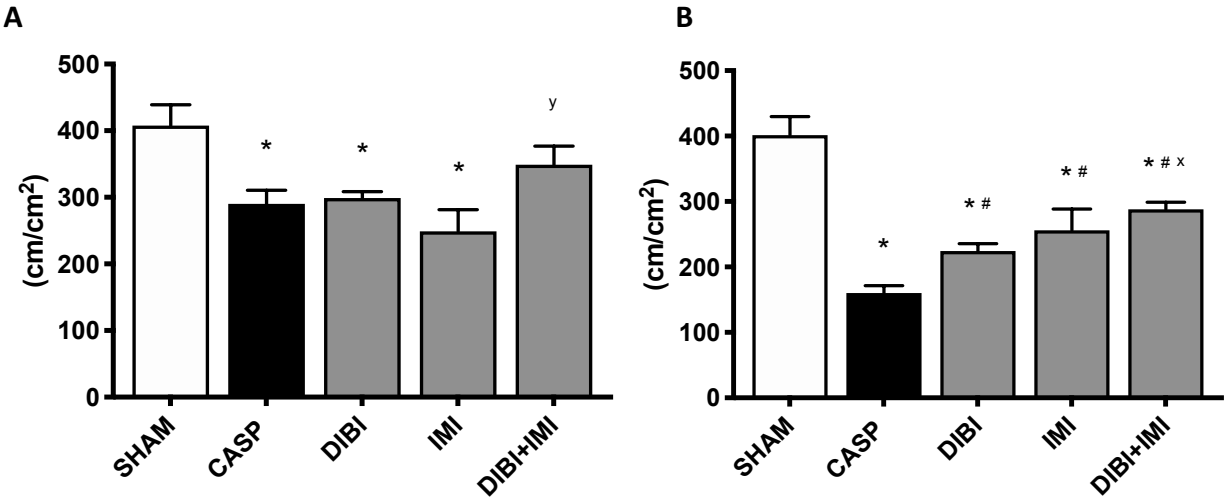

Figure 43 The effect of DIBI and/or imipenem on FCD in the intestinal muscle (A) and mucosa (B) layer 8 hours after sepsis induction (cells/mm^2).

Each bar graph represents mean values ± SEM (n = 7-14 per group). The white bars represent animals from the surgical control group, the black bars represent the untreated septic group, and the gray bars represent treated septic group. (A)* P<0.05 compared to SHAM group; y P<0.05 compared to IMI group. (B)* P<0.05 compared to SHAM group; # P<0.05 compared to CASP group; x P<0.05 compared to DIBI group.

3.3.2 Cytokines

3.3.2.1 Tumor Necrosis Factor-Alpha

We observed a significant increase ($P<0.05$) in TNF-α plasma levels in the CASP group compared to the SHAM group 8.5 hours after sepsis induction (figure 44). The new iron chelator DIBI at the dose of 80 mg/kg had no significant effect on CASP-induced increases of plasma TNF-α levels. However, imipenem at the dose of 25 mg/kg alone and in combination with DIBI significantly reduced TNF-α plasma levels compared to the untreated CASP group.

3.3.2.2 Interleukin-6

Compared to the baseline (SHAM), CASP surgery induced a significant increase ($P<0.05$) in IL-6 plasma levels 8.5 hours after sepsis induction (figure 45). The new iron chelator DIBI at the dose of 80 mg/kg and/or the antibiotic imipenem at the dose of 25 mg/kg significantly decreased plasma IL-6 levels compared to the untreated CASP group.

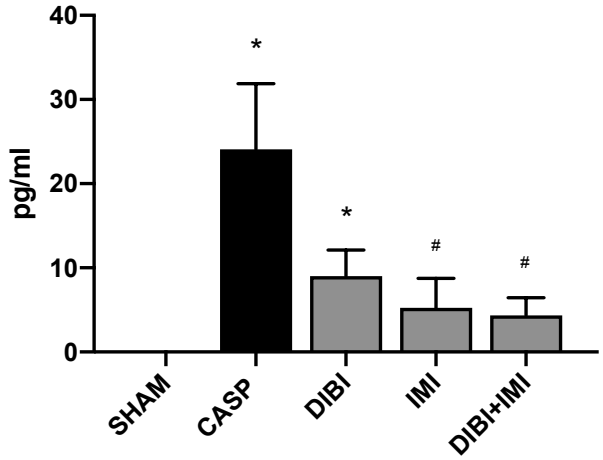

Figure 44 The effect of DIBI and/or imipenem on Tumor Necrosis Factor-Alpha (TNF-α) plasma levels 8.5 hours after sepsis induction (pg/ml).
Each bar graph represents mean values ± SEM (n = 7-14 per group). The white bar represents animals from the surgical control group, the black bar represents untreated septic groups, and the gray bars represent treated septic group. * P<0.05 compared to SHAM group; # P<0.05 compared to CASP group.

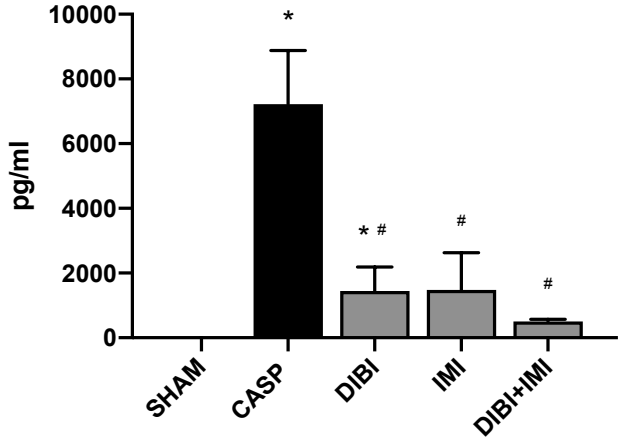

Figure 45 The effect of DIBI and/or imipenem on IL-6 plasma levels 8.5 hours after sepsis induction (pg/ml).
Each bar graph represents mean values ± SEM (n = 7-14 per group). The white bar represents animals from the surgical control group, the black bar represents untreated septic groups, and the gray bars represent treated septic groups. * P<0.05 compared to SHAM group; # P<0.05 compared to CASP group.

3.3.2.3 Interleukin-10

In the CASP group we observed a significant increase ($P<0.05$) of interleukin IL-10 plasma levels evaluated 8.5 hours after sepsis induction compared to SHAM (figure 46). The new iron chelator DIBI at the dose of 80 mg/kg and/or the antibiotic imipenem at the dose of 25 mg/kg significantly decreased plasma IL-10 levels compared to the untreated CASP group.

3.3.2.4 Interleukin-1 beta

All values were below the detection threshold (data not shown).

3.3.2.5 Soluble Intercellular Adhesion Molecule-1

It was observed a significant increase ($P<0.05$) in plasma levels of sICAM-1 8.5 hours after sepsis induction (CASP) compared to SHAM (figure 47). The new iron chelator DIBI at the dose of 80 mg/kg did not attenuate CASP-induced increases of sICAM-1. However, imipenem at the dose of 25 mg/kg alone and in combination with DIBI significantly decreased ($P<0.05$) sICAM-1 plasma levels compared to untreated CASP animals.

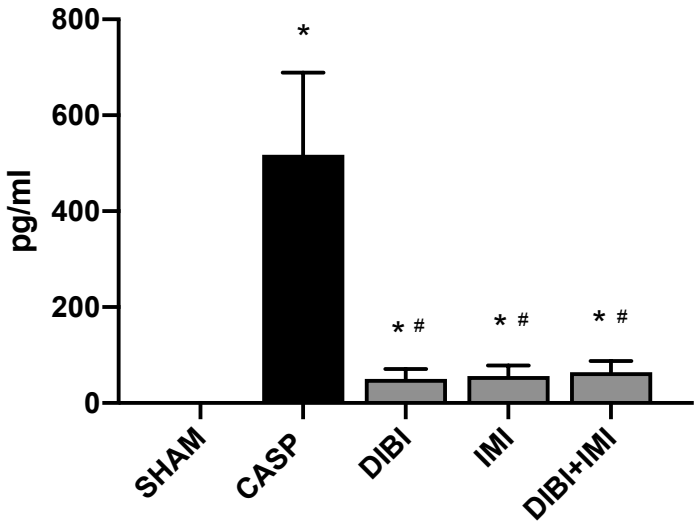

Figure 46 The effect of DIBI and/or imipenem on IL-10 plasma levels 8.5 hours after sepsis induction (pg/ml).

Each bar graph represents mean values ± SEM (n = 7-14 per group). The white bars represent animals from the surgical control group, the black bar represents the untreated septic group, and the gray bars represent treated septic groups. * P<0.05 compared to SHAM group; # P<0.05 compared to CASP group.

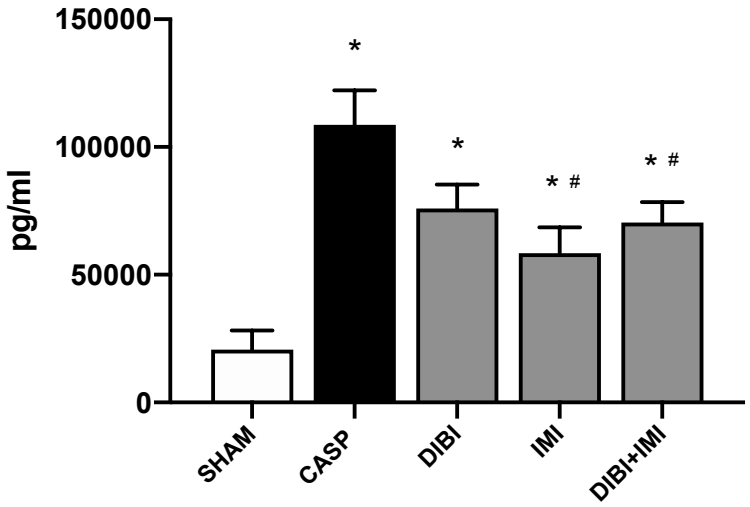

Figure 47 The effect of DIBI and/or imipenem on sICAM-1 plasma levels 8.5 hours after sepsis induction (pg/ml).

Each bar graph represents mean values ± SEM (n = 7-14 per group). The white bars represent animals from the surgical control group, the black bar represents the untreated septic group, and the gray bars represent treated septic groups. * P<0.05 compared to SHAM group; # P<0.05 compared to CASP group.

3.3.3 Histology

Assessment of morphological intestinal damage was performed using the Chiu scoring system (103). The surgical control group (SHAM) presented minimal morphological changes. Significantly higher levels of morphological damage in the intestine were observed in the untreated CASP compared to the SHAM group (figure 48 and 49). This damage is expressed by a rise in the Chiu score from grade 0 to grade 2. The administration of 80 mg/kg of DIBI did not reverse that damage since DIBI group was not significantly different than CASP group. Imipenem alone or in combination with DIBI significantly reduced the morphological damage ($P<0.05$) compared to the untreated CASP group. DIBI+IMI and IMI groups were not significantly different from SHAM in terms of morphological damages.

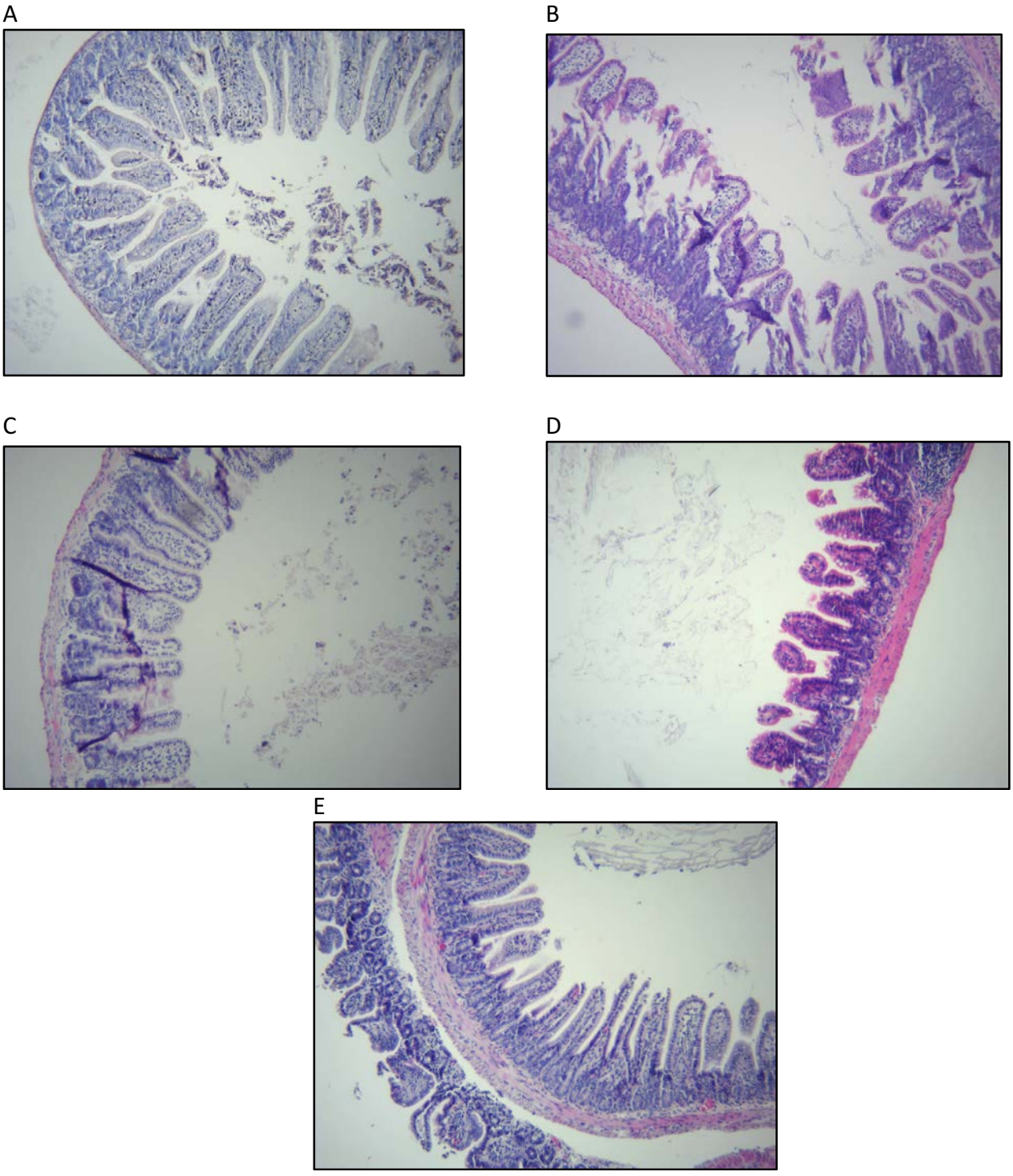

Figure 48 The effect of DIBI and/or imipenem on intestinal tissues 8.5h after CASP induced sepsis H&E staining of cross-sectional samples from the terminal ileum under 40X magnification. A. Surgical control SHAM; B. CASP; C. CASP+DIBI; D. CASP+IMI; E. CASP+DIBI+IMI

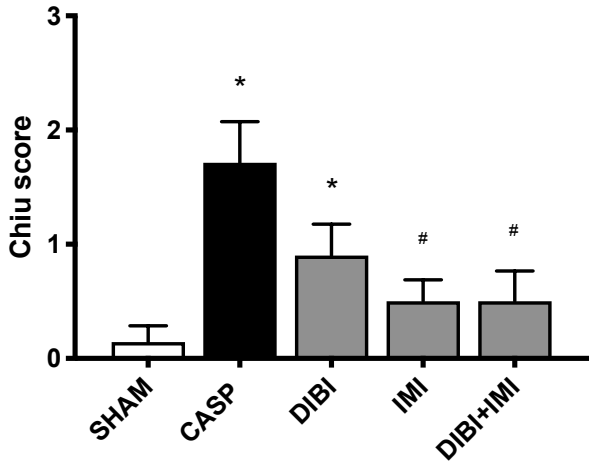

Figure 49 The effect of DIBI and/or imipenem on morphological changes of the intestine 8.5 hours after sepsis induction (Chi score (103)).
Each bar graph represents mean values ± SEM (n = 7-14 per group). The white bar represents animals from the surgical control group, the black bar represents untreated septic group, and the gray bars represent treated septic groups. * $P<0.05$ compared to SHAM group; # $P<0.05$ compared to CASP group.

3.3.4 Bacterial Burden

3.3.4.1 Peritoneal Lavage Fluid

In the PLF, bacterial growth was similar in both aerobic and anaerobic conditions. In the surgical control group (SHAM) we found minimal amounts of bacteria in the PLF. In the CASP group we observed a significant increase ($P<0.05$) of Gram-positive and negative bacterial burden in the PLF 7.5 hours after sepsis induction (figure 50). When comparing the Gram-positive and -negative population with the Gram-negative only population, it appeared that the bacteria that grew the most in the peritoneal cavity were Gram-negative bacteria. DIBI at the dose of 80 mg/kg did not significantly reduce bacterial growth compared to the untreated CASP group. However, imipenem at the dose of 25 mg/kg alone and in combination with DIBI decreased significantly ($P<0.05$) the bacterial growth compared to the untreated CASP group.

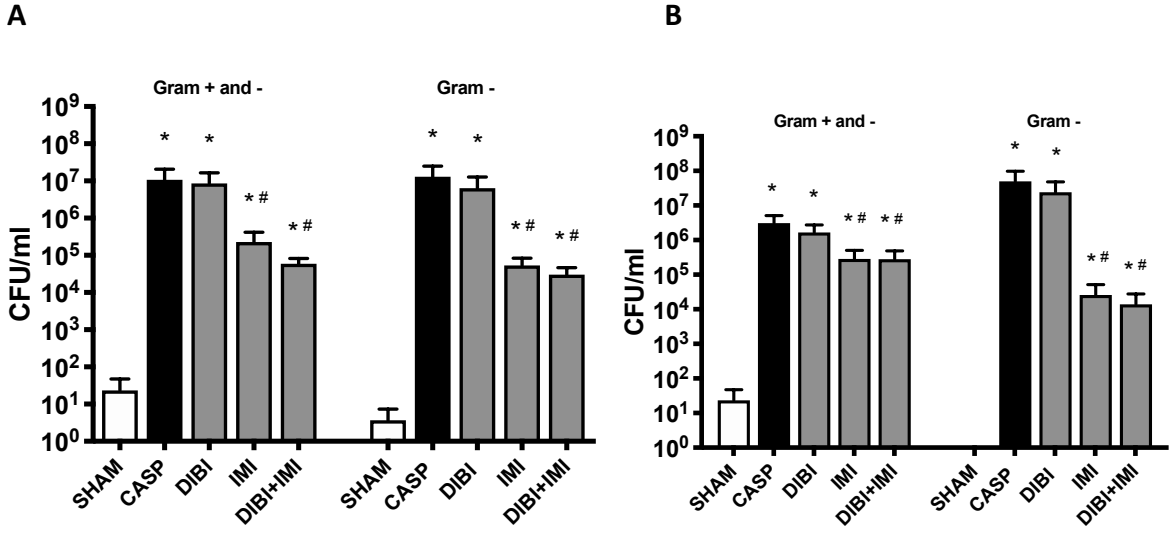

Figure 50 The effect of DIBI and/or imipenem on Gram positive and negative bacterial growth under aerobic (A) and anaerobic (B) conditions (CFU/ml).

Samples from peritoneal lavage fluid (PLF) 7.5 hours after sepsis induction. Each bar represents mean values ± SEM (n = 5-12 per group). The white bars represent animals from the surgical control group, the black bars represent the untreated septic group, and the gray bars represent treated septic groups. * P<0.05 compared to SHAM group; # P<0.05 compared to CASP group.

3.3.4.2 Blood

Minimal bacterial growth was noticed in surgical control animals (SHAM). In the CASP group, it was observed a significant increase ($P<0.05$) of Gram-positive and negative bacterial burden in the blood 9 hours after sepsis induction (Figure 51). As in the PLF it appeared that Gram-negative bacteria were the ones that grew the most. DIBI at the dose of 80 mg/kg did not significantly reduce bacterial growth compared to the untreated CASP group. However, imipenem at the dose of 25 mg/kg alone and in combination with DIBI significantly decreased ($P<0.05$) the bacterial growth compared to the untreated CASP group. In the blood, results of total bacterial growth (growth of Gram-positive and negative bacteria) were similar in both aerobic and anaerobic conditions.

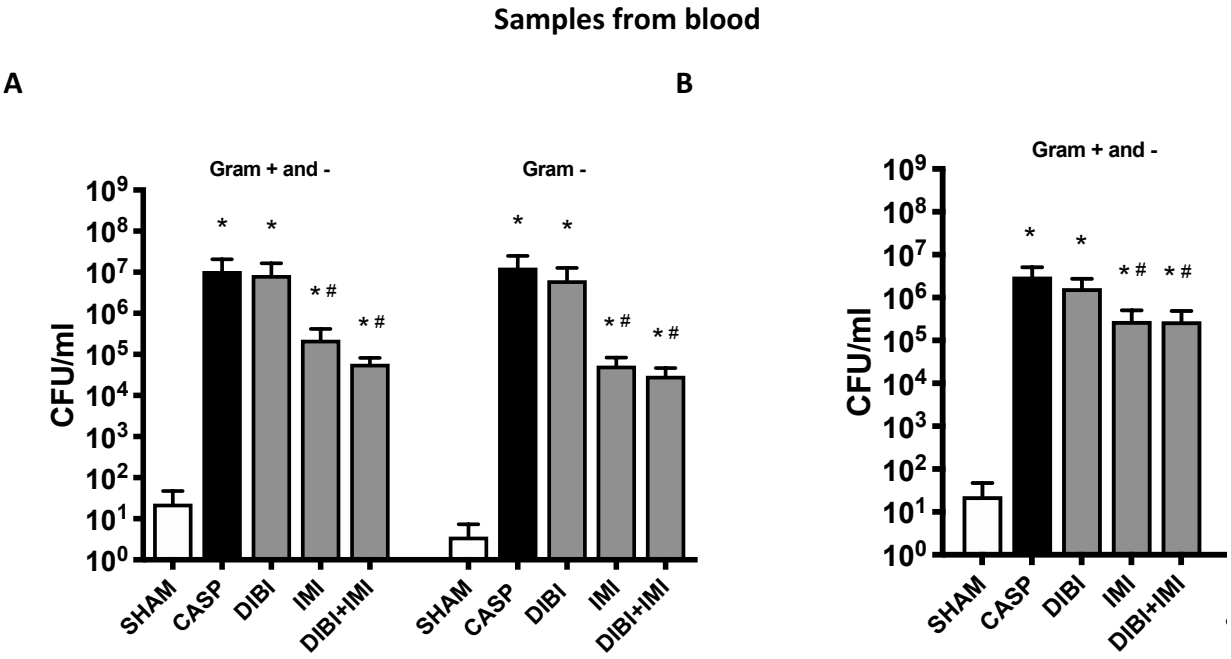

Figure 51 The effect of DIBI and/or imipenem on Gram positive and negative bacterial growth under aerobic (A) and anaerobic (B) conditions (CFU/ml).
Samples from whole blood 9 hours after sepsis induction. Each bar represents mean values ±SEM (n = 5-12 per group). The white bars represent animals from the surgical control group, the black bars represent the untreated septic group, and the gray bars represent treated septic groups. * P<0.05 compared to SHAM group, # P<0.05 compared to CASP group.

CHAPTER 4: DISCUSSION

4.1 LPS-Induced Cystitis

The goal here was to evaluate early systemic activation of the immune response in a murine model of local inflammation (LPS-induced cystitis). LPS-induced cystitis is a well-known and widely used model to study bladder inflammation in many species including mice (96, 97, 104). LPS has been used to induce inflammation in the bladder and activate the immune system. The systemic impact of LPS-induced cystitis has been compared to a standard LPS-induced model of systemic inflammation, i.e. endotoxemia. Systemic inflammation was evaluated by intravital microscopy (IVM) of the intestine, measurement of plasma inflammatory cytokine levels, and evaluation of morphological intestinal tissue damage histologically using H&E staining.

4.1.1 IVM

Since the focus was the systemic effects of local and systemic inflammation, an organ allowing the measurement of relevant inflammatory parameter by IVM had to be selected. The intestine has been chosen because of its important role during inflammatory processes. There is a normal physiological balance between the host and its intestinal bacterial colonizers (microbiome). Sepsis pathophysiology including tissue damage by oxidative stress and hypoxia leads to the disruptions of the intestinal mucosa barrier with potentially pathogens translocation from the gut into the systemic circulation (105–107). Those initially unharmful bacteria can join the pathogens responsible of sepsis and further boost septic damages. The more bacterial translocation across the intestinal barrier the higher leukocyte activation, and impaired intestinal microcirculation.

4.1.1.1 Leukocyte Adhesion

The primary endpoint using IVM was the assessment of leukocyte-endothelial interactions by measuring the number of adhering leukocytes in collecting and post-capillary venules. During inflammation, leukocytes and endothelial cells are activated. Leukocytes roll on the vascular endothelium, stick to the vessel wall and then transmigrate to the site of inflammation (108). Using IVM, it was possible to measure the number of adhering leukocytes per area. A baseline level of leukocyte adhesion was noticed in all control groups (no toxin administered) due to the surgical procedure including laparotomy and external positioning of the gut on the microscopy stage inducing minor local and systemic inflammation. Two hours after toxin challenge, LPS-induced cystitis triggered intestinal leukocyte adhesion at a level similar to inflammation induced by systemic (low or high dose) LPS administration. Those results could be explained by the fact that during inflammation, the activation of the NF-kB inflammatory pathway lead to vasodilation and increased vascular permeability to allow leukocyte migration toward the site of injury (109). The increased vascular permeability could have allowed a certain amount of endotoxin and pro-inflammatory cytokines to disseminate into the bloodstream and therefore induce leukocyte adhesion on intestine. In a study using the same two hours LPS-induced cystitis model (same LPS dose), leukocyte infiltration into the bladder wall associated with swelling and hemorrhagic areas were observed histologically (97). Although the dose of LPS used induces rather moderate than severe cystitis, damages to the bladder wall may have allowed pro-inflammatory molecules to spread systemically.

4.1.1.2 Capillary Perfusion

The second measured IVM parameter was the capillary blood flow in intestinal muscle and mucosa layers because, as aforementioned, microcirculatory dysfunction is a major issue in the pathophysiologic cascade of sepsis (62). The mucosa layer is more sensitive to damages and seems to have a more demanding metabolic activity. This layer receives approximately 80% of the total intramural blood flow whereas the muscle layer receives 20%. It was therefore relevant to assess blood flow impairment on both intestinal layers (110).

Although two hours after toxin challenge LPS-induced cystitis triggered systemic leukocyte activation measured in the intestine, the systemic effect of that local inflammation was not severe enough to cause intestinal blood flow impairments. Only the model of severe systemic inflammation has been able to impact the capillary blood flow in intestinal muscle and mucosa layers. Systemic consequences of local bladder inflammation on the intestinal microcirculation have not been studied yet. Therefore, the results are novel and can only be compared to studies of the intestinal microcirculation in systemic inflammation. Several endotoxemia studies showed that in severe systemic inflammation intestinal capillary blood flow was significantly decreased (99, 111).

4.1.2 Cytokines

To further assess systemic consequences of local inflammation, plasma levels of inflammatory cytokines and adhesion molecules were measured 3 hours after local LPS challenge in comparison to systemic LPS administration. Overall, local cystitis and low systemic inflammation did not increase plasma levels of TNF-α, IL-6, IL-1β, IL-10 and sICAM-1 in the same extent as in severe systemic inflammation. This is in discrepancy to the previously reported IVM results, where even low dose systemic inflammation induced leukocyte activation in the intestinal microcirculation similar to high dose LPS administration. Obviously, low dose LPS (locally and systemically) was able to induce limited leukocyte activation in some other tissues (gut), but did not result in a systemic cytokine storm. The observations are in line with a LPS dose response behaviour of immune cells in the systemic circulation.

4.1.3 Histology

Assessment of morphological intestinal tissue damage was done according to the Chiu scoring system (103). LPS-induced local inflammation and low dose systemic LPS administration did not cause significant damage to the intestinal tissue. Only the severe systemic inflammation induced measurable, but low-grade intestinal damage. This is again in contrast to the IVM findings, where already low dose LPS (locally and systemically) induced inflammatory changes in the gut. However, the observation time (3 hours) was potentially too short to see morphological changes with H&E staining in light microscopy.

All those data together allow to conclude that a systemic immune response can be observed early in local infection but without major changes in capillary blood flow, plasma levels of inflammatory markers, and intestinal tissue. Therefore, it could be suggested that a potential treatment for immune dysregulation should be initiated early during the course of sepsis.

4.2 Experimental Toxemia

After the LPS-induced cystitis model showed that systemic immune response was already activated when the inflammation was still local, it was interesting to now appreciate how, an early administration of an iron chelator, could influence the immune response during sepsis. However, since iron chelation also has a potential impact on bacterial growth, a sepsis model that does not involve bacteria, i.e. (endo)toxemia, has been chosen. Toxemia is an infection-free model which activates inflammatory pathways by the systemic administration of a controlled amount of toxin, a component of bacteria. Bacterial products trigger systemic inflammation characterized by increased leukocyte-endothelial interactions, release of plasma cytokines, adhesion molecules expression, and development of impaired capillary blood flow. Toxins chosen were from Gram-positive and negative bacteria. Because this model reproduces the pathophysiologic inflammatory features of sepsis, it allows therefore the focus on consequences of immune cells activation during a systemic inflammation and the potential role that DIBI, a new iron chelator, can play.

Inflammation was evaluated by intravital microscopy (IVM) of the intestine to measure leukocyte activation and capillary perfusion, measurement of plasma inflammatory cytokine levels, and evaluation of morphological intestinal tissue damage histologically using H&E staining.

4.2.1 IVM

4.2.1.1 Leukocyte Adhesion

Our primary endpoint was the assessment of leukocyte-endothelial interaction by measuring the number of adhering leukocytes in collecting and post-capillary venules. First of all, it was seen that our control group (CON), in collecting and post-capillary venules, had a baseline level of leukocyte adhesion. This could be explained by the fact that, even though they did not receive any toxin, they underwent a catheterization of the jugular vein followed by a laparotomy which induced a slight systemic inflammatory response due to the surgical trauma.

Secondly, the toxemia model worked effectively. All toxins were able to increase, at different levels, leukocyte adhesion in collecting and post-capillary venules compared to control animals. Although Gram-positive and Gram-negative toxins have been shown to increase inflammatory parameters (112), the Gram-negative LPS from *E. coli* seems to be the most potent of all the toxins used in this model. Only a few studies compared toxins directly. LPS from *E. coli* is one of the most used toxins to induce systemic inflammation in mice, rats or humans because of its high potency if the same amount of toxin is used (113). Studies to compare the pro-inflammatory properties of different intraperitoneally administered doses of LPS from *E. coli* and LTA from *Staphylococcus aureus* have been conducted. Inflammatory parameters measured were in vivo leukocyte adhesion using IVM and release of plasma cytokines. The results confirmed that LPS was more potent than LTA at the same dose but also that LTA administered at higher doses did not necessarily induce more cytokine excretion (114, 115).

Moreover, Yipp et al. compared the ability of LTA and PGN to induce leukocyte adhesion using IVM of the mouse cremaster muscle for leukocyte recruitment (116). The mechanism by which this increased leukocyte adhesion happens could be by the toxin-stimulation of Toll Like Receptors (TLR) 2 and 4 responsible of the activation of NF-κB inflammatory pathway. The fact that PAMPs of gram positive and negative bacteria do not trigger the same pathway can justify the difference in potency of these species. It has been suggested that each element (LPS, LTA, PGN, ...) can act differently depending on the bacterium (43). Slight structural differences and the sequence of amino acids that constitute them makes each element rather unique in term of potency and ability to induces an immune response. The Gram-positive LTA and PGN, although extracted from the same *S. aureus* and stimulating the same TLR2, do not have the same potency because they are two different molecules. For the Gram-negative, LPS of *E. coli* and *K. pneumoniae* show slight but important structural differences justifying the difference in term of immune activation. According to the literature, LPS, LTA and PGN could increase the expression of adhesion molecules and induce leukocyte-endothelial cells interaction through a ROS and iron-related process (78).

Thirdly, as expected, the new iron chelator, DIBI, in this two-hour toxin-challenge model, was able to significantly reduce the toxin-increased adhesion of leukocytes for all toxins in collecting and post-capillary venules. However, DIBI did not completely reverse to control level leukocyte adhesion. This effect is positive because, the goal of DIBI should be the decrease of the hyper-activation of leukocytes and not immunosuppression. Appropriate level of immune cell activation is still needed for a proper inflammatory process. These results agree with other studies. Arora et al. showed DIBI anti-inflammatory effect using IVM in a LPS-induced rat model of ocular inflammation. DIBI treated two hours LPS-challenged animal reduced ocular inflammation in local and systemic induced uveitis (95). No studies on the anti-inflammatory effects of DIBI in toxemia induced by Gram-positive bacterial toxins have been published yet. Greenshields et al. found interesting results by using DIBI in cancer in vitro experiments. DIBI alone has been able to reduce the growth of five type of breast cancer cell lines, but also enhance the effect of chemotherapeutic breast cancer treatment.

The cancer cells abnormally rapid growth is due to their increased iron related ROS production. Iron removal using DIBI was therefore able to reduce cancer cells growth (117). All the information together strongly suggests anti-inflammatory efficacy of DIBI.

4.2.1.2 Capillary Perfusion

The second parameter used to quantify inflammatory changes in the microcirculation was the intestinal FCD. All toxins were able to significantly decrease the FCD in intestinal muscle and mucosa layers compared to control. The effect of the iron chelator, DIBI, on the FCD changes was variable. While it improved the reduced capillary blood flow by LPS from *E. coli* and *S. aureus* peptidoglycan, no effect was seen on *K. pneumoniae* LPS and *S. aureus* LTA. However, a few other studies corroborate DIBI effects in similar *E. coli* LPS-induced toxemia models. Thorburn et al. using IVM showed that DIBI was able to bring the LPS-decreased capillary blood flow back to control levels in endotoxemic mice (99). Arora et al. reported that DIBI improved the reduced iridial microcirculation by *E. coli* LPS in experimental uveitis in both mice and rats (95). Impairment of capillary blood flow during severe inflammation is multifactorial, including contributing factors such as capillary leakage, disseminated intravascular coagulation, increased leukocyte-endothelial interaction, endothelial cell dysfunction, systemic redistribution of blood flow, and tissue edema externally compressing microvessels (62, 118). It can be speculated that while in some situations DIBI-related decrease of leukocyte-endothelial interaction could be sufficient to significantly improve capillary perfusion, in other cases the other factors may be more harmful therefore perpetuate damages and masked DIBI effects.

4.2.2 Cytokines

To further assess inflammation in this model, levels of inflammatory cytokines and adhesion molecules were measured in plasma collected 3 hours after toxin challenge. Cytokines are inflammatory molecules released during inflammation by a broad range of cells including immune cells (macrophages, neutrophils, T and B lymphocytes) as well as endothelial cells. Cytokines can be pro-inflammatory (e.g., TNF-α, IL-1β, IL-6) enhancing systematic inflammation, or anti-inflammatory (e.g., IL-10) inhibiting inflammation and promoting wound healing (46). Each cytokine has its own course of synthesis, release and half-life in the bloodstream. These parameters vary according to the intensity of the inflammation. TNF-α and IL-1β are the earliest inflammatory cytokines, produced and released within the first 30 minutes following a triggering event (45).

In this murine toxemia model, a few of the study cytokines had plasma levels too low to be detected 3h post toxin challenge especially in the PGN group. However, the trend was an increase in most of the plasma cytokine levels (mimicking the cytokine storm in sepsis). Wand et al. found comparable results when measuring TNF-α, IL-6 and IL-10 levels in plasma and in some organs (liver, lung, kidney) following *S. aureus* PGN challenge in rats (119). Variable levels of cytokines have been observed in the organs; the kidneys were the ones containing the lowest amount of the 3 cytokines. In general, plasma and organ levels of all these cytokines were elevated by PGN compared to control. When comparing the results from Wang et al. to our toxemia model, they had higher cytokines levels although both model measured cytokine levels 3h after PGN i.v. administration. The difference between what is reported here and their study is that they used 10 mg/kg PGN in rats when it was here 5 mg/kg in mice. PGN seems to have a dose-response effect. Another study using *S. aureus* LTA to stimulate human dermal microvascular endothelial cells showed increased IL-6 production (116). In the contrary, the same type of experiment on J774 cells (macrophage-like cell line) using *S. aureus* LTA, showed extremely low cytokine levels (114).

In a context where high levels of cytokine are expected, these results could be explained either by species differences (human vs rat vs mouse), or by the variability in the administered doses, or just by the mixed nature of the inflammatory response in sepsis involving both hyper-inflammation and immunosuppression phases.

Treatment with the novel iron chelator, DIBI, resulted in variable effects on plasma cytokine levels in experimental toxemia. A recently published study using the iron chelator, di-2-pyridylketone-4,4-dimethyl-3-thiosemicarbazone, reduced in a dose-response manner serum levels of IL-1β and TNF-α and tissue level of IL-1β, TNF-α, and IL-6 in a murine experimental model of allergic rhinitis (120). Others authors using the FDA-approved iron chelators, deferoxamine or deferasirox, respectively, in endotoxemic humans, mice and rats showed decreased LPS-induced activation of NF-κB, reduced plasma levels of TNF-α, IL-6, IL-1β, and IL-10, and lower levels of inflammatory parameters of liver injury (90, 91, 121, 122). Iron chelation by DIBI decreased the sICAM-1 rise induced by administration of Gram-positive and negative toxins. The adhesion molecule sICAM-1 is a key mediator of leukocyte migration and infiltration during sepsis. Its decrease is in correlation with the previously reported decrease of leukocytes adhesion by DIBI.

In summary, there is clearly a variability regarding cytokine levels in sepsis and DIBI-related effects on the cytokine release. Toxins appears to induce different patterns of cytokine release in experimental models of sepsis depending on differences in the amount of toxin administered, the route of administration, site of cytokine measurements, and the species used. The conflicting results seen with DIBI treatment could have 2 explanations (Figure 52). In this project, plasma cytokine levels were measure at one timepoint. Assuming that the red curve represents the time course of a cytokine release after LPS administration, it can be speculated that an increase in plasma cytokine measured at only one timepoint might not be a “real” increase in plasma. The high cytokine level (dark blue curve) in the DIBI treatment group compared to untreated controls could be due to a shift in the course of cytokine release: early cytokine peak levels (not detected with single time measurements in untreated animals) might have been delayed by DIBI administration and appear as increase.

Another possible explanation is that DIBI might decrease but expand the cytokine release (light blue curve). However, at present, potential (detrimental) DIBI-related side effects also can't be completely ruled out. Experiments including measurements of cytokines at different time points would be a way of clarification.

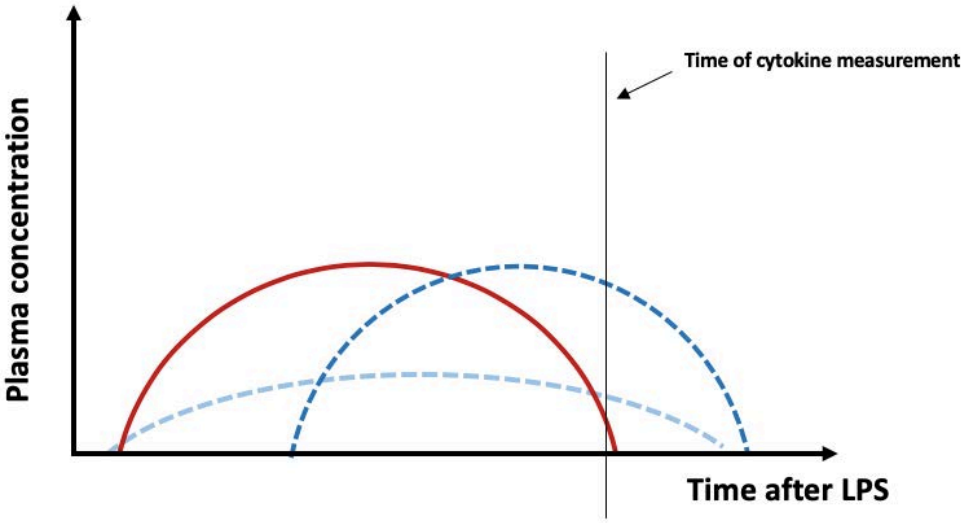

Figure 52: Possible DIBI's effect on plasma cytokine levels

4.2.3 Histology

Assessment of morphological intestinal tissue damage done according to the Chiu scoring system showed that *K. pneumoniae* LPS, *S. aureus* LTA and PGN induced measurable, but minor changes in intestinal tissue when compared to control. *E. coli* LPS induced more damage comparing to the other toxins, but the damage is still in the lower range of the Chiu score. DIBI administration was able to reduce those minimal *E. coli* LPS-induced changes. The previously reported results from the LPS-induced cystitis (this thesis) support those findings and strongly suggest that the 3 hours observation time might be too short to perceive morphological changes with H&E staining in light microscopy.

In review of the complete results, DIBI seems to have anti-inflammatory effects in this model of toxin-induced experimental sepsis. However, the toxemia model has some limitations. In this model, the amount of toxin has been tightly controlled and was administered in a rapid manner once only, which does not resemble clinical sepsis, where a more gradual release of toxins is seen. Those limitations can be improved by using a more clinically relevant model of sepsis that includes living bacteria.

4.3 Colon Ascendens Stent Peritonitis

After studying the consequences of immune cell (hyper-)activation during systemic inflammation and the anti-inflammatory effects of the novel iron chelator, DIBI, in that context, the next step was to assess the effects of iron chelation in a sepsis model combining both inflammation and infection. CASP-induced sepsis is a clinically relevant model mimicking the clinical course and the pathophysiology of human abdominal polybacterial sepsis (presence of living gram-positive and negative pathogens). Inflammation was evaluated by IVM of the intestine, measurement of plasma cytokine levels, evaluation of morphological intestinal tissue damage histologically using H&E staining, and bacterial burden by measuring bacterial growth in peritoneal lavage fluid and blood.

4.3.1 IVM

4.3.1.1 Leukocyte Adhesion

The surgical control group SHAM had a low baseline level of leukocyte adhesion in collecting and post-capillary intestinal submucosal venules due to the systemic inflammatory effects of the surgical CASP procedure and the second laparotomy 7.5 hours later.

CASP-induced sepsis increased leukocyte adhesion significantly. These findings are consistent with previous CASP studies that assessed leukocyte recruitment and infiltration in various organs (99, 101, 123–125) and were comparable to the previous 2h toxin models (LPS-induced cystitis and toxemia) where the immune response was at a similar level. Although all treatment regiments reduced leukocyte adhesion, the combination of iron chelation using DIBI and antibiotic therapy with imipenem had a stronger effect compared to DIBI only treated group. DIBI and/or imipenem did not completely reverse leukocyte adhesion to control level. This has also been seen in the toxemia model and is considered as beneficial, since the decrease of leukocyte (hyper-)activation did not prevent an appropriate level of immune cell activation for a proper anti-bacterial response. The reduction of ROS-induced damage by iron chelation, and the antimicrobial activity of imipenem (and DIBI), seems to have contributed equally to the decrease of leukocyte-endothelial interaction. A study in our lab using a slightly different CASP procedure found similar results. DIBI was administered at a lower dose (40 vs 80 mg/kg) and at a different route of administration (sc. vs i.p.). In another publication, the effects of different DIBI doses in CASP-induced sepsis were compared and DIBI at the same dose as in this study (80 mg/kg) was effective to improve leukocyte adhesion 8 hours after sepsis induction (99).

In summary, the data strongly suggest that the iron chelator DIBI alone or in combination with the antibiotic imipenem have anti-inflammatory properties in this experimental sepsis model.

4.3.1.2 Capillary Perfusion

Results for the capillary perfusion confirmed the findings seen for leukocyte adhesion. In CASP-induced sepsis, FCD was decreased in the intestinal muscle and mucosa layers 8 hours after infectious insult. The most sensitive layer, the mucosal layer, was more affected by CASP-induced sepsis. Those results are consistent with the literature. Previous CASP studies found reduction in capillary perfusion by the infectious condition (101, 123–125). Treatment with DIBI and/or IMI improved the capillary perfusion in the mucosa layer, but not in the muscle layer.

Only the combination of the two treatments improved the muscle layer FCD. Those results highlight, as in the toxemia model, the complexity of damages in the microvasculature in sepsis.

4.3.2 Cytokines

To further assess consequences of CASP-induced abdominal sepsis, levels of inflammatory cytokines were measured in plasma samples obtained 8.5 hours after the infectious insult. Unlike toxemia model where the treatment induced a mixed response (either increased or decreased in DIBI treated group comparing to untreated toxin group), all treatments - DIBI alone or in combination with imipenem - decreased significantly the rise of pro-inflammatory (TNF-α, IL-1β, IL-6) and anti-inflammatory (IL-10) cytokines. Islam et al. found similar results using CASP procedure. A decrease in both pro- and anti-inflammatory cytokine might be a sign of anti-inflammatory effects of DIBI. With less inflammation, less anti-inflammatory plasma cytokine might be needed for the healing process.

The present data do not allow an accurate discussion of the discrepancy between the CASP and toxemia models. Experiments including measurements of cytokines at different time points would be a way of clarification. Such difference between CASP and toxemia model highlight the importance of using clinically relevant models to test drug therapies.

4.3.3 Histology

Assessment of morphological intestinal tissue damage done according to the Chiu scoring system showed that the antibiotic imipenem is the key treatment allowing significant decrease of intestinal damage compared to CASP. DIBI alone did not have any significant effect. A study using a similar CASP procedure found no difference using DIBI and imipenem alone or in combination (101).

The mentioned study was slightly different than what has been done here: longer observation time (16h vs 8h) and lower dose of DIBI (40 vs 80 mg/kg). Imipenem dose was similar but the route of administration was different (s.c. vs i.p.). Comparable to the 2 hours of inflammation in the LPS-induced cystitis and toxemia models which were not enough to induce significant damage to the intestinal tissue, it appears that 16h hours of CASP-induced sepsis are still too short to result in severe intestinal morphological changes.

4.3.4 Bacterial Burden

In the CASP model, abdominal sepsis was triggered by allowing continuous leakage of intestinal fecal matter in the peritoneal cavity through a stent surgically inserted in the ascending colon. The goal of this part of the study was to estimate the average number of aerobic and anaerobic bacteria present in the abdominal cavity and the average number of bacteria that reached the bloodstream in order to evaluate potential anti-microbial activity of the iron chelator DIBI and/or antibiotic treatment. Since the results are similar for bacterial burden in the PLF and in the blood, they will be discussed together. CASP-induced leakage of intestinal bacteria into the peritoneal cavity also resulted in a huge amount of those bacteria in the bloodstream. DIBI, at the dose of 80 mg/kg, did not impact the bacterial burden in the blood and in the PLF. However, the antibiotic imipenem alone or in combination with DIBI did reduce the bacterial burden significantly. This is comparable to earlier findings of our group (101).

It has been previously shown that DIBI possesses anti-inflammatory effects, i.e attenuation of the immune response. Despite the fact that this effect would be beneficial in a context of acute sepsis where hyper-activation of immune cells is noticed, the risk that DIBI leads to immunosuppression was a possibility. DIBI-induced immunosuppression would then cause an increase of bacterial growth. The results of CASP bacterial studies showed that DIBI did not worsen bacterial growth. DIBI alone may not have reduced bacterial growth in this 8h CASP model, but it did not increase it either. Moreover, these results alone are not enough to conclude that DIBI does not have antimicrobial effects. Although clinically relevant, CASP has certain limitations.

The fact that in CASP the leakage of intestinal bacteria is continuous during the observation time could have overcome any slight anti-microbial effect of DIBI. In fact, studies have found some antimicrobial properties to DIBI. A study evaluating the minimum inhibitory concentration, the lowest concentration of a molecule that inhibits the growth of a specific strain of bacteria, has shown that the new iron chelator DIBI was strongly inhibitory to the Gram-positive bacteria *S. aureus*, the Gram-negative bacteria *A. baumannii*, and the fungus *C. albicans* (126). In addition, compared to other iron chelators, deferiprone and deferoxamine, DIBI displayed sometimes 100-fold more inhibitory activity.

The antimicrobial propriety of iron chelators comes from their ability to make iron unavailable for bacterial nutrition. The difference between DIBI and the other iron chelators can be explained by the fact that DIBI has the highest affinity for iron, and a molecule of DIBI can bind to 3 iron molecules, whereas other iron chelators binds to 1 or 2 iron molecules (93). In addition, iron chelator as Deferoxamine is a bacterial siderophore from *Streptomyces pilosus*, and Deferiprone bound to iron but keep it in active state (127, 128). In those two situations, bacteria is be able to utilize iron from Deferoxamine and Deferiprone. Other *in vitro* and *in vivo* studies have as well demonstrated DIBI's antibacterial characteristics and also the ability to enhance antibiotic effects and to even fully revert bacterial resistance to an antibiotic (129–133). To better investigate DIBI's anti-microbial effect in a clinically relevant sepsis model, a variant of the CASP procedure with surgical intervention (stent removal) might be useful. In such a model, the intestinal perforation is surgically fixed by a second operation, according to usual procedures in clinical practice. Furthermore, bacterial counts give total number of bacteria but not the species involved. Microbiome analyses are useful to study how different species are involved in experimental sepsis and better interpret DIBI effects.

4.4. Limitations and Future Directions

Some limitations can be identified in our study. First, experiments were done in experimental animal models. Although there are genetic and physiological similarities between human and mice, they are different species (134). The results reported here can't be directly applied in humans. A considerably high number of potential therapies for sepsis appeared promising in animal models, but failed in humans trials (27). However, the information presented here might be useful to design clinical trials with DIBI in human sepsis.

Second, experiments were performed on healthy young male mice. Even though men seem to be more at risk of having sepsis and dying from it (135), female subjects also suffer from the condition and should have been included in the study. Moreover, elderly cumulating different pathologies are more affected than healthy young subjects. Future experiments should include old mice with and without comorbidities.

Another limitation is investigator bias due to the fact that the same person performed (almost) all data collection, analysis and quantification of results. Although measures were taken to minimize sources of bias (videos analyzed and histological score assess in a blinded fashion), it was not possible to perform this study in a fully blinded manner because of the severity of the clinical symptoms on septic animals.

Future experiments should also test a second or more doses of DIBI to improve efficacy. The effect of the novel iron chelator, DIBI, in the immunosuppressive phase of sepsis should be studied as well. DIBI comparison with the FDA-approved iron chelators and microbiome analysis (PLF and blood from CASP model) are in progress in our lab. It might be useful to study also *in vitro* more in detail some of the observed clinical changes, e.g. endothelial cell dysfunction. Measuring key parameters of iron homeostasis in plasma is important. Measuring plasma cytokines at different timepoints to have a better idea of the release of those molecules in the 3 performed models will help understand the mixed response sometimes observed. Using DIBI in the CASP-I model with surgical stent removal in survival studies will be more relevant to evaluate DIBI's antimicrobial effect.

4.5. Conclusion

The present study investigated the impact of the novel iron chelator, DIBI, on intestinal microcirculation using three relevant *in vivo* experimental murine models of sepsis: LPS-induced cystitis, experimental toxemia and CASP-induced polybacterial abdominal sepsis. The dual role of iron in bacterial growth and the immune response during infection represents a potential therapeutic target for sepsis. First, the systemic impact of a model of local inflammation has been compared to a standard model of systemic inflammation. It has been shown that a systemic immune response can be observed early in local infection, yet without major changes in parameters such as capillary blood flow, plasma levels of inflammatory markers, and intestinal tissue damage. Early initiation of treatment was therefore suggested. Second, it has been studied how early administration of DIBI influences the immune response during sepsis.

DIBI showed anti-inflammatory properties in experimental sepsis induced by Gram-positive and Gram-negative toxins. The last step was the assessment of DIBI in a clinically relevant model of abdominal sepsis, i.e. CASP, combining infection and inflammation. Overall, it has been found that iron chelation using DIBI was able to decrease sepsis-induced leukocyte adhesion, preserved capillary perfusion, and reduced bacterial burden (when combined with antibiotic). These results strongly suggested DIBI as promising adjunct treatment for sepsis caused by Gram-positive and Gram-negative bacteria.

REFERENCES

1. M Singer; CS Deutschman; CW Seymour; M Shankar-Hari; D Annane; M Bauer; R Bellomo; GR Bernard; J-D Chiche; CM Coopersmith; RS Hotchkiss; MM Levy; JC Marshall; GS Martin; SM Opal; GD Rubenfeld; T van der Poll; J-L Vincent; DC Angus. The Third International Consensus Definitions for Sepsis and Septic Shock (Sepsis-3). *JAMA* 315, 801–10 (2016)

2. C Fleischmann; A Scherag; NKJ Adhikari; CS Hartog; T Tsaganos; P Schlattmann; DC Angus; K Reinhart. Assessment of global incidence and mortality of hospital-treated sepsis current estimates and limitations. *Am J Respir Crit Care Med* 193, 259–272 (2016)

3. JL Vincent. Increasing awareness of sepsis: World Sepsis Day, (2012)

4. CM Martin; F Priestap; H Fisher; RA Fowler; DK Heyland; SP Keenan; CJ Longo; T Morrison; D Bentley; N Antman. A prospective, observational registry of patients with severe sepsis: The Canadian Sepsis Treatment and Response Registry. *Crit Care Med* 37, 81–88 (2009)

5. C Rhee; Z Zhang; SS Kadri; DJ Murphy; GS Martin; E Overton; CW Seymour; DC Angus; R Dantes; L Epstein; D Fram; R Schaaf; R Wang; M Klompas. Sepsis Surveillance Using Adult Sepsis Events Simplified eSOFA Criteria Versus Sepsis-3 Sequential Organ Failure Assessment Criteria∗. *Crit Care Med* 47, 307–314 (2019)

6. S Finfer; FR Machado. The Global Epidemiology of Sepsis. Does It Matter That We Know So Little? *Am J Respir Crit Care Med* 193, 228–230 (2016)

7. JE Gotts; MA Matthay. Sepsis: pathophysiology and clinical management. *BMJ* 353, i1585 (2016)

8. T Navaneelan; Statistics Canada. Deaths involving sepsis in Canada. (2016)

9. J Hajj; N Blaine; J Salavaci; D Jacoby. The Centrality of Sepsis: A Review on Incidence, Mortality, and Cost of Care. *Healthc (Basel, Switzerland)* 6 (2018)

10. C Brun-Buisson. Incidence, Risk Factors, and Outcome of Severe Sepsis and Septic Shock in Adults. *JAMA* 274, 968 (1995)

11. R Luhr; Y Cao; B Söderquist; S Cajander. Trends in sepsis mortality over time in randomised sepsis trials: A systematic literature review and meta-analysis of mortality in the control arm, 2002-2016, (2019)

12. A Kwizera; I Baelani; M Mer; N Kissoon; MJ Schultz; AJ Patterson; N Musa; JC Farmer; MW Dünser; N Adhikari; PR Arriaga; MR Baldisseri; S Bhagwanjee; DH Ceraso; APL Clift; LA Harmon; J Hellman; JL Hidalgo; HS Kabara; RM Kleinpell; A Latif; G Lundeg; B Patel; NO Raimondi; N Rungta; GS Shrestha; JM Teles; G Thiery; JL Zimmerman. The long sepsis journey in low- and middle-income countries begins with a first step but on which road?, (2018)

13. C Rhee; TM Jones; Y Hamad; A Pande; J Varon; C O'Brien; DJ Anderson; DK Warren; RB Dantes; L Epstein; M Klompas. Prevalence, Underlying Causes, and Preventability of Sepsis-Associated Mortality in US Acute Care Hospitals. *JAMA Netw open* 2, e187571 (2019)

14. M Heron. National Vital Statistics Reports Volume 68, Number 6, June 24, 2019, Deaths: Leading Causes for 2017. (2019)

15. CJ Paoli; MA Reynolds; M Sinha; M Gitlin; E Crouser. Epidemiology and Costs of Sepsis in the United States—An Analysis Based on Timing of Diagnosis and Severity Level*. *Crit Care Med* 46, 1889–1897 (2018)

16. CM Torio; BJ Moore. National Inpatient Hospital Costs: The Most Expensive Conditions by Payer, 2013: Statistical Brief #204. (2006)

17. L Husak; A Marcuzzi; J Herring; E Wen; L Yin; DD Capan; G Cernat. National analysis of sepsis hospitalizations and factors contributing to sepsis in-hospital mortality in Canada. *Healthc Q* 13 Spec No, 35–41 (2010)

18. J Letarte; CJ Longo; J Pelletier; B Nabonne; HN Fisher. Patient characteristics and costs of severe sepsis and septic shock in Quebec. *J Crit Care* 17, 39–49 (2002)

19. B Tiru; EK DiNino; A Orenstein; PT Mailloux; A Pesaturo; A Gupta; WT McGee. The Economic and Humanistic Burden of Severe Sepsis, (2015)

20. JS Hernandez Botero; MC Florian Perez. The History of Sepsis from Ancient Egypt to the XIX Century. In: Sepsis - An Ongoing and Significant Challenge. InTech (2012)

21. F Gül; MK Arslantaş; İ Cinel; A Kumar. Changing definitions of sepsis, (2017)

22. American College of Chest Physicians/Society of Critical Care Medicine Consensus Conference: definitions for sepsis and organ failure and guidelines for the use of innovative therapies in sepsis. In: Critical care medicine (1992)

23. MM Levy; MP Fink; JC Marshall; E Abraham; D Angus; D Cook; J Cohen; SM Opal; JL Vincent; G Ramsay. 2001 SCCM/ESICM/ACCP/ATS/SIS International Sepsis Definitions Conference. In: Intensive Care Medicine (2003)

24. JL Vincent. The Clinical Challenge of Sepsis Identification and Monitoring. *PLoS Med* 13 (2016)

25. J Rello; F Valenzuela-Sánchez; M Ruiz-Rodriguez; S Moyano. Sepsis: A Review of Advances in Management, (2017)

26. PE Marik; AM Taeb. SIRS, qSOFA and new sepsis definition, (2017)

27. E Kyriazopoulou; EJ Giamarellos-Bourboulis. Pharmacological management of sepsis in adults with a focus on the current gold standard treatments and promising adjunctive strategies: evidence from the last five years. *Expert Opin Pharmacother* 20, 991–1007 (2019)

28. H Il Kim; S Park. Sepsis: Early recognition and optimized treatment, (2019)

29. PE Marik; JD Farkas. The Changing Paradigm of Sepsis. *Crit Care Med* 46, 1690–1692 (2018)

30. R Ferrer; I Martin-Loeches; G Phillips; TM Osborn; S Townsend; RP Dellinger; A Artigas; C Schorr; MM Levy. Empiric antibiotic treatment reduces mortality in severe sepsis and septic shock from the first hour: Results from a guideline-based performance improvement program. *Crit Care Med* 42, 1749–1755 (2014)

31. A Rhodes; LE Evans; W Alhazzani; MM Levy; M Antonelli; R Ferrer; A Kumar; JE Sevransky; CL Sprung; ME Nunnally; B Rochwerg; GD Rubenfeld; DC Angus; D Annane; RJ Beale; GJ Bellinghan; GR Bernard; JD Chiche; C Coopersmith; DP De Backer; CJ French; S Fujishima; H Gerlach; JL Hidalgo; SM Hollenberg; AE Jones; DiR Karnad; RM Kleinpell; Y Koh; TC Lisboa; FR MacHado; JJ Marini; JC Marshall; JE Mazuski; LA McIntyre; AS McLean; S Mehta; RP Moreno; J Myburgh; P Navalesi; O Nishida; TM Osborn; A Perner; CM Plunkett; M Ranieri; CA Schorr; MA Seckel; CW Seymour; L Shieh; KA Shukri; SQ Simpson; M Singer; BT Thompson; SR Townsend; T Van Der Poll; JL Vincent; WJ Wiersinga; JL Zimmerman; RP Dellinger. Surviving Sepsis Campaign: International Guidelines for Management of Sepsis and Septic Shock: 2016, (2017)

32. X Bai; W Yu; W Ji; Z Lin; S Tan; K Duan; Y Dong; L Xu; N Li. Early versus delayed administration of norepinephrine in patients with septic shock. *Crit Care* 18 (2014)

33. A Signore. About inflammation and infection, (2013)

34. H Wang; CX Wei; L Min; LY Zhu. Good or bad: gut bacteria in human health and diseases, (2018)

35. DD Chaplin. Overview of the immune response. *J Allergy Clin Immunol* 125 (2010)

36. D Tang; R Kang; CB Coyne; HJ Zeh; MT Lotze. PAMPs and DAMPs: Signal 0s that spur autophagy and immunity. *Immunol Rev* 249, 158–175 (2012)

37. E Vénéreau; C Ceriotti; ME Bianchi. DAMPs from Cell Death to New Life. *Front Immunol* 6, 422 (2015)

38. G Santoni; C Cardinali; M Morelli; M Santoni; M Nabissi; C Amantini. Danger- and pathogen-associated molecular patterns recognition by pattern-recognition receptors and ion channels of the transient receptor potential family triggers the inflammasome activation in immune cells and sensory neurons. *J Neuroinflammation* 12, 21 (2015)

39. A Rubartelli; MT Lotze. Inside, outside, upside down: damage-associated molecular-pattern molecules (DAMPs) and redox. *Trends Immunol* 28, 429–436 (2007)

40. MR Thompson; JJ Kaminski; EA Kurt-Jones; KA Fitzgerald. Pattern recognition receptors and the innate immune response to viral infection, (2011)

41. L Oliveira-Nascimento; P Massari; LM Wetzler. The role of TLR2 ininfection and immunity, (2012)

42. YC Lu; WC Yeh; PS Ohashi. LPS/TLR4 signal transduction pathway, (2008)

43. K Dickson; C Lehmann. Inflammatory response to different toxins in experimental sepsis models, (2019)

44. T Liu; L Zhang; D Joo; SC Sun. NF-κB signaling in inflammation, (2017)

45. J Cohen. The immunopathogenesis of sepsis, (2002)

46. H Chaudhry; J Zhou; Y Zhong; MM Ali; F Mcguire; PS Nagarkatti; M Nagarkatti. Role of cytokines as a double-edged sword in sepsis, (2013)

47. JM Zhang; J An. Cytokines, inflammation, and pain, (2007)

48. BG Chousterman; FK Swirski; GF Weber. Cytokine storm and sepsis disease pathogenesis, (2017)

49. SM Opal; VA DePalo. Anti-inflammatory cytokines. *Chest* 117, 1162–1172 (2000)

50. NGC (UK). Finding the source of infection. (2016)

51. NS Ward; B Casserly; A Ayala. The Compensatory Anti-inflammatory Response Syndrome (CARS) in Critically Ill Patients, (2008)

52. AM Binkowska; G Michalak; R Slotwiński. Current views on the mechanisms of immune responses to trauma and infection, (2015)

53. C Konradt; CA Hunter. Pathogen interactions with endothelial cells and the induction of innate and adaptive immunity, (2018)

54. HF Langer; T Chavakis. Leukocyte - Endothelial interactions in inflammation. *J Cell Mol Med* 13, 1211–1220 (2009)

55. D De Backer; J Creteur; JC Preiser; MJ Dubois; JL Vincent. Microvascular blood flow is altered in patients with sepsis. *Am J Respir Crit Care Med* 166, 98–104 (2002)

56. J Birnbaum; O V Hein; C Luhrs; O Ruckbeil; C Spies; S Ziemer; M Grundling; T Usichenko; K Meissner; D Pavlovic; WJ Kox; C Lehmann. Effects of coagulation factor XIII on intestinal functional capillary density, leukocyte adherence and mesenteric plasma extravasation in experimental endotoxemia. *Crit Care* 10, R29 (2006)

57. J-L Teboul; J Duranteau. Alteration of microcirculation in sepsis. *Crit Care Med* 40, 1653–1654 (2012)

58. S Trzeciak; RP Dellinger; JE Parrillo; M Guglielmi; J Bajaj; NL Abate; RC Arnold; S Colilla; S Zanotti; SM Hollenberg. Early microcirculatory perfusion derangements in patients with severe sepsis and septic shock: Relationship to hemodynamics, oxygen transport, and survival. *Ann Emerg Med* 49 (2007)

59. S Trzeciak; J V. McCoy; RP Dellinger; RC Arnold; M Rizzuto; NL Abate; NI Shapiro; JE Parrillo; SM Hollenberg. Early increases in microcirculatory perfusion during protocol-directed resuscitation are associated with reduced multi-organ failure at 24 h in patients with sepsis. *Intensive Care Med* 34, 2210–2217 (2008)

60. Y Sakr; MJ Dubois; D De Backer; J Creteur; JL Vincent. Persistent-microcirculatory alterations are associated with organ failure and death in patients with septic shock. *Crit Care Med* 32, 1825–1831 (2004)

61. M Charlton; M Sims; T Coats; JP Thompson. The microcirculation and its measurement in sepsis. *J Intensive Care Soc* 18, 221–227 (2017)

62. D De Backer; D Orbegozo Cortes; K Donadello; J-L Vincent. Pathophysiology of microcirculatory dysfunction and the pathogenesis of septic shock. *Virulence* 5, 73–9 (2014)

63. M Miranda; M Balarini; D Caixeta; E Bouskela. Microcirculatory dysfunction in sepsis: pathophysiology, clinical monitoring, and potential therapies. *Am J Physiol Circ Physiol* 311, H24–H35 (2016)

64. G Schlag; H Redl. Pathophysiology of Shock, Sepsis, and Organ Failure. Springer Berlin Heidelberg (1993)

65. AD Sheftel; AB Mason; P Ponka. The long history of iron in the Universe and in health and disease, (2012)

66. N Abbaspour; R Hurrell; R Kelishadi. Review on iron and its importance for human health. *J Res Med Sci* 19, 164–74 (2014)

67. BJ Crielaard; T Lammers; S Rivella. Targeting iron metabolism in drug discovery and delivery. *Nat Rev Drug Discov* 16, 400–423 (2017)

68. Y Kohgo; K Ikuta; T Ohtake; Y Torimoto; J Kato. Body iron metabolism and pathophysiology of iron overload, (2008)

69. ER Monsen. Iron nutrition and absorption: dietary factors which impact iron bioavailability, (1988)

70. E Nemeth; E V. Valore; M Territo; G Schiller; A Lichtenstein; T Ganz. Hepcidin, a putative mediator of anemia of inflammation, is a type II acute-phase protein. *Blood* 101, 2461–2463 (2003)

71. T Ganz. Molecular pathogenesis of anemia of chronic disease, (2006)

72. S Sharma; E Nemeth; YH Chen; J Goodnough; A Huston; GD Roodman; T Ganz; A Lichtenstein. Involvement of hepcidin in the anemia of multiple myeloma. *Clin Cancer Res* 14, 3262–3267 (2008)

73. S Di Meo; TT Reed; P Venditti; VM Victor. Role of ROS and RNS Sources in Physiological and Pathological Conditions. *Oxid Med Cell Longev* 2016, 1245049 (2016)

74. A Covarrubias; V Byles; T Horng. ROS sets the stage for macrophage differentiation. *Cell Res* 23, 984–5 (2013)

75. Q Xu; S Choksi; J Qu; J Jang; M Choe; B Banfi; JF Engelhardt; Z Liu. NADPH Oxidases Are Essential for Macrophage Differentiation. *J Biol Chem* 291, 20030–20041 (2016)

76. Y Zhang; S Choksi; K Chen; Y Pobezinskaya; I Linnoila; Z-G Liu. ROS play a critical role in the differentiation of alternatively activated macrophages and the occurrence of tumor-associated macrophages. *Cell Res* 23, 898–914 (2013)

77. B Brüne; N Dehne; N Grossmann; M Jung; D Namgaladze; T Schmid; A von Knethen; A Weigert. Redox control of inflammation in macrophages. *Antioxid Redox Signal* 19, 595–637 (2013)

78. M Mittal; MR Siddiqui; K Tran; SP Reddy; AB Malik. Reactive oxygen species in inflammation and tissue injury. *Antioxid Redox Signal* 20, 1126–67 (2014)

79. H She; S Xiong; M Lin; E Zandi; C Giulivi; H Tsukamoto. Iron activates NF-κB in Kupffer cells. *Am J Physiol - Gastrointest Liver Physiol* 283 (2002)

80. Z Zhang; F Zhang; P An; X Guo; Y Shen; Y Tao; Q Wu; Y Zhang; Y Yu; B Ning; G Nie; MD Knutson; GJ Anderson; F Wang. Ferroportin1 deficiency in mouse macrophages impairs iron homeostasis and inflammatory responses. *Blood* 118, 1912–1922 (2011)

81. A Sindrilaru; T Peters; S Wieschalka; C Baican; A Baican; H Peter; A Hainzl; S Schatz; Y Qi; A Schlecht; JM Weiss; M Wlaschek; C Sunderkötter; K Scharffetter-Kochanek. An unrestrained proinflammatory M1 macrophage population induced by iron impairs wound healing in humans and mice. *J Clin Invest* 121, 985–997 (2011)

82. P Lan; K han Pan; S jia Wang; Q cheng Shi; Y xian Yu; Y Fu; Y Chen; Y Jiang; X ting Hua; J cang Zhou; Y song Yu. High Serum Iron level is Associated with Increased Mortality in Patients with Sepsis. *Sci Rep* 8 (2018)

83. PN Paradkar; I De Domenico; N Durchfort; I Zohn; J Kaplan; DM Ward. Iron depletion limits intracellular bacterial growth in macrophages. *Blood* 112, 866–874 (2008)

84. T Ganz; E Nemeth. Iron homeostasis in host defence and inflammation, (2015)

85. S Saikia; D Oliveira; G Hu; J Kronstad. Role of ferric reductases in iron acquisition and virulence in the fungal pathogen cryptococcus neoformans. *Infect Immun* 82, 839–850 (2014)

86. JR Sheldon; HA Laakso; DE Heinrichs. Iron Acquisition Strategies of Bacterial Pathogens. In: Virulence Mechanisms of Bacterial Pathogens, Fifth Edition. American Society of Microbiology (2016)

87. N Mobarra; M Shanaki; H Ehteram; H Nasiri; M Sahmani; M Saeidi; M Goudarzi; H Pourkarim; M Azad. A review on iron chelators in treatment of iron overload syndromes, (2016)

88. L Li; B Frei. Iron chelation inhibits NF-κB-mediated adhesion molecule expression by inhibiting p22phox protein expression and NADPH oxidase activity. *Arterioscler Thromb Vasc Biol* 26, 2638–2643 (2006)

89. E Messaris; PT Antonakis; N Memos; E Chatzigianni; E Leandros; MM Konstadoulakis. Deferoxamine administration in septic animals: Improved survival and altered apoptotic gene expression. *Int Immunopharmacol* 4, 455–459 (2004)

90. M Vulcano; RP Meiss; MA Isturiz. Deferoxamine reduces tissue injury and lethality in LPS-treated mice. *Int J Immunopharmacol* 22, 635–644 (2000)

91. LT van Eijk; S Heemskerk; RW van der Pluijm; SM van Wijk; WHM Peters; JG van der Hoeven; M Kox; DW Swinkels; P Pickkers. The effect of iron loading and iron chelation on the innate immune response and subclinical organ injury during human endotoxemia: A randomized trial. *Haematologica* 99, 579–587 (2014)

92. MR Power Coombs; T Grant; AL Greenshields; DJ Arsenault; BE Holbein; DW Hoskin. Inhibitory effect of iron withdrawal by chelation on the growth of human and murine mammary carcinoma and fibrosarcoma cells. *Exp Mol Pathol* 99, 262–270 (2015)

93. H Heli; S Mirtorabi; K Karimian. Advances in iron chelation: An update, (2011)

94. E Poggiali; E Cassinerio; L Zanaboni; MD Cappellini. An update on iron chelation therapy, (2012)

95. N Arora; A Caldwell; K Wafa; A Szczesniak; M Caldwell; N Al-Banna; N Sharawy; S Islam; J Zhou; BE Holbein; MEM Kelly; C Lehmann. DIBI, a polymeric hydroxypyridinone iron chelator, reduces ocular inflammation in local and systemic endotoxin-induced uveitis. *Clin Hemorheol Microcirc* 69, 153–164 (2018)

96. S-J Lee; SW Kim; Y-H Cho; MS Yoon. Anti-inflammatory effect of an Escherichia coli extract in a mouse model of lipopolysaccharide-induced cystitis. *World J Urol* 24, 33–38 (2006)

97. TJ Jerde; DE Bjorling; H Steinberg; T Warner; R Saban. Determination of mouse bladder inflammatory response to E. coli lipopolysaccharide. (2000)

98. T Thorburn; M Aali; L Kostek; C LeTourneau-Paci; P Colp; J Zhou; B Holbein; D Hoskin; C Lehmann. Anti-inflammatory effects of a novel iron chelator, DIBI, in experimental sepsis. *Clin Hemorheol Microcirc* 67, 241–250 (2017)

99. TV Thorburn. IRON-RELATED IMMUNE CELL FUNCTION IN SEPSIS. (2018)

100. C Lehmann; F Götz; L Schuster; J Zhou. Improved setup for intestinal intravital microscopy in mice - the "floating table." *Minerva Anestesiol* 102–103 (2013)

101. S Islam; S Jarosch; J Zhou; MDC Parquet; JT Toguri; P Colp; BE Holbein; C Lehmann. Anti-inflammatory and anti-bacterial effects of iron chelation in experimental sepsis. *J Surg Res* 1–8 (2015)

102. I Burkovskiy; J Zhou; C Lehmann. Experimental cannabinoid 2 receptor inhibition in CNS injury-induced immunodeficiency syndrome. *Microcirculation* 1, n/a-n/a (2016)

103. CJ Chiu; AH McArdle; R Brown; HJ Scott; FN Gurd. Intestinal Mucosal Lesion in Low-Flow States: I. A Morphological, Hemodynamic, and Metabolic Reappraisal. *Arch Surg* 101, 478–483 (1970)

104. S Tambaro; MA Casu; A Mastinu; P Lazzari. Evaluation of selective cannabinoid CB1 and CB2 receptor agonists in a mouse model of lipopolysaccharide-induced interstitial cystitis. *Eur J Pharmacol* 729, 67–74 (2014)

105. Q Li; Q Zhang; C Wang; X Liu; N Li; J Li. Disruption of tight junctions during polymicrobial sepsis in vivo. *J Pathol* 218, 210–221 (2009)

106. M Gatt. The role of the gut in sepsis, (2015)

107. KT Fay; ML Ford; CM Coopersmith. The intestinal microenvironment in sepsis. *Biochim Biophys Acta - Mol Basis Dis* 1863, 2574–2583 (2017)

108. M Schnoor; P Alcaide; MB Voisin; JD Van Buul. Crossing the Vascular Wall: Common and Unique Mechanisms Exploited by Different Leukocyte Subsets during Extravasation, (2015)

109. S Grover; A Srivastava; R Lee; AK Tewari; AE te. Role of inflammation in bladder function and interstitial cystitis, (2011)

110. PR Kvietys. The Gastrointestinal Circulation, https://www.ncbi.nlm.nih.gov/books/NBK53099/

111. T Thorburn; M Aali; L Kostek; C LeTourneau-Paci; P Colp; J Zhou; B Holbein; D Hoskin; C Lehmann. Anti-inflammatory effects of a novel iron chelator, DIBI, in experimental sepsis. *Clin Hemorheol Microcirc* 1–10 (2017)

112. K Triantafilou; M Triantafilou; RL Dedrick. Interactions of bacterial lipopolysaccharide and peptidoglycan with a 70 kDa and an 80 kDa protein on the cell surface of CD14+ and CD14- cells. *Hum Immunol* 62, 50–63 (2001)

113. MN Guentzel. Escherichia, Klebsiella, Enterobacter, Serratia, Citrobacter,and Proteus. (1996)

114. SJ Finney; SK Leaver; TW Evans; A Burke-Gaffney. Differences in lipopolysaccharide- and lipoteichoic acid-induced cytokine/chemokine expression. *Intensive Care Med* 38, 324–32 (2012)

115. BG Yipp; G Andonegui; CJ Howlett; SM Robbins; T Hartung; M Ho; P Kubes. Profound Differences in Leukocyte-Endothelial Cell Responses to Lipopolysaccharide Versus Lipoteichoic Acid. *J Immunol* 168, 4650–4658 (2002)

116. MR Gillrie; L Zbytnuik; E McAvoy; R Kapadia; K Lee; CCM Waterhouse; SP Davis; DA Muruve; P Kubes; M Ho. Divergent roles of Toll-like receptor 2 in response to lipoteichoic acid and Staphylococcus aureus in vivo. *Eur J Immunol* 40, 1639–1650 (2010)

117. AL Greenshields; MR Power Coombs; W Fernando; BE Holbein; DW Hoskin. DIBI, a novel 3-hydroxypyridin-4-one chelator iron-binding polymer, inhibits breast cancer cell growth and functions as a chemosensitizer by promoting S-phase DNA damage. *BioMetals* (2019)

118. MJ Massey; PC Hou; M Filbin; H Wang; L Ngo; DT Huang; WC Aird; V Novack; S Trzeciak; DM Yealy; JA Kellum; DC Angus; NI Shapiro. Microcirculatory perfusion disturbances in septic shock: results from the ProCESS trial. *Crit Care* 22, 308 (2018)

119. JE Wang; MK Dahle; A Yndestad; I Bauer; MC McDonald; P Aukrust; SJ Foster; M Bauer; AO Aasen; C Thiemermann. Peptidoglycan of Staphylococcus aureus causes inflammation and organ injury in the rat. *Crit Care Med* 32, 546–552 (2004)

120. HY Kim; NR Han; HM Kim; HJ Jeong. The Iron Chelator and Anticancer Agent Dp44mT Relieves Allergic Inflammation in Mice With Allergic Rhinitis. *Inflammation* 41, 1744–1754 (2018)

121. J Cermanova; Z Kadova; E Dolezelova; M Zagorova; V Safka; M Hroch,; T Laho; M Holeckova; J Mokry; P Kovarikova; J Bures; M Sterba; S Micuda. Deferoxamine but not Dexrazoxane Alleviates Liver Injury Induced by Endotoxemia in Rats. *Shock* 42, 372–379 (2014)

122. S Wang; C Liu; S Pan; Q Miao; J Xue; J Xun; Y Zhang; Y Gao; X Duan; Y Fan. Deferoxamine attenuates lipopolysaccharide-induced inflammatory responses and protects against endotoxic shock in mice. *Biochem Biophys Res Commun* 465, 305–311 (2015)

123. C Lehmann; M Kianian; J Zhou; I Kuster; R Kuschnereit; S Whynot; O Hung; R Shukla; B Johnston; V Cerny; D Pavlovic; A Spassov; MEM Kelly. Cannabinoid receptor 2 activation reduces intestinal leukocyte recruitment and systemic inflammatory mediator release in acute experimental sepsis. *Crit Care* 16, R47 (2012)

124. C Fuchs; E Ladwig; J Zhou; D Pavlovic; K Behrend; S Whynot; O Hung; M Murphy; V Cerny; C Lehmann. Argatroban administration reduces leukocyte adhesion and improves capillary perfusion within the intestinal microcirculation in experimental sepsis. *Thromb Haemost* 104, 1022–8 (2010)

125. MK Lustig; VH Bac; D Pavlovic; S Maier; M Grundling; O Grisk; M Wendt; CD Heidecke; C Lehmann. Colon ascendens stent peritonitis--a model of sepsis adopted to the rat: physiological, microcirculatory and laboratory changes. *Shock* 28, 59–64 (2007)

126. MTC Ang; R Gumbau-Brisa; DS Allan; R McDonald; MJ Ferguson; BE Holbein; M Bierenstiel. DIBI, a 3-hydroxypyridin-4-one chelator iron-binding polymer with enhanced antimicrobial activity. *Medchemcomm* 9, 1206–1212 (2018)

127. M Aali; A Caldwell; K House; J Zhou; V Chappe; C Lehmann. Iron chelation as novel treatment for lung inflammation in cystic fibrosis. *Med Hypotheses* (2017)

128. Y Xia; N Farah; A Maxan; J Zhou; C Lehmann. Therapeutic iron restriction in sepsis. *Med Hypotheses* 89, 37–39 (2016)

129. M del C Parquet; KA Savage; DS Allan; RJ Davidson; BE Holbein. Novel iron-chelator DIBI inhibits Staphylococcus aureus growth, suppresses experimental MRSA infection in mice and enhances the activities of diverse antibiotics in vitro. *Front Microbiol* 9 (2018)

130. KA Savage; M del Carmen Parquet; DS Allan; RJ Davidson; BE Holbein; EA Lilly; PL Fidel. Iron restriction to clinical isolates of candida albicans by the novel chelator dibi inhibits growth and increases sensitivity to azoles in vitro and in vivo in a murine model of experimental vaginitis. *Antimicrob Agents Chemother* 62 (2018)

131. BE Holbein; R Mira de Orduña. Effect of trace iron levels and iron withdrawal by chelation on the growth of Candida albicans and Candida vini. *FEMS Microbiol Lett* 307, 19–24 (2010)

132. MDC Parquet; KA Savage; DS Allan; MTC Ang; W Chen; SM Logan; BE Holbein. Antibiotic-Resistant Acinetobacter baumannii Is Susceptible to the Novel Iron-Sequestering Anti-infective DIBI In Vitro and in Experimental Pneumonia in Mice. *Antimicrob Agents Chemother* 63 (2019)

133. KA Savage; M del Carmen Parquet; DS Allan; RJ Davidson; BE Holbein; EA Lilly; PL Fidel. Erratum for savage et al., “Iron restriction to clinical isolates of candida albicans by the novel chelator dibi inhibits growth and increases sensitivity to azoles in vitro and in vivo in a murine model of experimental vaginitis” (American Society for Microbiology (2018) 62:8 (e02576-17) DOI: 10.1128/AAC.02576-17), (2019)

134. RL Perlman. Mouse Models of Human Disease: An Evolutionary Perspective. *Evol Med Public Heal* eow014 (2016)

135. N Nasir; B Jamil; S Siddiqui; N Talat; FA Khan; R Hussain. Mortality in sepsis and its relationship with gender. *Pakistan J Med Sci* 31, 1201–1206 (2015)

APPENDICES

A

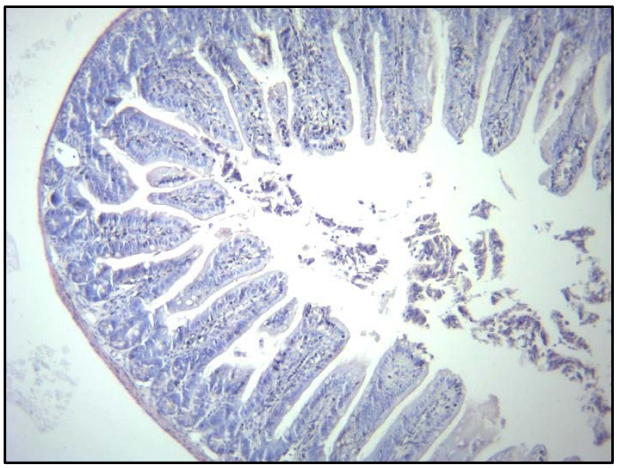

B

C

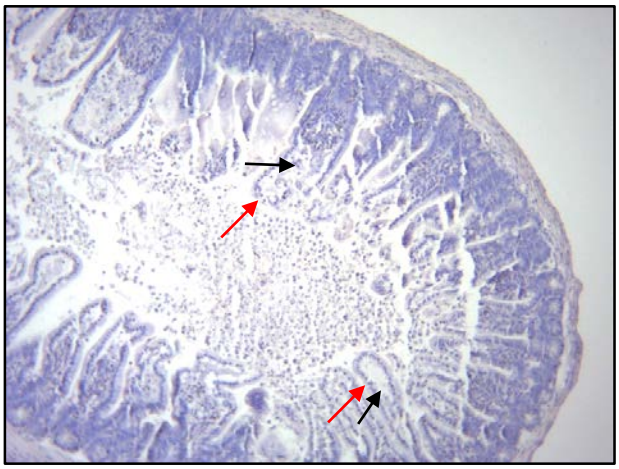

Figure 53 Representation of histological changes observed during experiments (Chiu score(103)). Cross section of murine intestine showing different degree of tissue damage due to inflammation. H&E staining under 40X magnification.

(A) grade 0: Normal mucosal villi, epithelial cells well aligned and intact;

(B) grade 1: Development of spaces called Gruenhagen's space at the apex of villi (shown by black arrow), epithelial cells well aligned and intact;

(C) grade 2: Extension of Gruenhagen's space along the villi with damage/missing epithelial cells shown by red arrow;